University of Strathclyde Glasgow

A Tissue-Engineered Approach to Hernia Repair

Ivan J. Hall Barrientos, MEng

Biomedical Engineering,

University of Strathclyde

Thesis submitted for the degree of Doctor of Engineering (EngD)

December 2017

Declaration

This thesis is the result of the author's original research. It has been composed by the author and has not been previously submitted for examination that has led to the award of a degree.

The copyright of this thesis belongs to the author under the terms of the United Kingdom Copyright Acts as qualified by University of Strathclyde Regulation 3.50. Due acknowledgement must always be made of the use of any material contained in, or derived from, this thesis.

Signed:

Date:

Dedicated to my family and Colette.

Acknowledgements

Abstract

Hernia repairs are among the most common surgical procedures performed, with more than 20 million hernias estimated to be repaired every year around the world. Mesh insertion is the most common method of treatment, with the mesh typically being made from polypropylene (PP). Significant complications can arise from PP meshes that include chronic infection, inflammation and pain.

Electrospinning, a technique that utilises electric forces to create micro- and nano-fibres, was used to fabricate a new-generation of hernia mesh (drug-loaded polymeric mesh). Solutions of polycaprolactone (PCL) or polylactic acid (PLA), two aliphatic polymers commonly used in various clinical applications, were individually mixed with irgasan (IRG) (an antibacterial agent) or levofloxacin (LEVO) (a broad-spectrum antibiotic). Type I collagen was later included into the polymer-drug solutions in order to increase the biocompatibility of the samples. Electrospun samples were subsequently analysed for mechanical, physicochemical, drug release and biological characteristics.

Electrospinning was useful in creating micro- and nano- fibres for polymer-drug combinations. IRG-loaded scaffolds displayed a sustained release behaviour, whilst LEVO-loaded scaffolds showed a burst release. The addition of type I collagen modified the release rate of PLA-LEVO scaffolds from burst to sustained release, and modified surface characteristics from hydrophilic to hydrophobic. Biological studies demonstrated smooth muscle cells affinity to LEVO-loaded scaffolds, with high adhesion and proliferation, whilst also demonstrating significant resistance to bacterial growth (*E. coli* and *S. aureus*).

Nomenclature

AFM	Atomic Force Microscopy
API	Active Pharmaceutical Ingredient
BET	Brunauer-Emmett-Teller
BrdU	5-bromo-2'-deoxyuridine
CAG	Contact Angle Goniometry
CLF	Chloroform
DDS	Drug Delivery System
DSC	Differential Scanning Calorimetry
DMF	*N,N*-Dimethylformamide
EC$_{50}$	Half-Maximal Effective Concentration
E. coli	Escherichia Coli
ECM	Extracellular Matrix
η	Shear Viscosity
g	Grams (Weight)
G'	Elastic/Storage Modulus
G''	Viscous/Loss Modulus
HFP	1,1,1,3,3,3-Hexafluoro-2-propanol

Hr	Hours (Time)
IGC	Inverse Gas Chromatography
IR	Infrared
IRG	Irgasan
LB	Luria-Bertani
LEVO	Levofloxacin
LVER	Linear Viscoelastic Region
Pa	Pascal (Pressure)
PBS	Phosphate Buffer Solution
PCL	Polycaprolactone
PLA	Polylactic Acid
PP	Polypropylene
N	Newton (Force)
NMR	Nuclear Magnetic Resonance
Ra	Roughness Average
RAOSMC	Rat Aortic Smooth Muscle Cell
S. aureus	Staphylococcus Aureus
SDS	Sodium Dodecyl Sulphate

SEA	Surface Energy Analysis
SEM	Scanning Electron Microscopy
SMC	Smooth Muscle Cell
$\mathbf{T_c}$	Crystallisation Temperature
$\mathbf{T_g}$	Glass Transition Temperature
$\mathbf{T_m}$	Melting Temperature
ToF-SIMS	Time-of-Flight Secondary Ion Mass Spectrometry
UV	Ultraviolet
XRPD	X-Ray Powder Diffraction
λ	Wavelength

Contents

List of Figures

List of Tables

Chapter 1: General Introduction

1.1   Introduction

Hernia repairs are among the most common surgical procedures performed, with an estimate of more than 20 million hernias to be repaired every year around the world (Kingsworth & LeBlanc 2003), and approximately over 100,000 procedures are carried out in the UK per year (Dabbas et al. 2011). The most common type of hernia is the 'inguinal hernia', which is a protrusion of abdominal-cavity contents through the inguinal canal – this typically occurs when tissue structure and function is lost at the load-bearing muscle, tendon and fascial layer (Franz 2008).

There are three current methods of hernia repair that include *tension-free, low-tension* and *tension repair*. Tension-free repair has now become the standard surgical procedure for the repair of inguinal hernias, and this is normally accompanied by the insertion of a mesh at the site of hernia in order to strengthen the weakened abdominal cavity. The meshes are predominately found in 3 various forms; standard non-absorbable implants, composite synthetic implants, and bio implants (mainly arranged from human or animal tissues) (Lukasiewicz & Drewa 2014).

The topic of this thesis is centered around the need to improve on the existing line of hernia repair mesh products, relative to the basic patient needs that has the potential to reduce recurrence rates, encourage healthy cellular growth at site of repair and maintain a level of biocompatibility between the surrounding tissue and mesh. These needs have been specifically selected due to the current polymer used, *polypropylene*, which according to reports (circa 1990s – 2000s) is the best repair material so far been

used in hernia repair operations (Gaoming et al. 2005) and is the most widely used polymer in hernia repair (Akolekar et al. 2008). However, recent reports have begun to reveal problems. A number of serious complications have been occurring for operations where PP has been used that are related to chronic pain caused by the formation of scar tissue (Bendavid et al. 2014), chronic inflammation in association with a foreign body (Moriarty et al. 2012), and chronic infection due to the formation of biofilm and the contamination with micro-organisms (Patel et al. 2012). Clinical studies have been recently published highlighting the adverse events after PP mesh surgical procedures (Morling et al. 2016), and highly publicised cases of litigation from patients against the NHS and mesh manufacturers (Devlin 2017) further establish the fundamental need to develop a new generation of mesh material that will begin to impact post-operative patient care in a positive manner. Other polymers commonly used for surgical meshes are polyester (PET) and polytetrafluoroethylene (PTFE) – early complications associated with the use of these meshes include seroma, hematoma, wound breakdown, bowel injury and deep vein thrombosis (Iannitti et al. 2008).

The need to design and develop a new generation of hernia meshes is clear; it is now apparent that using inert polymers is not enough for patient recovery. It may be critical to develop a type of mesh that closely resembles the extracellular matrix (ECM) and there are numerous fabrication methods that can form polymers into this shape, and in conjunction with biocompatible polymers (or natural polymers). It should be noted that during wound healing, there is a fine balance between biosynthesis and degradation of the ECM. The ECM is comprised of 70 – 80% collagen, and having the correct ratio of type I to type III collagen has been suggested as critical to the

overall success of wound healing related to hernia repair (Zheng et al. 2002). However, wound infection has the capability to delay parts of the surgical wound-healing pathway (Robson et al. 2000), therefore a progression from the current mesh design may be to integrate anti-bacterial materials that will enable the proper mechanism of action for the ECM post-surgery. Chronic pain, inflammation, and infection all interact in a number of different ways, and given the importance of these factors, this situation poses a number of different research questions:

Can a different mesh material be used within hernia repair? In particular, can we appropriately use biocompatible polymers, and possibly in conjunction with natural polymers?

Can a new-generation drug-loaded mesh that is bio-available to the surrounding tissues be created? The healthy growth of surrounding cells may be vital to the success of this mesh; therefore can we fabricate a drug-loaded mesh that will allow for cellular growth in order to predict possibly tissue behaviour and interaction?

Can a mesh that fulfils the patients' needs, whilst reducing the negative side effects associated with polypropylene mesh repair be created? We have already identified three major needs that must be addressed; chronic pain, chronic inflammation and chronic infection – can a mesh be created that actively reduces these three major problems?

Chapter 2: Literature Review

2.1 Hernia Repair

There are a number of different diseases that are widely acknowledged as the more serious or important diseases to research in order to find a potential cure. Illnesses such as cancer, heart disease and Parkinson's disease fit into this category, however there are a number of other health problems that are almost decidedly overlooked. In particular, a hernia is an example of an ailment that is less often newsworthy and any development in research is not widely seen as a breakthrough in mainstream media. However, hernia repair is one of the most common operations a general surgeon will be required to carry out (Earle 2010). There are a number of different types of hernias, and these are generally organised via the location of the incurred hernia on the human body. The four main types of hernia that occur are:

- Inguinal Hernias: these are the most common types of hernia that occur in the abdominal wall of the body, in particular the inguinal canal.

- Ventral Hernias: this is also known as an incisional hernia, given that this type of hernia commonly occurs after surgery at the site of initial incision. Ventral hernias have a high degree of severity, with an average recurrence rate of 50% (Franklin et al. 2004).

- Femoral Hernias: are very similar to inguinal hernias, due to common occurrence in the groin area. This commonly occurs in women during

pregnancy or childbirth due to a weakness in the groin (due to excessive weight strain), which causes the intestine to move into the femoral canal.

- Umbilical Hernias: these occur near the navel and are common in infants. This is due to the natural weaknesses in the blood vessels of the umbilical cord – although this occurs in infants, it can be carried into adult life and the repair of this type of hernia becomes extremely difficult to rectify.
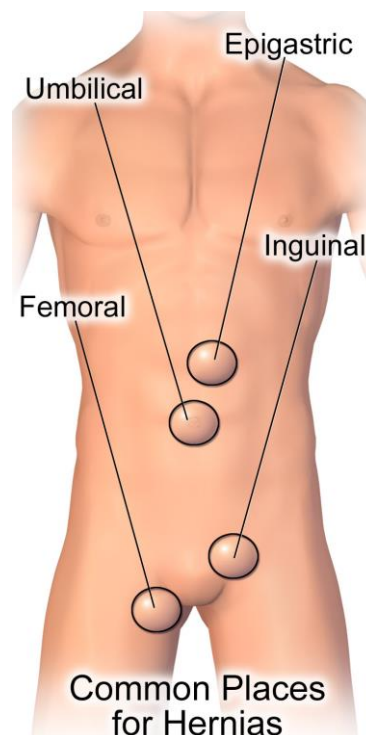
Figure 2.1 – Diagram detailing common areas of hernia occurrence

These different types of hernia occur (but are not limited to) mainly in the lower torso, specifically in the abdominal area. Within the abdominal area there are a number of different muscles including a superficial group (consisting of over 5 types of muscle) and a deep group (consisting of over 5 types of muscles) (Tahan et al. 2016) – even at this level of understanding the anatomy of the abdominal area, it can be strongly

suggested that any surgical procedure for hernia is inherently difficult to perform. The large number of muscles surrounding the abdominal wall suggests that there will be a varying number of stress and strain forces being applied to the abdomen at all times, therefore if a hernia is to be repaired it needs to be able to withstand the variant forces and prevent any further or potential perforation of the abdominal wall. In particular, the abdominal wall is seen to exhibit nonlinear elastic, anisotropic behaviour, with a Young's Moduli of 50 kPa and 20 kPa in the transversal and longitudinal directions (Förstemann et al. 2011). Repairing a hernia is effectively a reconstructive surgery, and the main goals for reconstructing an abdominal wall are to restore the structural and functional ability of the abdominal wall and surrounding tissue, achieve muscular stability, and to achieve optimal wound healing (Grevious et al. 2006).

2.1.1 Methods of Treatment

In most cases of hernia occurrence, surgery will most likely be required. However, there are number of different factors that will affect the treatment – for example hernia location, size and shape of the defect, and whether or not the herniated contents are reducible, chronically incarcerated, or acutely incarcerated (Deeba et al. 2009). Within this, there are number of different surgical procedures that are used:

- Prosthetic reinforcement (i.e. surgically inserting a mesh),
- Component separation,
- Laparoscopic hernioplasty.

The more popular procedures involve mesh repair (prosthetic reinforcement) and laparoscopic hernioplasty. It should be noted, however, that most hernia injury are

unique to the patient; therefore a tailored procedure for each surgery is required (Kawaguchi et al. 2015). This means that the current methods of hernia repair will not always have the same result across different patients. Whilst it was previously mentioned that there are a number of factors affecting hernia procedure, similarly there are factors about the patient that will affect their hernia recovery. Factors such as age, sex and health (i.e. smoker, diabetic, cardiac problems) will all play a vital role in whether surgery will be a success (relative to whether the hernia occurs again).

With mesh insertion, this can be achieved using either open or laparoscopic surgical techniques. With open [inguinal] repair, the procedure involves initially making an incision near the site of the hernia protrusion. The protrusion is then placed back into the abdomen, and a mesh is placed within the abdominal wall at the site of hernia. The mesh is then fixed in place, usually, with either surgical sutures or staples (Hassler & Baltazar-Ford 2017). This method is the more commonly used procedure; however, there have been studies demonstrating the benefit of laparoscopic repairs with regards to improved post-operative pain, quality of life and post-operative complications (Koju et al. 2017). Both techniques still focus on the use of mesh insertion, and there are a number of side effects currently associated with this that include:

- Chronic infection

- Chronic inflammation

- High recurrence rate of hernia

- Adhesion of surrounding tissue to the mesh

- Obstruction of small/large intestine

- Fistula

- Seroma

- Perforation of organs. (FDA 2017)

2.1.2 User Requirements of Mesh

Given the number of complications using a mesh in a surgical scenario, it is vital to understand and articulate user requirements that will determine what the ideal surgical mesh will be. The following have been determined in literature as the more important properties: Sufficient mechanical strength, chemical stability, lack of carcinogenic properties, easy sterilisation, ability to limit foreign body reactions, fabrication in required size and shape, infection resistance, biomechanical properties resembling native tissues (Lukasiewicz & Drewa 2014; Hamer-Hodges & Scott 1985)
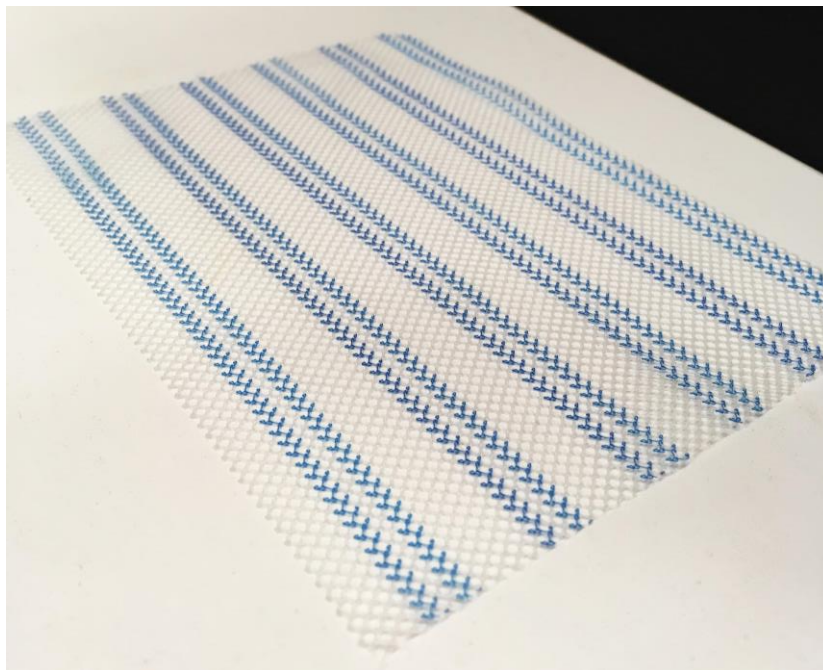
Figure 2.2 – An example of a polypropylene mesh, used in hernia repair

Within these requirements, there are a number of sub-factors that will affect the success of achieving the desired requirement – factors such as mesh material,

strength/elasticity, weight and pore size are all crucial components to understand. As mentioned in the previous section, there are a number of different materials used in the current line of hernia meshes, in particular polypropylene (PP), polyester (PE) and polytetrafluoroethylene (PTFE). Whilst these are common materials, each of these materials do not meet all the exact requirements outlined.

Elasticity and tensile strength of the mesh is extremely important given that any changes in either of these (e.g. if the elasticity increases, or the strength decreases) will cause major defects in the mesh. Any potential defects in a mesh will then lead to further reduction in its functionality, which may have potentially serious consequences to the recovery and health of the patient. The difficulty with this factor lies in finding the balance between something that is strong, but flexible enough to allow liberal movement in the patient. The natural elasticity of the abdominal wall at 32 N/cm is about 38%, whereas lightweight meshes have an elasticity of 20 – 35% and heavyweight meshes have an elasticity of between 4 – 15% (Klosterhalfen et al. 2005). The strength of the polymer mesh is also affected by the fabrication method, and relative to the three common polymer mesh types (PP, PE and PTFE), these are normally either woven or knitted. Woven meshes have a great degree of strength but with poor directional stretch, whereas knitted meshes have a lesser strength but a greater degree of flexibility. It is possible that an anisotropic mesh would be the optimum way for meeting an elasticity and strength requirement.

The porosity of the mesh is also important, and again therein lays a difficulty in choosing the optimum porosity size. Pores must be more than 75 µm in order to allow infiltration by macrophages, fibroblasts, blood vessels and collagen (Bilsel & Abci

2012). Meshes can be classified into four different types according to their porosity: type I macro porous (porosity greater than 75 µm), type II micro porous (porosity less than 10 µm), type III macro porous with micro porous components and type IV biomaterials with sub-micronic pore size. As mentioned previously, the difficulty here lies in finding a balance in porosity size: increased porosity in macro porous meshes allows for improved soft tissue ingrowth (which in turn allows for greater abdominal recovery) but there is a greater risk of adhesions, and a reduction in strength. Whereas with micro porous meshes, there are significantly less adhesions, however micro porous meshes require sutures for fixation and the piercing of a micro porous mesh will increase the risk of infection (Zogbi et al. 2010). Therefore, it is important to find an optimum porosity size, in which adhesions can be kept to a minimum, strength and flexibility are not greatly sacrificed, and soft tissue ingrowth can occur.

The porosity also links with the weight of a mesh – weight is always grouped into categories of lightweight and heavyweight. Generally, lightweight meshes have larger porosity, composed of thin filaments and are more elastic. Heavyweight meshes, on the other hand, have a small porosity size, are composed of thicker filaments and have a high degree of tensile strength. Therefore, both types of meshes have both advantages and disadvantages of equal proportion. The choice between a lightweight and a heavyweight mesh is multifactorial and superiority is yet to be proven (Bilsel & Abci 2012).

2.2 Drug Delivery Systems

A drug delivery system is a formulation or a device that enables the introduction of a therapeutic substance in the body and improves its efficacy and safety by controlling

the rate, time, and place of release of drugs in the body (Jain & Jain 2008). By this particular definition of a drug delivery system (DDS), it can be assumed that this covers a number of different and conventional DDS types such as oral, parenteral, or transdermal drug delivery. Outside of these three examples, there are number of methods that are used in conjunction with the type of disease or ailment being remedied. However, within these conventional methods of DDS there are two new main categories that are being researched and developing at an impressive rate: targeted drug delivery and sustained release formulations. New techniques of DDS are being developed primarily because the systemic route of drug administration is the mainstay of pharmacotherapy. However, it is limited because of their toxic side effects, degradation of drugs before reaching their target site, low permeability and poor patient compliance (Wu et al. 2009).

With a number of new drug delivery fabrication methods being researched, it is clear that DDS have a relevance and importance in the medical field. If a drug is being administered it should fundamentally target the desired area of treatment, at the highest efficacy possible and at an optimal rate. Yet this simple requirement for drug delivery is one that is seldom fulfilled – there are still a number of unwanted side effects associated with conventional DDS's due to some drugs reacting with various tissues and organs that are not intended for interaction with the drug. These unwanted reactions will naturally cause a decrease in efficacy of drugs and creates a major limitation in the design and manufacture of medicines for major illnesses, such as cancer or cardiovascular diseases (Tiwari et al. 2012).

Despite the major limitations of current medicines, there have been a number of breakthroughs and major advances in DDSs due to the development of modern fabrication techniques – the most widely used being electrospinning and 3D printing. This emergence of successful fabrication of DDSs is parallel with the development of new biocompatible materials for drug delivery which provides an alternative means of engineering release profiles by control of spatial distribution within a given polymer composition (Moulton & Wallace 2014). Biocompatible polymer research has become an important factor within DDS development, with a number of new and old polymers capable of being fabricated in a manner which suit the properties of particular drugs (e.g. drug solubility related to polymer porosity) and have also allowed for the ability to create limitless drug dosages (Sandler et al. 2011).

2.2.1 Fabrication Methods

With the relatively broad area of pharmaceuticals, and within that, the areas of drug implants, drug delivery systems and other various pharmaceutical delivery methods, the other end of this dramatic rise in technology regarding fabrication of DDSs is within the area of *tissue engineering*. Given the correlation between increasing world population and an increase in major diseases (i.e. diseases that directly affect the human body's organs), it is therefore vital to realize that there is inevitably a major shortage in available organs for transplant. So in order tackle this rapidly growing and potentially serious problem, there is now a bridge between using synthetic materials and the culture of live cells (cells that would be found in any particular organ of the human body).

With the fundamentals of tissue engineering, there are a number of different requirements that all must be effectively achieved in order to create a synthetic, working organ or tissue. Typically, in tissue engineering, a *scaffold*, such as a 3D artificial structure that must allow specific cultured cells to attach to it and allow easy growth and maintenance of these expanding and replicating cells. The scaffold material must also have a number of different desirable characteristics in order for the successful implementation and growth of potential cells on the structure. The material must be biodegradable (must be readily absorbable to the surrounding tissues once the cells have grown and covered the scaffold), have a high porosity and optimal pore size (this allows for nutrients to be transported across the material and cells), and the rate of degradation is also hugely important (the rate of scaffold degradation must be linked with the rate of cell growth. This allows the scaffold to provide adequate structure and support until the newly formed cells are plentiful in order to sustain their own 'natural' structure). Finally, the scaffold and cell cultures must be contained (and usually are) contained within a bioreactor, which allows for an ideal environment that adheres to the optimum growing conditions (growth factors).

2.2.1.1 Electrospinning

Electrospinning is a fabrication technique that has been widely researched within the scientific field, and in particular within the creation of DDSs. Electrospinning is immediately useful for the creation of scaffolds, given that the fibre formation can result in the creation of nanomaterials with a high surface area (Reneker & Fong 2006). The mechanism of electrospinning is illustrated in Figure 2.3 – the process fundamentally involves applying electric charges across a metallic needle that contains

a polymeric solution. When a droplet is formed at the tip of the needle, (the electric field causes a conical droplet called a Taylor cone), the induction of charges causes instability – however, there is also a repulsion of charge happening that will overcome the surface tension (of the polymeric solution). This then results in the solution accelerating in the direction of the electric field, towards a metallic collector (or target) (Shah et al. 2014; McKee et al. 2004; McManus et al. 2006; Deitzel et al. 2001).
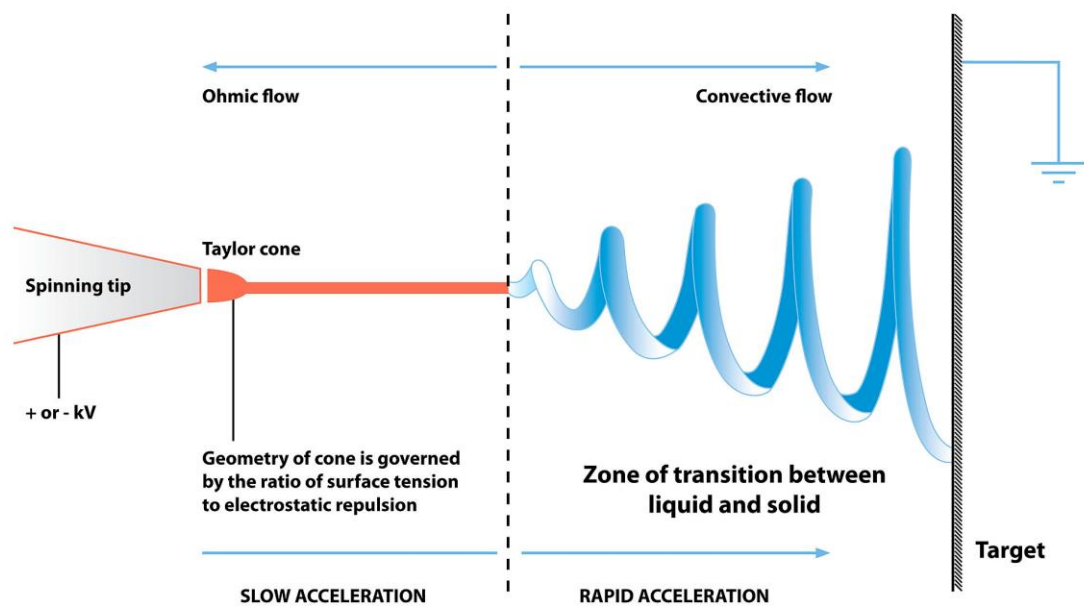
Figure 2.3 – Diagram detailing fibre formation via the process of electrospinning

There are a number of different parameters and factors that can affect the overall process of electrospinning, which typically means that in order to create 'optimal' nanofibres specific parameters must be optimised according to the type of polymeric solution being used. Some parameters include:

- **Voltage**: there is a *critical value* for voltages being applied to polymeric solutions. If the voltage is too low, the Taylor cone will drop and the polymeric

solution will not stretch. If the voltage is above the critical value, beading and 'spitting' of the solution will occur (Sill & von Recum 2008).

- **Flow rate**: the flow of the solution (how fast the polymeric solution moves through the needle) is typically controlled using a pump, and similarly to voltage, there is a *critical flow rate*. Increasing the flow rate beyond the critical value will cause beading of fibres. However, alterations (increased or decreased) close to the critical value are important in modifying the diameter of the fibres being created (Megelski et al. 2002).

- **Solution conductivity**: the conductivity of polymeric solutions will directly affect the formation of the Taylor cone, which in turn will affect the overall diameter of the fibres being produced. Typically, an increase in conductivity will cause a decrease in fibre diameter (Sun et al. 2014).

- **Needle – target distance**: a *critical distance* is another important parameter that affects the overall quality of electrospun fibres. Small distances between needle and target will usually result in large fibre diameters and beading (due to the lack of time for solvent to evaporate from needle to target), and larger distances will cause smaller fibre diameters but poor uptake of the fibres onto the target (Matabola & Moutloali 2013).

There are other various factors alongside the previously mentioned parameters (such as humidity, temperature, solvent choice etc.), however; it appears that the afore mentioned appear to the more crucial parameters to consider in order to successfully create a polymeric scaffold. Electrospinning offers a number of advantages that are ideal for the potential creation of hernia mesh, such as the ease and flexibility in which drugs can be encapsulated (provided they have a particular solubility with the solvent

used in the polymeric solution). Another advantage of electrospinning is the speed in which samples can be created – this is ideal for experimental work, which would allow for quick modification of polymer-drug formulations that will be suitable for the electrospinning process. Some of the major limitations of electrospinning include the use of toxic solvents to breakdown polymers and drugs – if the scaffolds produced are to be used in a surgical setting, it is vital that there is no presence of the solvent on the scaffold (Agarwal & Greiner 2011).

2.2.1.2 3D Printing

3D printing has become one of the most rapidly growing technologies since its inception in the late 1980s – initially described as a process for the manufacture of tooling and functional prototype parts directly from computer models (Sachs et al. 1990). It is technically known as a method of solid freeform fabrication (or rapid prototyping), and has been proven as a feasible method of improving drug delivery systems. With regards to drug delivery, there are currently two main areas that are being researched: targeted drug delivery in which the drug is only active in the target area of the body, and sustained release formulations in which the drug is released over a period of time in a controlled manner from a formulation (Moulton & Wallace 2014). Research in both types of drug delivery systems has advanced greatly due to the introduction and enhancement of 3D printing technologies and subsequent supporting materials. Development of biocompatible polymers (e.g. Polylactic acid, polycaprolactone) has allowed for various critical factors in drug delivery such as porosity, drug dispersion rate and tensile strength to be tailored specifically to suite both the drug type and disease being treated.

3D printing is a process that incorporates the use of computer aided design (CAD) software to create initial 3D designs and programming. The 3D printer then extrudes material from a nozzle onto a substrate, and a 2D foundation is created across the X and Y planes. Material is then deposited along the z-axis, and in some types of 3D printing (i.e. inkjet printing) a liquid binder is then applied across each layer of the object. This process is repeated until the desired 3D object is created (Maulvi et al. 2017).

Human tissue such as bone, vascular grafts and heart tissue have been engineered through the use of various new 3D printing techniques. Despite the relative success of 3D inkjet printing, there are a number of limitations associated with the method. For example, the overall process is one that takes a substantial amount of time, and the more layers of powder needed; the longer the process will take. Not all polymers can be fabricated at room temperature in powder form, which therefore excludes a number of polymers that can be used in this method. There may also be limitation in the time taken if a complex shape of object is required – given that the process incorporates repeating certain steps in order to apply different materials (e.g. powders). Therefore, it can be concluded that the current range of 3D printers may be suited to current drug implant/DDS fabrication given that the modern extruders used within the current 3D printing allows for variable extrusion temperatures, multiple material feeds (there is a possibility of extruding two different materials at once during the print), reduced print times (dependent on material and shape however) and the ability to input a CAD model file in order to print complex models and shapes.

2.2.2 Drug Delivery Applications

Currently, a number of different applications are being researched and tested. The type of drugs being experimented with range from levofloxacin (a type of antibiotic, typically used for treating urinary tract infection, respiratory tract infections, meningitis) (Cheow et al. 2010; Wu et al. 2009) to dexamethasone (a form of steroid, typically used as an anti-inflammatory or to counteract potential side effects in anti-tumour treatments) (Sivashankari & Prabaharan 2016; Chou et al. 2015). A number of DDSs are being developed using these types of drugs, specifically as drug implants. Drug implants are very useful DDSs because they can be implanted at the required tissue site, meaning any sustained released of the drug will be high in efficacy (it will achieve the desired therapeutic effect), low in toxicity and reduces the chance of unwanted reactions with irrelevant organs or tissue (Kaurav & Kapoor 2017).

One particular area of drug implants that has been widely cited is a multi-drug implant for the treatment of bone tuberculosis. The challenge faced in this particular application (i.e. multi-drug drug implant DDSs), is that with fabrication of these drug implants comes lack of control over the shape and internal architecture of the implants (Wu et al. 2009). Typically, having a lack of regulation of shape will result in either an irregular or monotonic mode drug release – which fundamentally lowers the efficacy of the drug implant in cases where the disease is severe. In this particular study, the multi-drug implant was created using a polymer of poly (DL-lactic acid) (PDLLA) which is known as a biocompatible polymer, isoniazid (INH) and rifampicin (RFP) which are common anti tuberculosis drugs, and were fabricated using a 3D printing process. The materials were fabricated by printing INH and RFP binder

solutions onto the selected areas of sequentially deposited layers of PDLLA powder in a specific sequence. The drug implant was physically printed as a cylinder design, and the porosity of the drug implant was then calculated. The implants were then tested both in vitro and in vivo and a distinct drug release pattern was observed in both methods – it was found that INH and RFP were released orderly in a certain sequence, as the drugs were ranged in the order of INH-RFP-INH-RFP from the periphery to the centre of the drug implant. It was also found that the levels of INH and RFP were lower in arterial blood than in comparison to bone levels – this may indicate that this drug implant has the ability to administer its loaded drugs without having to raise the serum level of the drugs. This is an important factor in demonstrating that 3D printing of DDSs and has the potential to have their loaded drugs released in an accurately controlled manner. However, within this study there is no comparison of various polymers across the drug implants; for example, testing INH and RFP with other biocompatible polymers such polyglycolide (PGA) or polylactic acid (PLA). A comparison of drug implants fabricated from different materials may allow for an optimum porosity size to be calculated, degradation time of the polymers could be analysed in order to determine which polymer is suitable during bone regeneration and even the optimum size (i.e. dimensions of the cylinder) of the drug implants could be determined dependent on the mechanical or thermal properties of the polymers being tested (for example, drug dissolution of INH and RFP may be dependent on the microstructures formed during the 3D printing – the drug/polymer mixture may crystallize under high extrusion temperatures).

Other types of drug implants have been also designed successfully, for example drug implants fabricated by electrospinning for the controlled delivery of levofloxacin

(LEVO), a broad-spectrum fluoroquinolone antibiotic against gram-positive, gram-negative and atypical bacteria (Huang et al. 2007). LEVO was encapsulated in composite mats of PCL and mesoporous silica – in this case, the encapsulation of LEVO was chosen in order to alter the release rate of the drug from burst to sustained release (Jalvandi et al. 2015). This change in behaviour was achieved by encapsulating the LEVO into the mesoporous silica nanoparticles, with the nanoparticles then being integrated into the core region of PCL through core-shell electrospinning. This study was successful in achieving incorporation, and also demonstrating the necessity to alter the release behaviour of LEVO.

Electrospinning has also been used to integrate a number of important drugs into polymers such as tetracycline (which utilised a blend of PLA and PCL 50/50, and demonstrated a sustained release behaviour compared to commercial wound dressings), cefoxitin (a PLGA scaffold that initially demonstrated a burst release behaviour, that was extended to week-long sustained released behaviour due to the use of amphiphilic block copolymer of PEG-b-PLA), ampicillin (using core-shell electrospinning to encapsulate the drug in poly(methyl methacrylate) (PMMA) that demonstrated sustained release behaviour), and triclosan (incorporating triclosan-cyclodextrin inclusion complexes into electrospun PLA that indicated a high antibacterial efficacy against *E. coli* and *S. aureus*) (Zahedi et al. 2012; Kim et al. 2004; Sohrabi et al. 2013; Kayaci et al. 2013). In particular, the use of triclosan within electrospun scaffolds appeared to demonstrate a high level of efficacy against the growth of certain bacteria (Del Valle et al. 2011). This drug may prove useful in the hernia repair context, if the drug can be released at a sustained rate it may be possible to contain infection at the site of mesh insertion.

A different study of drug delivery research, in which various drugs were loaded in different types of bioceramics, for example 3 different drugs of vancomycin (antibiotic for bacterial infections), ofloxacin (a fluroroquinolone antibiotic) and tetracycline (a broad spectrum polyketide antibiotic) were loaded into 3 different types of bioceramics (hydroxyapatite, brushite and monetite) (Gbureck et al. 2007). In this study, instead of the drug being loaded into a polymer either prior to 3D printing (through a mixture) or being loaded during the 3D printing process using a binder solution, 3 different bioceramics were printed using a 3D powder printing system to create physical models which were then subsequently immersed in different drug solutions. This approach was used to observe whether drug loaded could be achieved through adsorption through various (and possibly ideal) porosities, surface area and pore size distribution of the 3D printed bioceramics used.

2.3 Polymers Used in Tissue Engineering

2.3.1 Polylactic Acid

One of the most commonly used and researched materials across drug delivery appears to be polylactic acid and other variations of this (e.g. poly-DL-lactide (PDLLA)). This type of polymer is widely considered as a biopolymer and its high level of biocompatibility and has allowed this polymer to be used in a number of different industrial applications. Biopolymers are produced from natural resources and crude oil; and in the case of PLA, it is produced by chemical synthesis from bio-derived monomers such as polylactic acid (Jamshidian et al. 2010). Lactic acid (2-hydroxy propionic acid), the monomer backbone of PLA, is produced via fermentation or chemical synthesis, and the resulting polymers have a variable molecular weight. PLA

is an ideal polymer for use within forming drug implants/tablets since it can be prepared using a number of different manufacturing methods such as electrospinning injection moulding, blow moulding, thermoforming and extrusion (Lee et al. 2016). In particular, extrusion of PLA works satisfactorily given that it is one of the finest ways to form and melt particular thermoplastic materials – normally a twin extruder would be ideal given that the thermal energy produced by the process is enough to melt the PLA pellets (melt temperature of between 200°C – 220°C).
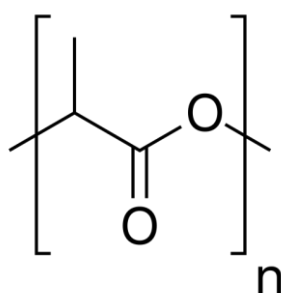
Figure 2.4 – Chemical structure of polylactic acid

PLA has a number of different mechanical, thermal and physical properties that makes it an ideal candidate for use within the area of drug delivery systems. PLA generally shows a good tensile strength with higher values than polystyrene (PS) materials which is lower than polyethylene terephthalate (PET) materials (PLA tensile strength = 48 to 53 MPa, PS tensile strength = 34 to 50 MPa and PET tensile strength = 48 to 72 MPa) (Signori et al. 2009). The tensile strength is important for DDSs in order for the drug-loaded scaffold to retain is structural integrity and is a suitably malleable. With regards to the glass transition temperatures of PLA, are cited between 40°C and 70°C, which seems an ideal temperature range given that the drugs or drug implants will not be within an environment in which it will exposed to high temperatures. Similarly, PLA

has a melting temperature of between 200°C and 220°C, which again means that for use within the human body, the melting point will not be reached meaning its properties will not potentially change. PLA currently has clinical use in a range of applications such as sutures, rods for fracture fixation and intestinal slings (Athanasiou et al. 1996). Overall, the use of PLA has a number of various advantages, including its safety, biocompatibility, mechanical and thermal properties (Ramot et al. 2016).

2.3.2 Polycaprolactone

Polycaprolactone is a member of the biodegradable aliphatic polyesters family, and has been widely used in a range of clinical and research applications. PCL is produced through the ring opening polymerisation of ε-caprolactone (a cyclic monomer) (Woodruff & Hutmacher 2010). PCL a number of advantageous characteristics; it is low-cost, it has a low melting point of approximately 60°C (which is useful for processing materials in melt form), and has good solubility against common solvents (Nair & Laurencin 2007). The molecular weight of PCL can vary from 3,000 to 80,000 g/mol, with increasing molecular weight typically resulting in a decrease in crystallinity (Hayashi 1994). Given that PCL already has FDA approval, it is an ideal choice for experimental use with a route into clinical applications.
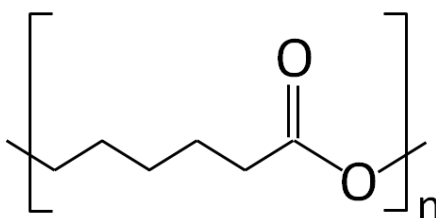
Figure 2.5 – Chemical structure of polycaprolactone

PCL has a particularly advantageous characteristic, whereby it has a biodegradation rate that is longer compared to PLA (PCL degrades hydrolytically over 2 – 3 years); however, this may be useful within a long-term surgical implant context if PCL can retain its tensile strength during the duration of any drug-elution phase (assuming that the implant is drug-loaded). PCL has a tensile strength of approximately 23 MPa, but has a high elongation breakage at beyond 700% (Gunatillake et al. 2006). PCL falls into the *biocompatible polymers* category, and this is due to its responses in relation to cytotoxicity, immunological and carcinogenic measures. There have been studies indicating that PCL has been used successfully within animal models, with no necrosis of cells observed, implying that PCL has successful biocompatibility with certain animal tissue (Menei et al. 1994; Jackson et al. 2002).

PCL has been used in medical applications such as sutures, however typically PCL is used in combination with other polymers to achieve modify the stiffness of the sutures e.g. PCL-glycolide (Middleton & Tipton 2000). Wound dressings are another major application for PCL given the relatively slow rate of degradation, and has been used in wound dressings for cutaneous wounds, sub-dermal implants and ureteral inserts (Ng et al. 2007; Cha & Pitt 1988; Jones et al. 2002). PCL has also been used within tissue engineering contexts; in particular, a number of studies have used PCL as scaffolds for creating bone tissue – aligned fibres of PCL have been used as a substrate for human skeletal muscle cells, with the fibres inducing efficient and proliferative cell growth along fibres (Choi et al. 2008; Thomas et al. 2006).

2.3.3 Natural Polymers

A number of *natural* polymers are widely used in research and medical contexts, and they are often used in combination with synthetic polymers – this allows for a balance between increased strength and durability (from synthetic polymers) with flexibility and increased biocompatibility (from natural polymers). Typical natural polymers can also be referred to as polypeptides – the most common one being *collagen*. Collagen is a structural protein that is a major component within various tissues in the human body (and animals). There are many different types of collagen that range from type I to X – with type I being the most abundant (Hayashi 1994).

The use of collagen within tissue engineering is highly advantageous for a number of reasons: firstly, collagen provides various binding sites in order for cells to attach to – this means where a synthetic polymer has poor cell affinity, the addition of collagen will circumvent this issue (Ospina-Orejarena et al. 2016). Type I collagen has an interesting structure, whereby a 'strand' of collagen is made up of smaller *fibrils* – these collagen fibrils (also commonly termed as collagen fibres) are 50 – 70 nm in diameter and are a densely packed collagen strand. Collagen fibres exhibit high tensile strength, and can be stretched without being broken (Lodish et al. 2000).

Despite the numerous advantages of collagen use within scaffold creation, it should be noted that it is an expensive material – extracting collagen (from human or animal) that is suitable for research purposes cannot be acquired in large quantities (Lee et al. 2008). Another major disadvantage is that there is significant difficulty in breaking down collagen without denaturing the proteins. This creates in issue when using collagen in relation to the development of electrospinning solutions. Hexfluoro-2-

propanol (HFP) is a solvent that is commonly used to break down collagen without denaturation, however it is highly toxic, expensive and has a low boiling point (which may yield unstable fibres during the electrospinning process) (Leszczak et al. 2014). Cross-linking collagen also may yield a number of problems, by decreasing biodegradability, reducing flexibility and increasing the toxicity (through presence of residual cross-linking agent on collagen material) (Charulatha & Rajaram 2003).

Other natural polymers commonly used in scaffold creation include *gelatin* – a collagen-based product, derived through the hydrolysis of collagen fibres (Djagny et al. 2001). In a similar fashion to collagen, it exhibits high mechanical strength, and is biocompatible. Gelatin has been widely incorporated within electrospinning practices, primarily through water-based formulations (gelatin is water-soluble) however it can also be used with acid and binary solvent systems (Topuz & Uyar 2017). One significant disadvantage of gelatin is the high rate of mass loss from fibres, typically caused through renaturation when a gelatin-polymer scaffold is exposed to water environments (Dulnik et al. 2016). *Elastin* is another natural polymer that can be used within tissue engineering contexts. Elastin is a highly elastic protein that is typically formed alongside collagen – it is approximately 1000 times more flexible than collagen, and therefore elastin provides the necessary elasticity to tissue (Buttafoco et al. 2006). Elastin has been used within electrospinning contexts, however is it not typically electrospun without combination to other synthetic or natural polymers. Elastin composites include PCL-collagen-elastin, elastin-PLGA and collagen-elastin hydrogels (Aguirre-Chagala et al. 2017; Foraida et al. 2017; Dunphy et al. 2014).

2.4 Analytical Techniques

2.4.1 Mechanical Analysis

There are various mechanical analyses that can be performed in order to successfully determine various aspects of both polymeric solutions and polymeric samples. Firstly, *rheological* measurements are important in assessing various mechanical aspects of a polymeric solution, such as the viscosity and viscoelasticity. Rheology is the study of the flow of a liquid, and the basic law describes the behaviour of an ideal liquid:

$$\tau = \eta \cdot \dot{\gamma}$$

Shear Stress = Viscosity · Shear Rate

Flow is typically measured between two flat, parallel plates – this creates *laminar flow*, and any displacement or disruption in the liquid will be measured (Schramm 2016). The outputs from rheological measurements result in values corresponding to elastic modulus (storage modulus), viscous modulus (loss modulus), and shear viscosity. Rheology is very useful in detecting in changes in laminar flow, due to the presence of drug, or any other added materials to the polymeric solution. Any changes to the polymeric solution will be indicative of how it will behave during the electrospinning process.

In order to measure the *mechanical strength* of the fabricated samples, *tensile testing* is the optimal method to determine this. This is a test where a material, or in particular a mesh, is subjected to elongation (through an applied force) until failure. Elongation of the material is used to calculate the *strain*, which is defined by:

$$\varepsilon = \frac{\Delta L}{L_0} = \frac{L - L_0}{L_0}$$

ΔL is defined as the *change* in length of material, L is the *final* length, and L_0 is the *original* length. Due the applied force, *stress* can be calculated as followed:

$$\sigma = \frac{F_n}{A}$$

During the measurements, the applied force is changed (typically increased); therefore stress (σ) is calculated as applied force (F_n) value over the cross-sectional area (A) of the material. As the force is changed, the final output results in a *stress-strain curve*. A stress-strain curve is a graph that will indicate important mechanical aspects of the material under tension: Young's modulus, elastic limit, ultimate tensile strength, and breakage point.

2.4.2 Solid State Characterisation

Solid-state characterisation is useful in determining physical aspects of polymer-drug materials – this is especially important in determining whether a drug is in a crystal or amorphous state (especially if embedded in a polymer), as either solid form may display varying chemical and physical properties (Bugay 2001). The use of *differential scanning calorimetry* (DSC), a thermal analysis technique, is one approach that determines potential interactions between polymer-drug and which solid-state the polymer or drug exists within. DSC works by examining the heat capacity of a material during controlled heating and cooling and various transitions can be observed through resulting data. Results are typically displayed as a heat flow versus temperature (or time) thermogram – endothermic (positive) and exothermic (negative) reactions are

identified through the direction of peaks on a graph, with other various transitions easily identified such as glass transition (T_g), crystallisation temperature (T_c), and melting temperature (T_m). Material states can also be identified through peak observation with sharp peaks representing crystalline structures, and broad peaks representing amorphous structures.

Another important analytical technique for understanding the physical form of polymer-drug materials is *x-ray powder diffraction* (XRPD). This technique utilises the use of x-rays (short wave), whereby the secondary x-ray beams are scattered once they interact with atom within the polymeric sample – bright spots are produced at various angles, and the spacing of the diffraction can be determined using these angles (Bragg's law):

$$n\lambda = 2d \sin \theta$$

n = order of reflection; λ = wavelength; d = interplaner spacing causing diffraction;

θ = diffraction angle

A diffraction pattern will result, which typically represents crystalline structures (sharp peaks) and amorphous structures (broad peaks). The values obtained relating to crystallinity of a material should be comparable to those found in DSC results.

2.4.3 Spectroscopy

If particular drugs are to be integrated with polymers to create a drug-loaded material, it is important to determine whether the drug has been integrated fully into the polymeric matrix. In particular, there are cases where drug molecules simply do not embed within a polymer, and may be found at the surface of the material – this may

not suitable for those looking to achieve a particular drug release rate (i.e. sustained release behaviour). Using *infrared spectroscopy* (IR) is a quick and relatively simple approach in identifying any potential drug on the surface of a material. IR works through the absorbance of infrared frequencies in various organic compounds, measured as percentage transmittance. IR can be used to identify different functional groups (bond stretching, bending) that may be present within particular polymers or drugs – therefore if the functional groups of drug can be identified, it may be possible to observe these functional groups in drug-loaded materials (especially if there is a large amount of drug at the surface of the material).

IR spectroscopy may be useful for indicative results relating to drug embedding, however the use of *time-of-flight secondary ion mass spectrometry* (ToF-SIMS) is a technique that will yield highly accurate results concerning drug placement within a polymer. ToF-SIMS involves the use of an ion beam exciting the surface of a material – this causes secondary ions to release from the surface. The exact mass of these ions are determined using a time-of-flight analyser, and subsequent SIMS peaks will help identify what element or molecule is being observed. This technique can be used in conjunction with ion sputtering which will provide information of *depth distribution*. This depth distribution will allow for 3D analysis of the material, and a nano-level analysis of exactly where drug molecules are distributed within a polymeric matrix.

2.4.4 Imaging

Electrospinning yields either nano or micro fibres, therefore imaging these fibres at a high resolution will determine whether the fabrication process has been successful in creating useful fibres. *Scanning electron microscopy* is a widely used imaging

technique that produces images using an electron beam – the detection of secondary electrons (emitted from the sample) provides information about the surface topography. For materials (such as most polymers) that have a low conductivity, it is important to sputter coat the sample using a conductive material, typically gold or platinum.

SEM will allow for a clear picture of the surface; however, there may be limitations with certain types of equipment that will not image at a nano-scale. *Atomic force microscopy* (AFM) is a technique that has the potential to image at a nano-scale, at a high resolution. AFM is a form of scanning probe microscopy that uses a mechanical probe to touch the surface of the material (either tapping, contact or non-contact mode). AFM images can be produced through a *tapping mode* – tapping mode is where the cantilever oscillates at its resonant frequency (via piezoelectric elements), with an image being formed from the recurrent contact made between the cantilever tip and the material surface (Geisse 2009). Tapping mode is useful for imaging polymers, as the mode causes less damage to the material surface than using contact mode; therefore it may be a useful technique in imaging any samples that have a small thickness, or susceptible to damage.

2.4.5 Biological Studies

Examining the biological relevance of materials is important, especially if there is a need for clinical relevance. There are a vast number of different studies that are available that vary in complexity; however, for the purposes of this project there should be a focus on two main aspects that includes *antibacterial relevance* and *cell interaction*. Given that one of the main issues with hernia repair is related to chronic

infection, understanding the antibacterial efficacy of materials will be incremental in determining whether these materials are suitable for potential clinical use. One method of testing antimicrobial responses is through an *agar diffusion method.* This is a commonly practiced procedure, where agar plates are inoculated with the inoculum of the desired test bacteria. Material (usually a disc shape) is placed in the centre of the agar surface and the Petri dishes are subsequently incubated. If the material has antimicrobial qualities, then zones of inhibition (of the bacteria) will be observed in the agar plate. This method is simple, low in cost, has been standardised and is a useful indicator to determine the antibacterial efficacy of materials (Balouiri et al. 2016).

The main methods of testing cellular response against materials (such as scaffolds) are through *cell adhesion, cell proliferation* and *cell viability* studies. Cell adhesion assays involve examining whether specific cells will attach to a substrate, in this case an electrospun polymeric scaffold. This process involves seeding cells directly onto the scaffold surface, and detecting attached cells using either colorimetric or fluorometric detection/imaging. Cell adhesion assays are useful in indicating whether particular scaffolds demonstrate an affinity for cell attachment, which may determine suitability for further development. If a cell adhesion assay reveals a high level of cell attachment, it is imperative to examine the proliferation of cells on the scaffold over a particular time period. This can be monitored through fluorescent imaging of the scaffolds at designated time points (e.g. 3, 7 and 14 days), via fluorescent staining of the proliferative cell culture on the scaffold (e.g. propidium iodide staining). Cell proliferation can be quantified through cell count software analysis (ImageJ).

Cell viability techniques can be used to show what dosages of drug used in electrospun scaffolds are potentially harmful to cell growth. The most common (and fastest) method of testing viability is through a *resazurin assay*; this assay indicates viable cells, as active cells will metabolically reduce resazurin (blue in colour) into resorufin (fluorescent pink). Fluorescence can be quantified using a microplate fluorimeter (at 560 nm excitation and 590 nm emission). Other techniques, such as a bromodeoxyuridine (BrdU) assay can be used to measure the cell proliferation against varying drug concentrations. BrdU assays involve incorporating BrdU into the DNA of replicating cells and then using BrdU antibodies to detect presence of the chemical.

2.5 Aims & Objectives

The aims and objectives for this project are:

- **To create a drug-loaded mesh that would help reduce chronic infection in hernia mesh repair**;
  - o Electrospinning will be used to create a mesh that integrates antibiotics and polymer. Physicochemical characterisation will determine whether the meshes created are suitable for further development.

- **To integrate natural polymer into the mesh in order to increase the biocompatibility of the fabricated mesh**;
  - o Integration of type I collagen may increase the biocompatibility, and potentially alter characteristics of the fabricated mesh. Any changes will be measured using imaging techniques and physicochemical characterisation.

- **To determine whether the fabricated meshes have an ideal biological response**;
  - o Biological studies (such as antibacterial studies, cell proliferation and viability assays) will be used to determine whether there is an optimal biological response. These results should help understand whether the meshes have potential use in a clinical environment.

Chapter 3: Electrospinning Synthetic Polymers

3.1 Introduction

Given the imperative need to change polymeric materials for hernia mesh repair, as outlined in the previous literature review Chapter, the two main polymers identified for experimental use are polycaprolactone and polylactic acid. The integration of anti-bacterial drugs with these polymers has become a necessity given the high risk of chronic infection (and other associated side effects such as inflammation) associated with the implementation of hernia meshes. There are a number of primary goals for the research of drug delivery devices (De Jong & Borm 2008):

- Specific drug targeting and delivery,

- Reduction in toxicity whilst maintaining therapeutic effects,

- Greater biocompatibility.

In order to successfully create a drug delivery device that can be suitable for hernia repair, a suitable fabrication method must be chosen. Fabrication methods for incorporating biomaterials and drug encapsulation in novel mesh matrices, such as hot-melt extrusion (Li et al. 2013), electrospinning (Toncheva et al. 2011), 3D printing (Holländer et al. 2016) and high-speed rotary spinning (Sebe et al. 2013) have been widely researched. In particular, electrospinning is the most popular and preferred technique for nanofiber fabrication due to its simplicity, cost-effectiveness, flexibility, and ability to spin a broad range of polymers (Zamani et al. 2013). The method allows for the simple and direct functionalization of fibres with drug compounds and is compatible with solvents such as chloroform and dimethyl sulfoxide. In addition, the

process of electrospinning with the use of solvents such as chloroform, dimethyl sulfoxide etc., allows functionalisation of the scaffolds through the inclusion of drugs in the polymer-solvent solution without the need for a complicated preparation process (M. He et al. 2015). Electrospinning has previously been applied to the fabrication of triclosan/cyclodextrin inclusion complexes (Celebioglu et al. 2014), the construction of scaffolds with perlecan domain IV peptides (Hartman et al. 2011), manufacture of biocatalytic protein membranes (Kabay et al. 2016), and encapsulation of levofloxacin in mesoporous silica nanoparticles (Jalvandi et al. 2015). Electrospinning produces scaffolds containing micro-fibres and this is an advantageous feature not observed in braided mesh commercial devices – these microfibers also introduce mechanical anisotropy and provide topographic features to guide cell alignment (Goldstein & Thayer 2016). However, electrospun fibres typically incorporate the use of organic solvents and for applications such as hernia repair or tissue engineering, the toxicity of organic solvents used could be highly critical – avoiding organic solvents is of outmost importance for applications in medicine and pharmacy (Agarwal & Greiner 2011; Bubel et al. 2014).

The purpose of this Chapter is to examine the physicochemical properties, bacteria response, and drug loading of electrospun scaffolds. The polymers chosen for this study is *polycaprolactone* (PCL); a biodegradable polyester commonly used in biomedical applications for controlled release and targeted drug delivery (Bhavsar & Amiji 2008). PCL, a biodegradable aliphatic polyester (Azimi et al. 2014), is an obvious candidate for drug delivery systems due to its high biocompatibility and ease of degradation in the human body (Bikiaris et al. 2007). Drug loading of structures that mechanically resemble interfacial tissue and which allows short or long-term

release of suitable bioactives may be utilisable in hernia-repair meshes. The matrix was loaded and electrospun with two drugs, *irgasan* (an antibacterial agent used commonly in soaps, detergents and surgical cleaning agents) or *levofloxacin* (a broad-spectrum antibiotic used commonly to treat gastrointestinal infections). These two drugs were used to their relevance within clinical environments (IRG is commonly incorporated on the surfaces of medical devices, and LEVO is commonly used to treat intra-abdominal infections in conjunction with other antibiotics such as ciprofloxacin). The mechanical characteristics, morphology, surface hydrophobicity, drug efficacy and chemical distribution were characterised with an array of analytical techniques. The results from the studies described in this Chapter should help to understand the electrospinning process of scaffolds and polymer-drug interactions within the scaffolds.

3.2 Materials & Methods

3.2.1 Materials

PCL with a mean molecular weight of 80 kD, PLA with a mixed molecular weight, IRG (variation of Triclosan, >97%), LEVO (>98%), and all the solvents used for the electrospinning were obtained from Sigma Aldrich. The solvents consisting of chloroform (anhydrous, containing amylenes as stabilizers, >99%) and N,N-dimethylformamide (DMF, anhydrous 99.8%).

3.2.2 Preparation of Synthetic Polymer Solutions

Initially, concentrations ranging from 8 – 12% were tested initially in order to determine what concentration was suitable for the electrospinning apparatus. Different

solutions with a polymer concentration of 12% and 8% (w/w) were prepared to be used within the electrospinning method – this particular concentration was used due to its possessed suture retention and tensile strengths appropriate for hernia repair, as specified for similar electrospun scaffolds described by Ebersole and colleagues (Ebersole et al. 2012). Various PCL and PLA formulations were constructed of a total weight of 25 g per solution, which allowed for PCL (12% w/w), PLA (8% w/w) and a 9:1 (w/w) ratio of chloroform (CLF) to N,N-dimethylformamide (DMF). These solvents were used due to their ideal solubility characteristics related to both IRG and LEVO. For the unloaded polymer solution, 3 g of polymer was dissolved in 22 g of CLF: DMF (9:1) which was initially mixed through 30 min in a centrifuge, a further 30 min in a sonicator (Elma S30 Elmasonic®) and a final 1 h with a magnetic stirrer. This process was vital to ensure that the solution was fully homogeneous. The solution was left overnight, and a further 30 min of sonication applied the following morning in order to confirm the homogeneity of the solution. For the irgasan-loaded solutions, the same method was applied, except the solution contained 1% (w/w) irgasan. This concentration was used in order to obtain an accurate measurement during UV analysis. The concentration of the levofloxacin-loaded solutions was 0.5% (w/w), providing sufficient sensitivity in the release cell for accurate UV analysis. All the preparations turned to clear solutions. These observations were interpreted to determine that the solutions had successfully homogenised. The solutions were then subsequently used in the electrospinning process and for rheological analysis.

3.2.3 Electrospinning of Polymer Solutions

The polymer test specimens were fabricated for each polymeric solution, using a custom in-house electrospinning apparatus, which consisted of a syringe pump (Harvard Apparatus PHD 2000 infusion, US) and two 30kV high-voltage power supplies (Alpha III series, Brandenburg, UK). The polymer solution was loaded into glass syringe and fed through tubing with a metal needle tip attached at the end. The needle was clamped into place, to allow a high-voltage supply to run through it, which allowed an electric field to be created between the needle and the target plate. The syringe was clamped to a pump, which determined the specific injection flow rate of the polymeric solutions. For each of the three solutions (e.g. unloaded, irgasan-loaded, and levofloxacin-loaded), 3 varying flow rates of 0.5, 1 and 1.5 ml h^{-1} were applied across varying voltages of 2 kV – 5 kV (needle) and 10 kV – 18 kV (target plate) (Hall Barrientos et al. 2016). The variation in flow rate and applied voltages was to correct any problems that occurred during fabrication, i.e. 'spitting' of solution at the target plate, or any potential beading (which was examined through SEM). The fabrication of this solution was electrospun onto the target that was covered with aluminium foil, in order for the final material to be removed and used for further characterisation. The final yield of electrospun polymers resulted in thin, flexible sheets of material.

3.2.4 Rheological Studies

A Thermo Scientific HAAKE MARS II® rheometer with a P35 TiL cone and plate was used to measure the rheological and mechanical behaviour of the different unloaded and loaded polymeric solutions. The objective of this experiment was to examine the viscoelastic properties of the PCL and PLA solutions, specifically to determine

whether the irgasan or levofloxacin is having an effect on the mechanical properties of the polymer. The method used was taken and modified from the rheological study undertaken by Bubel et al. 2014. In brief, an oscillating amplitude sweep between 0.1 Pa – 1000 Pa at a frequency of 1 Hz was used to determine the linear viscoelastic region (LVER) of the samples. Once the LVER is determined from the amplitude sweep, a downwards oscillating frequency sweep from 10 Hz – 0.1 Hz with a shear stress (Pa) within the LVER was then used in order to help understand the nature of the solutions concerning strength and stability. The experiments were repeated 4 times per solution, and for each experiment, each data point (20 data points per method) was optimised to repeat each measurement 5 times.

3.2.5 SEM

The morphology and diameter of individual fibres spun from PCL solution were determined from scanning electron micrographs of each sample (TM-1000®, Hitachi, UK, Ltd.). The samples were mounted on an aluminium plate with conductive tape. Images of fibres were taken at various locations of each electrospun PCL scaffold in order to determine the overall uniformity of fibres. Prior to imaging, the samples were sputter coated with gold for 30 s using a Leica EM ACE200® vacuum coater, the process being repeated four times in order to increase the conductivity of the samples. The samples were imaged in secondary electron mode at 5 kV.

3.2.6 AFM

Further morphological analysis was undertaken through atomic force microscopy. A Multimode 8 microscope (Bruker, USA), with Scanasyst-Air® probes (Bruker, USA)

was used in Peak Force Quantitative Nano Mechanics (QNM) mode, as described by Lamprou et al. 2013. The imaging of the fibres was performed under ambient conditions, with a silicon cantilever probe. The tip radius of the probe and the spring constant were calculated to be in the regions of 0.964 nm (18° tip half angle) and 0.4935 N/m, respectively. The scan sizes ranged from 200 nm to 25 µm, at a scan rate of 0.977 Hz with 256-sample resolution. The Roughness Average (Ra) values were determined by entering surface scanning data, and digital levelling algorithm values were determined using Nanoscope Analysis software V1.40® (Bruker USA). AFM images were collected from two different samples and at random spot surface sampling.

3.2.7 DSC

Differential scanning calorimetry (DSC) was carried out using a Mettler Toledo DSC822 in order to examine the thermal properties of the electrospun PLA scaffolds. Firstly, the scaffolds were cut, weighed and placed in the DSC specific aluminium discs. The disc was then sealed using a press and subsequently placed in the DSC instrument. The parameters for DSC analysis were set (parameters are detailed below) via the computer software. The analysis was then run which took approximately 20 min. The method included heating from 25 ℃ to 220 ℃ at 10 ℃ steps, using standard 40 µl aluminium discs, and each sample consisted of 4 mg.

3.2.8 XRPD

XRPD was performed in a Bruker D2 Phaser machine and measurements were taken under CuKα radiation (λ= 1.5406 Å), 40 kV and 30 mA as X-ray source with K_b (Ni) filter. Diffraction patterns were collected with 2θ ranging from 3° to 70°.

3.2.9 CAG

To monitor changes in wettability of the scaffolds, sessile drop contact angle for distilled water was measured by contact angle goniometry, using a contact angle goniometer (Kruss G30, Germany) as described by Lamprou et al. 2010.

3.2.10 *In-Vitro* Drug Release Studies

The drug releases of the irgasan/levofloxacin loaded polymeric scaffolds were measured in order to determine the release profile of the drugs. For the irgasan loaded electrospun scaffolds, a buffer solution consisting of phosphate buffer solution (PBS, pH 7.4) was mixed with 0.5% sodium dodecyl sulphate (SDS, a surfactant was used due to the hydrophobic nature of irgasan). SDS was used after initial trials of dissolution determined that IRG release could not be detected without the use of surfactant. 8 ml of this solution was placed in a vial and the polymer-irgasan scaffolds were cut, weighed, and subsequently placed in the vial of PBS/SDS. A similar method was adopted for the PCL-levofloxacin scaffold, except PBS was used (Duan et al. 2013).

Calibration curves were created for both irgasan and levofloxacin using a UV spectrophotometer, in order to help determine the relative concentration (mg ml^{-1})

found eluted in the buffer solutions. The UV absorbance of both drugs was measured: irgasan at 280 nm (Piccoli et al. 2002), and levofloxacin at 292 nm (Maleque et al. 2012) respectively. Measurements were taken at intervals at 15 min, 30 min, 1 h, 2 h, 4 h, 8 h, 24 hrs and every day after the 24 h mark for up to 7 days at 37 ºC. At each point, 4 ml of solution was taken from the vial and replaced with fresh in order to satisfy the perfect-sink conditions and keeping the volume of the solution constant.

3.2.11 ToF-SIMS

ToF-SIMS data was acquired using a ToF-SIMS V mass spectrometer (ION-TOF GmbH, Münster, Germany) based at the Wolfson Foundation Pharmaceutical Surfaces Laboratory at the University of Strathclyde. The instrument is equipped with a bismuth liquid metal ion gun (LMIG), an argon gas cluster ion beam (GCIB) and a gridless reflectron time-of-flight mass analyser.

Three different acquisition modes, detailed below, were used to analyse the fibres: high mass resolution spectroscopy, depth profiling, high lateral resolution imaging. Owing to the insulative nature of the materials, a low-energy electron beam (21 V) was used to compensate for charging.

3.2.11.1 High Mass Resolution Spectroscopy

For an optimal mass resolution, the primary ion beam (Bi3+ primary ions) was pulsed at 10 kHz frequency with a pulse width of 17.0 ns. The primary ion gun energy was set at 30 kV and the pulsed target current was approximately 0.63 pA. Data was collected both in the positive and in the negative secondary ion polarities, in three replicates; each acquisition was made from different areas of the samples used in this

study. The analysed area and the acquisition time, for each repetition, were respectively 100 μm × 100 μm and 120 seconds, delivering a primary ion dose density (PIDD) of approximately 4.6×1012 (primary ions/cm^2). Reference spectra for pure levofloxacin and irgasan compounds were acquired in positive and negative ion mode from 0 to 400 Da.

3.2.11.2 High Lateral Resolution Imaging

The LMIG was operated using the imaging mode, with high lateral resolution, and Bi3^{++} was selected as primary ion beam. The primary ion gun energy was 30 kV and the pulsed target current was approximately 0.048 pA. High lateral resolution ion images were collected over a surface area of 100 μm × 100 μm, using a pulsed analysis beam (pulse width = 100 ns). The resolution was 256×256 pixels per image (pixel width was circa 0.4 μm). Each image was obtained with a final ion dose of 6.5×1012 primary ions/cm^2 or less. The dose was kept below the static limit of 1013 primary ions/cm^2 to minimize surface damages during the analysis. The images were processed with the ION-TOF SurfaceLab 6.6 software (Münster, Germany).

3.2.11.3 3D Imaging

The LMIG and the GCIB were employed in a dual-beam configuration to collect the depth profile and the 3D image data. The LMIG was operated in pulsed mode to investigate the lateral distribution of chemical species, while the Argon source was operated in DC mode to remove multiple layers of material from the sample surface between the analytical cycles. For the depth profiling analysis, the dual beam experiment used a 30 kV Bi3^{++} primary ion beam for analysis and a 10 kV Ar1500$^+$

beam for sputtering. The pulsed current of the Bi_3^+ primary ion beam was 0.048 pA and the DC current of the cluster $Ar1500^+$ was 10.22 nA, with a 500 seconds analysis time and 4 seconds sputtering time. The raster areas of the pulsed analysis beams and the DC sputter were 100 μm × 100 μm and 300 μm × 300 μm, respectively. The resolution was 256 × 256 pixels per image (pixel width of about 0.4 μm). Data was collected in the negative secondary ion mode. In the course of each acquisition, mass spectral information at each image pixel was collected in the m/z range of 0-917 m/z.

3.2.12 Statistical Analysis

All experiments were performed in triplicate with calculation of means and standard deviations. Two-way analysis of variance (ANOVA) was used for multiple comparisons along with Tukey's multiple comparing tests, followed by T-test to access statistical significance for paired comparisons. Significance was acknowledged for p values lower than 0.05.

3.3 Results

3.3.1 Rheological Studies

PCL

The results for various PCL solutions (PCL, PCL-IRG and PCL-LEVO) are shown in Figure 3.1. For PCL-unloaded solutions, it can be clearly seen across the three graphs (elastic modulus (A), viscous modulus (B), and shear viscosity (C)) that the solution exhibit a similar behaviour; the curve peaks at approximately ~100 Pa before degradation of the solution occurs. The viscous modulus value peaks at ~75 Pa, which is significantly greater than the elastic modulus peak value (~ 5.5 Pa). The addition of

both IRG and LEVO increased the LVER for both solutions – no decrease in G' or G''
can be observed until ~ 500 Pa in each case. The viscous modulus for PCL-IRG is
shown at below 50 Pa and PCL-LEVO at below 40 Pa. PCL-LEVO samples exhibited
the lowest values for both viscous modulus and shear viscosity results (shear viscosity
= under 6000 Pa.s).

Figure 3.2 shows the frequency sweep data for the various PCL formulations. For all
solutions, the viscous modulus values were greater than the elastic modulus with no
crossover point between the 0.1 – 10 Hz ranges. PCL-unloaded exhibited the lowest
G' value of ~ 10 Pa at 10 Hz, PCL-IRG of ~ 15 Pa at 10 Hz, and PCL-LEVO at the
highest value of ~ 30 Pa at 10 Hz.
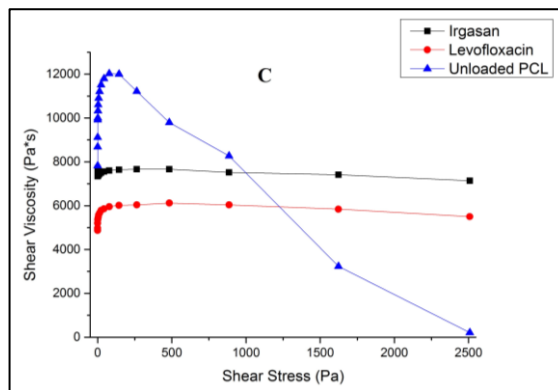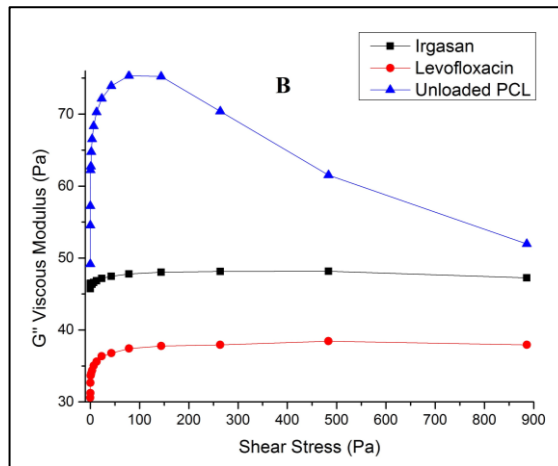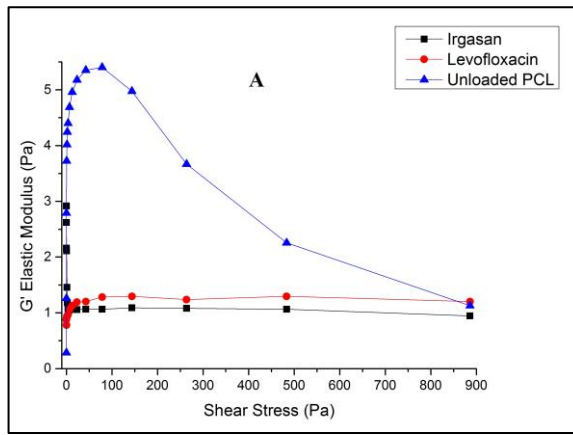
Figure 3.1 – Amplitude sweep data for PCL, PCL-IRG and PCL-LEVO. (a) Elastic modulus (b) Viscous modulus (c) Shear viscosity
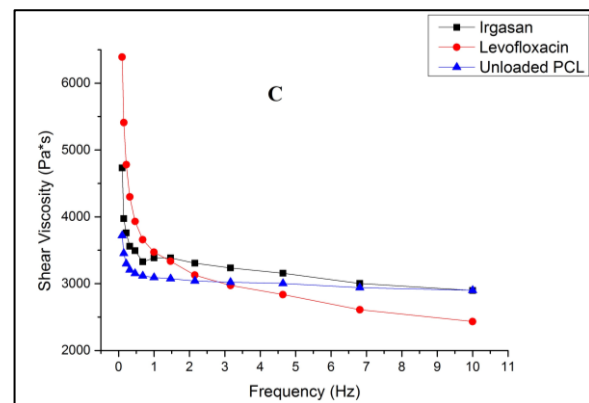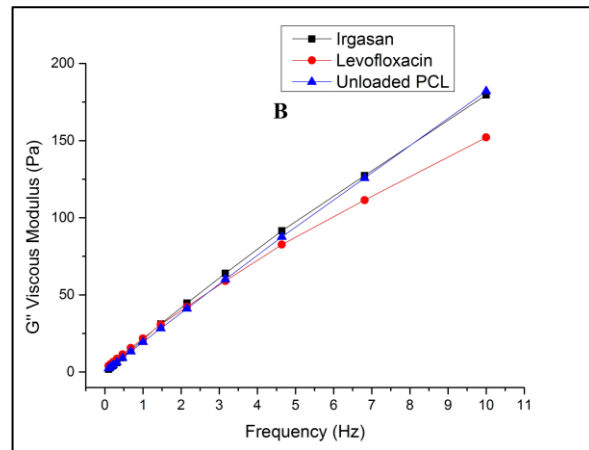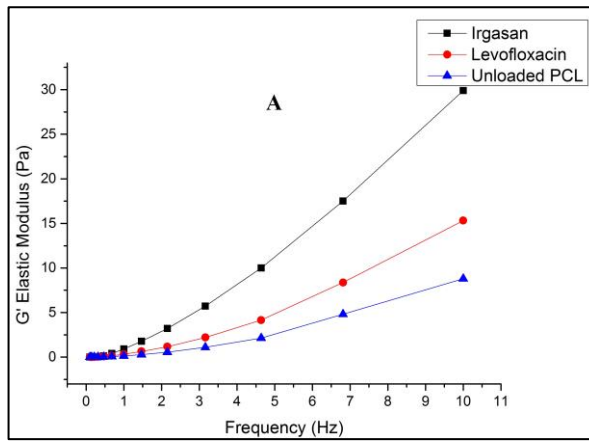
Figure 3.2 – Frequency sweep data for PCL, PCL-IRG and PCL-LEVO. (a) Elastic modulus (b) Viscous modulus (c) Shear viscosity

PLA

The data presented in Figure 3.3 indicates an increase in G' values for both PLA-IRG and PLA-LEVO – PLA-unloaded solutions peaking at ~ 23 Pa at a shear stress of ~ 18 Pa, PLA-IRG peaking at ~ 35 Pa at a shear stress of ~10 Pa, and PLA-LEVO peaking at ~ 33 Pa at a shear stress of ~ 21 Pa. The G'' values for PLA-unloaded peaked at ~ 55 Pa, PLA-LEVO at ~70 Pa (both at a shear stress of ~15 Pa), and PLA-IRG peaking at ~ 55 Pa at a shear stress of ~ 21 Pa. These values determine that the addition of levofloxacin to the PLA solutions causes both G' and G'' to increase within the same LVER (10 – 20 Pa), and the irgasan solutions to shift in value across the shear stress axis (shift from 10 – 20 Pa, to 20 – 30 Pa). The shear viscosity of the solutions similarly indicated an increase in value within the same LVER for PLA-unloaded to PLA-LEVO (~ 9500 Pa to ~ 12000 Pa), and a shift in LVER across the shear stress axis from 10 – 20 Pa to 20 – 30 Pa.

The frequency sweep data in Figure 3.4 shows that PLA-unloaded solutions have a higher G'' value to G' (G': G'', ~ 400: ~ 550 Pa), whilst the PLA-IRG and PLA-LEVO have a higher G' value to G'' (G': G'', ~ 800: ~ 500 Pa; ~ 1200: ~ 300 Pa, respectively).
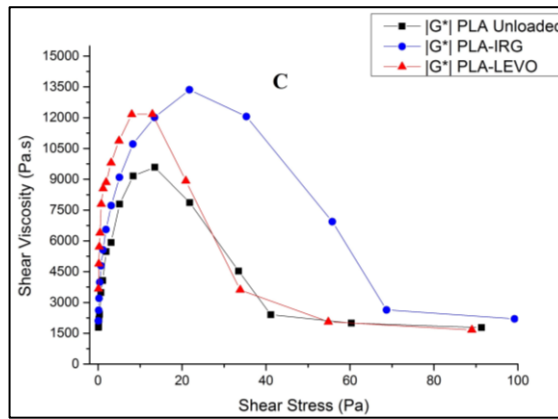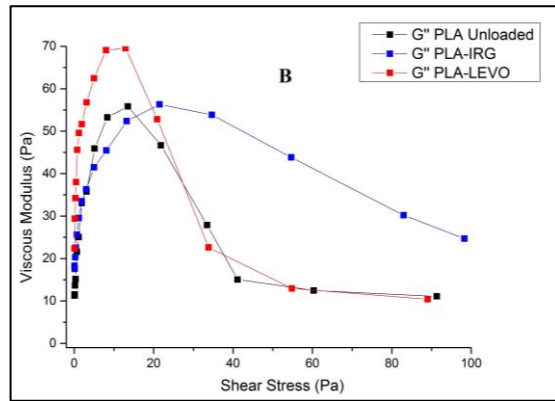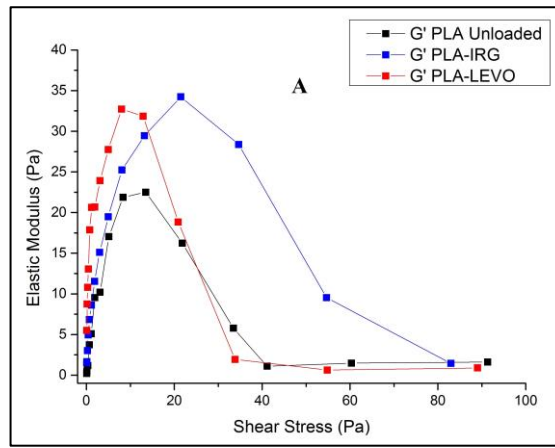
Figure 3.3 – Amplitude sweep data for PLA, PLA-IRG and PLA-LEVO. (a) Elastic modulus (b) Viscous modulus (c) Shear viscosity
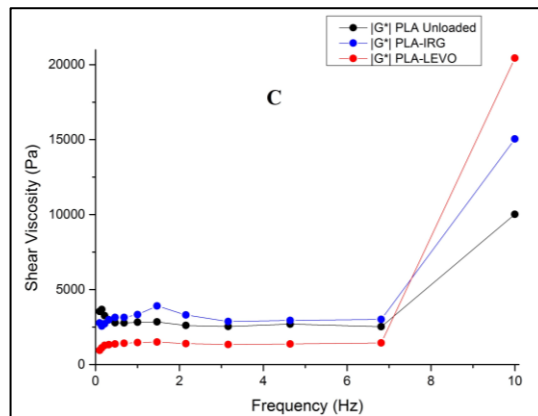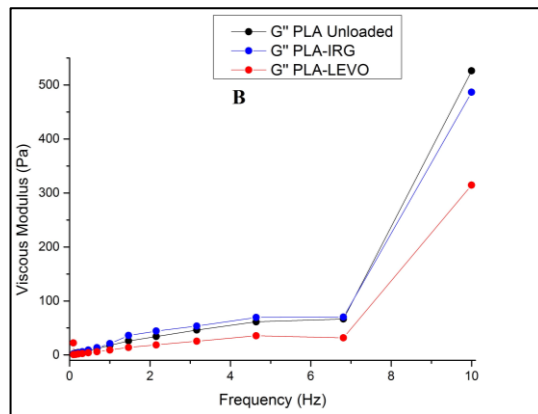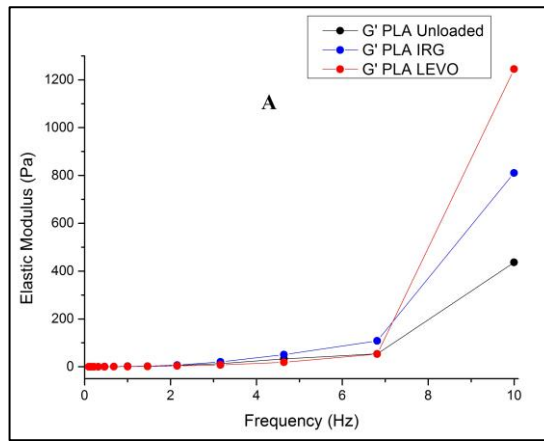
Figure 3.4 – Frequency sweep data for PLA, PLA-IRG and PLA-LEVO. (a) Elastic modulus (b) Viscous modulus (c) Shear viscosity

3.3.2 Fibre Morphology

Initially, a range of concentrations of PCL/PLA and IRG/LEVO were used to determine the most suitable polymeric/drug concentrations that yielded the most consistent fibres; consistent meaning that there were no signs of obvious beading, a smooth morphology of fibre, and an apparent uniformity in fibre size. Figure 3.5 shows SEM images of fibres (A and B) of varying polymer concentrations (8% and 12%, respectively) and varying drug concentrations (C and D, 2% IRG and 2% LEVO). It can be seen clearly in images A – D that the fibre morphology does not meet the suitability criteria mentioned previously. Images C and D show significantly heavy beading of the fibres, due to the higher concentration of IRG and LEVO used.
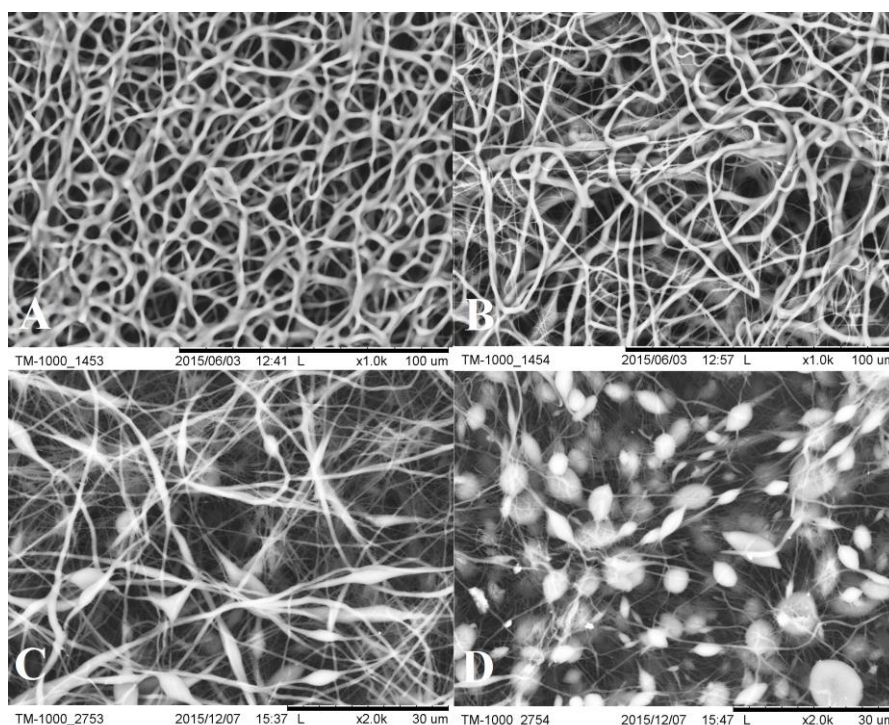
Figure 3.5 – SEM images of electrospun fibres. (a) PCL 8% (b) PLA 12% (c) 2% IRG (d) 2% LEVO

Figure 3.6 shows 3 different fibre formations for PCL, PCL-IRG and PCL-LEVO that yielded the most consistent fibres. A comparison and analysis of fibre diameters for all samples can be found in Chapter 4, section 4.3.1. PCL-unloaded samples were found to have an average fibre diameter of 2.0 µm, PCL-IRG with 1.6 µm, and PCL-LEVO with 2.9 µm. The AFM images were indicative of the surface morphology of the fibres, with Figure 3.7A showing regions of PCL-IRG, with no visible signs of drug at the surface. Figure 3.7B, however, showed irregular regions of morphology, which appears to be drug at the surface of the fibres.
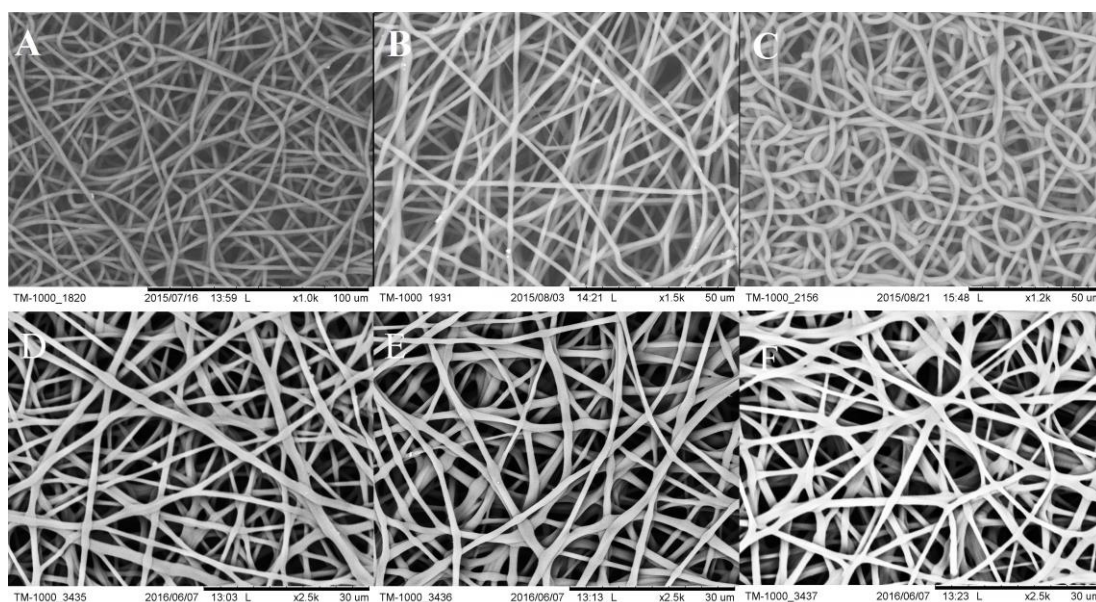
Figure 3.6 – SEM images of PCL and PLA fibres. (a) PCL (b) PCL-IRG (c) PCL-LEVO (d) PLA (e) PLA-IRG (f) PLA-LEVO

PLA

Fibre formation was at uniformity at an 8% concentration for PLA – the fibres shown in Figure 3.6 D – F shows a consistency in the fibre morphology. Fibre diameters across the samples were 2.7 µm for PLA, 2.5 µm for PLA-IRG, and 2.1 µm for PLA-LEVO. AFM images D and E in Figure 3.7 show a smooth morphology with no

apparent signs of API at the surface – however, a rough morphology can be observed in Figure 3.7 F, which may indicate there is LEVO present at the surface of the fibres.
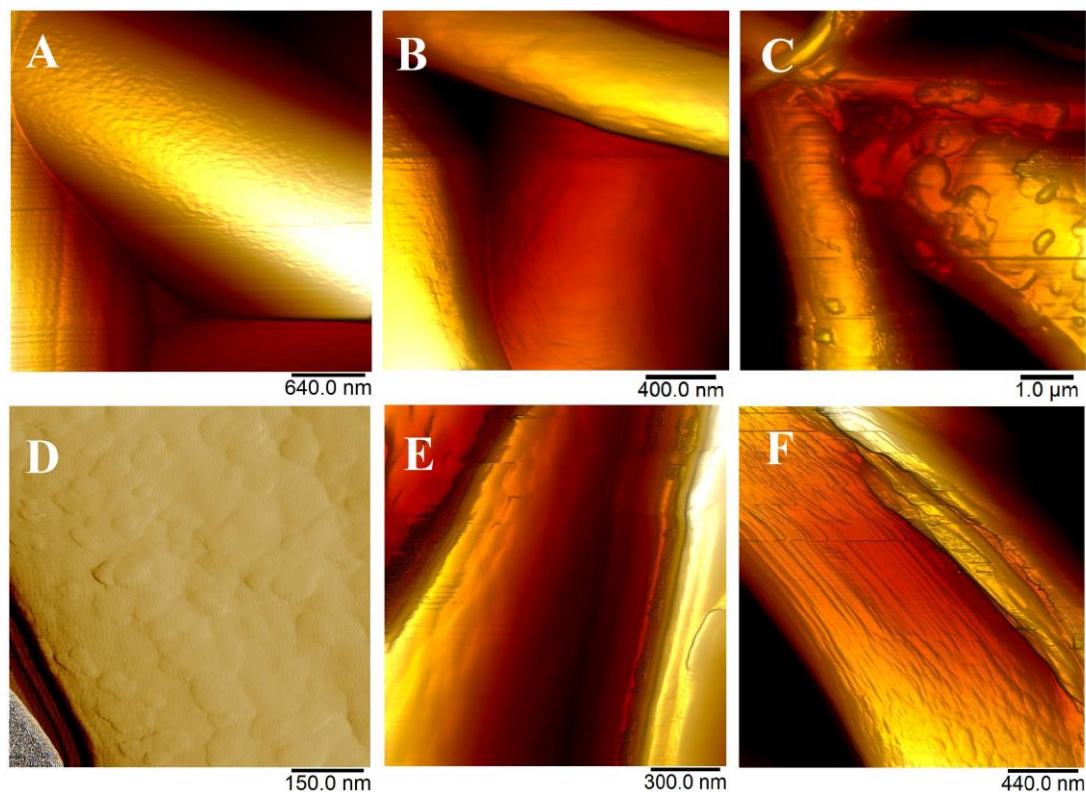
Figure 3.7 – AFM images of PCL and PLA fibres. (a) PCL (b) PCL-IRG (c) PCL-LEVO (d) PLA (e) PLA-IRG (f) PLA-LEVO

3.3.3 Solid State Characterisation

PCL

The DSC curves shown in in Figure 3.8 indicate a melting temperature (T_m) of around 60 °C for all three PCL samples. The glass transition temperature (T_g) is not observable within the measured temperature range (T_g of PCL = - 60°C (Domingos et al. 2009)), therefore no comment can be made regarding the suppression of the T_g related to the addition of IRG or LEVO. The DSC curves for raw powder samples of IRG and LEVO are displayed in Figure 3.9. The raw IRG curve exhibits a T_m of around 60 °C, and the

LEVO exhibiting an endothermic peak at ~ 90 °C and a T_m of ~ 230 °C. The XRPD data was inconclusive in showing any potential interactions between polymer and drug, or changes the polymeric structure.
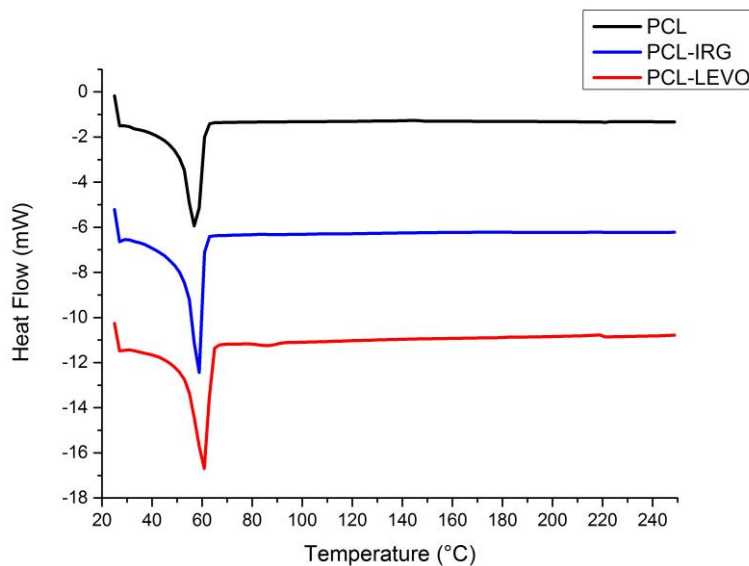
Figure 3.8 – DSC thermograms for PCL, PCL-IRG and PCL-LEVO samples
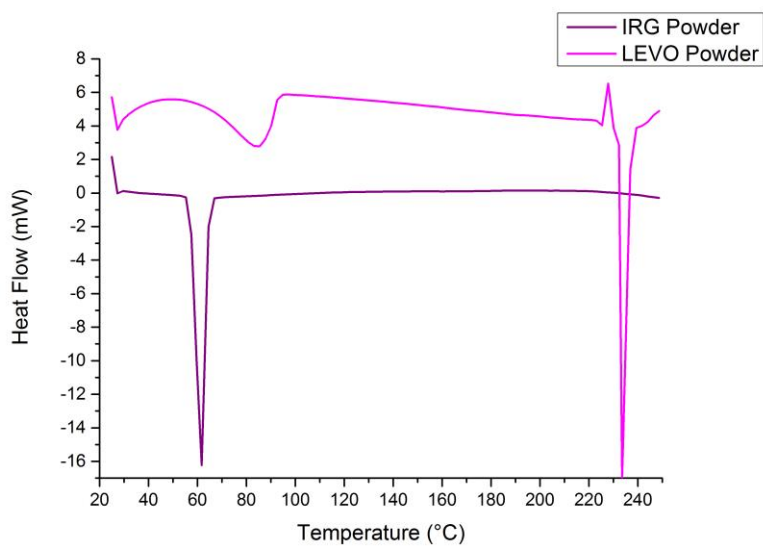
Figure 3.9 – DSC thermograms for raw drugs IRG and LEVO

Figure 3.10 shows the DSC curves for 3 samples of PLA, PLA-IRG and PLA-LEVO. For PLA, a T_g is observed at around 65 °C, a crystallisation temperature (T_c) at 90 °C and a final T_m at ~ 150 °C. The PLA-IRG curve appears to a suppressed (or reduced) T_g and no apparent T_c at the previously mentioned temperatures for PLA. There also appears to be a shift of the T_m for PLA. It can be observed in the PLA-LEVO curve an exothermic peak at ~ 60 °C before an apparent T_g value of 65 °C – this exothermic peak may be from the LEVO. There is a slight shift in the T_c value for PLA-LEVO sample at around 93 °C. The T_m for PLA and PLA-LEVO remained the same; however, a shift in T_m appears in the PLA-IRG sample at ~ 140 °C.

 XRPD data is presented in Figures 3.11 and 3.12. The PLA curve in Figure 2.11 shows the start of a broad peak beginning at 5° and ending at around 26° - there appears to be a crystalline peak at 17°. The curve for PLA-IRG closely mimics the curve for PLA, and there are no apparent crystalline peaks that are prominent at 8° and 24° as seen in the raw IRG data. However, in Figure 3.12 the prominent crystalline peaks of raw LEVO at 7° and 10° can be seen within the PLA-LEVO curve.
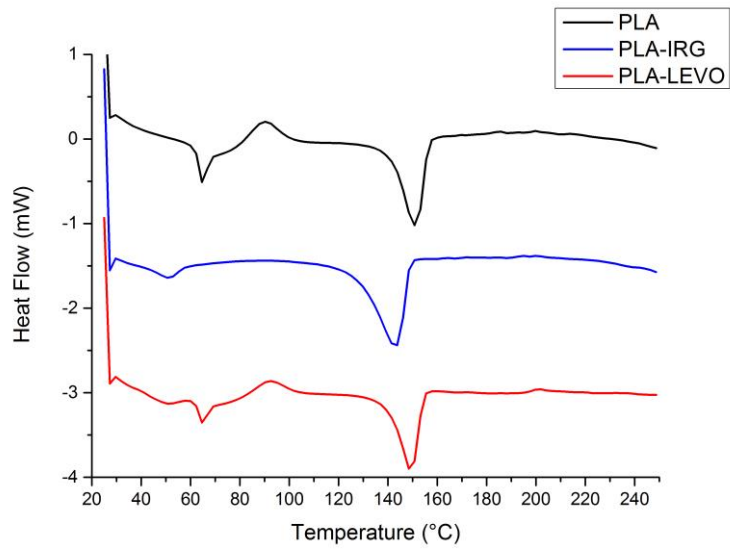
Figure 3.10 – DSC thermograms for PLA, PLA-IRG and PLA-LEVO
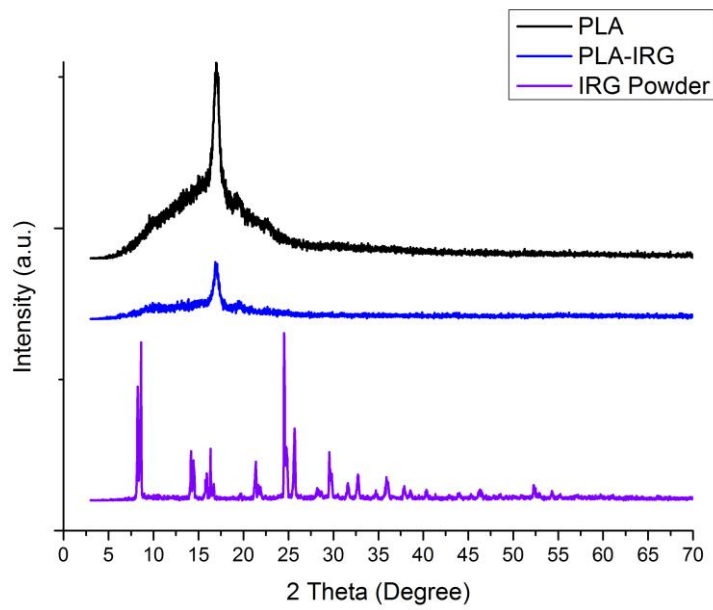
Figure 3.11 – XRPD curves for PLA, PLA-IRG and IRG powder
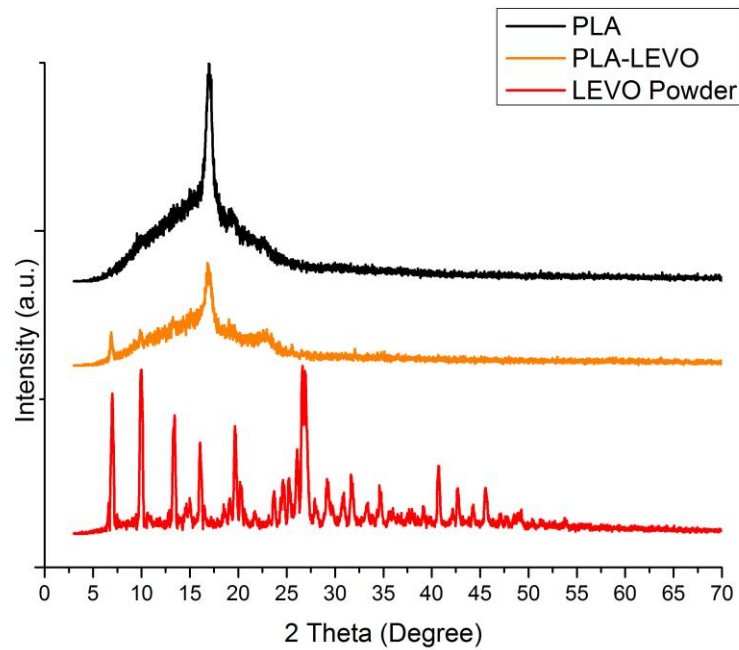
Figure 3.12 – XRPD curves for PLA, PLA-LEVO and LEVO powder

3.3.4 Surface Characterisation

PCL

The contact angle measurements (Figure 3.13) found that PCL-unloaded exhibited hydrophobic behaviour with a starting angle of ~ 80° (0 min) and finishing at ~ 75° (20 min). PCL-IRG exhibited a higher starting contact angle of ~ 110° (0 min) and finishing at ~ 80°. PCL-LEVO exhibited hydrophilic behaviour due to the angle decreasing rapidly from 100° to 0° within the first two minutes of the experiment.

PLA

PLA and PLA-IRG samples exhibited similar starting and finishing angles (~ 125° and 80°, respectively), with PLA-LEVO starting with a lower angle of ~105° and finishing at ~55°.
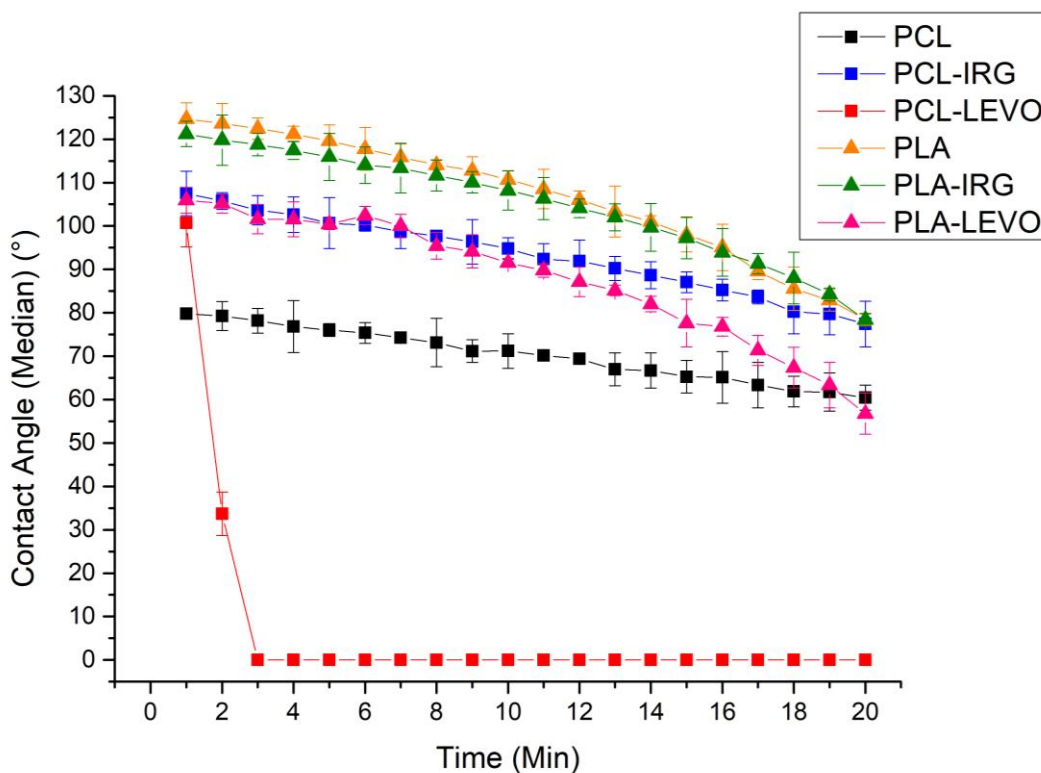
Figure 3.13 – CAG graph showing the contact angle median values versus time for PCL, PCL-IRG, PCL-LEVO, PLA, PLA-IRG and PLA-LEVO (*n=3*)

3.3.5 Drug Efficacy of Synthetic Scaffolds

The cumulative drug release profiles of both IRG and LEVO with PCL and PLA are shown in Figure 3.14. For both PCL-IRG and PLA-IRG, sustained release behaviour was exhibited with PCL-IRG eluting at ~ 50% cumulative drug release at the final time point (196 hr). PLA-IRG finished at ~ 40 % cumulative drug release at the final time point. Similarly, both PCL-LEVO and PLA-LEVO samples released the drug as burst release type behaviour. PCL-LEVO released ~ 50% of the antibiotic within the first 10 hours of study, followed by equilibrium until the final time point. PLA-LEVO released ~ 20% of the drug within 10 hours of the study.
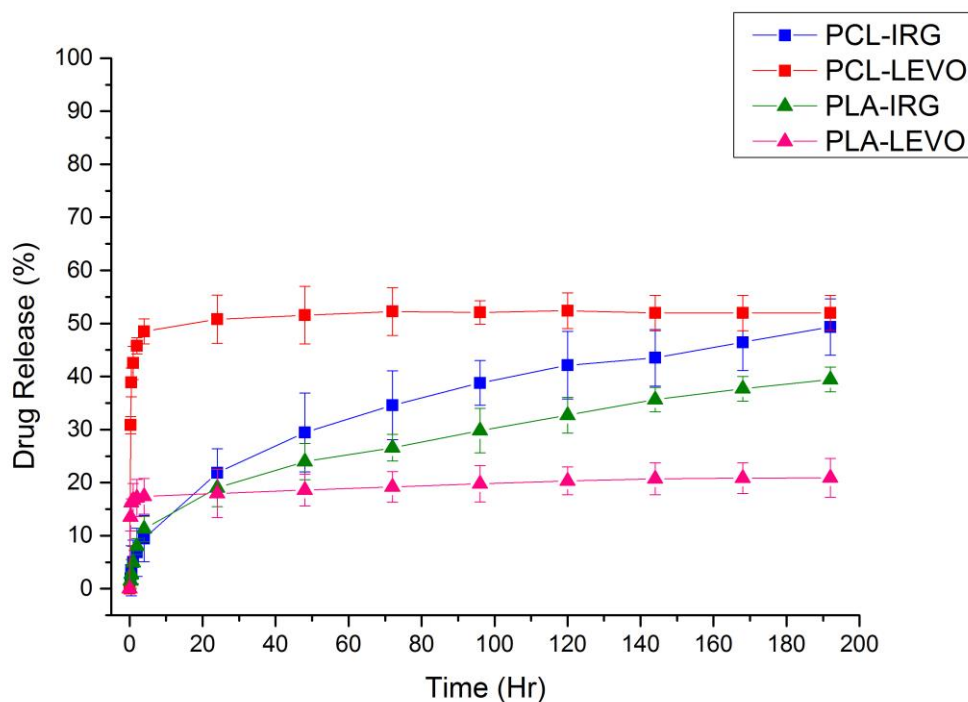
Figure 3.14 – *In vitro* release rate data for PCL-IRG, PCL-LEVO, PLA-IRG and PLA-LEVO (*n=6*)

3.3.6 ToF-SIMS Analysis

PCL

Imaging and 3D imaging techniques showed a difference in the distribution of the active pharmaceutical ingredients (API) between irgasan-loaded and levofloxacin-loaded fibres. PCL is identified by the ion at m/z 113, levofloxacin ($C_{18}H_{20}FN_3O_4$) by the ions at m/z 320 and m/z 360, and irgasan by the ions at m/z 287 and m/z 289. The total ion images and the overlays of single ion images for the characteristic peaks of PCL (grey) and the two drugs (yellow) are reported in Figure 3.15.
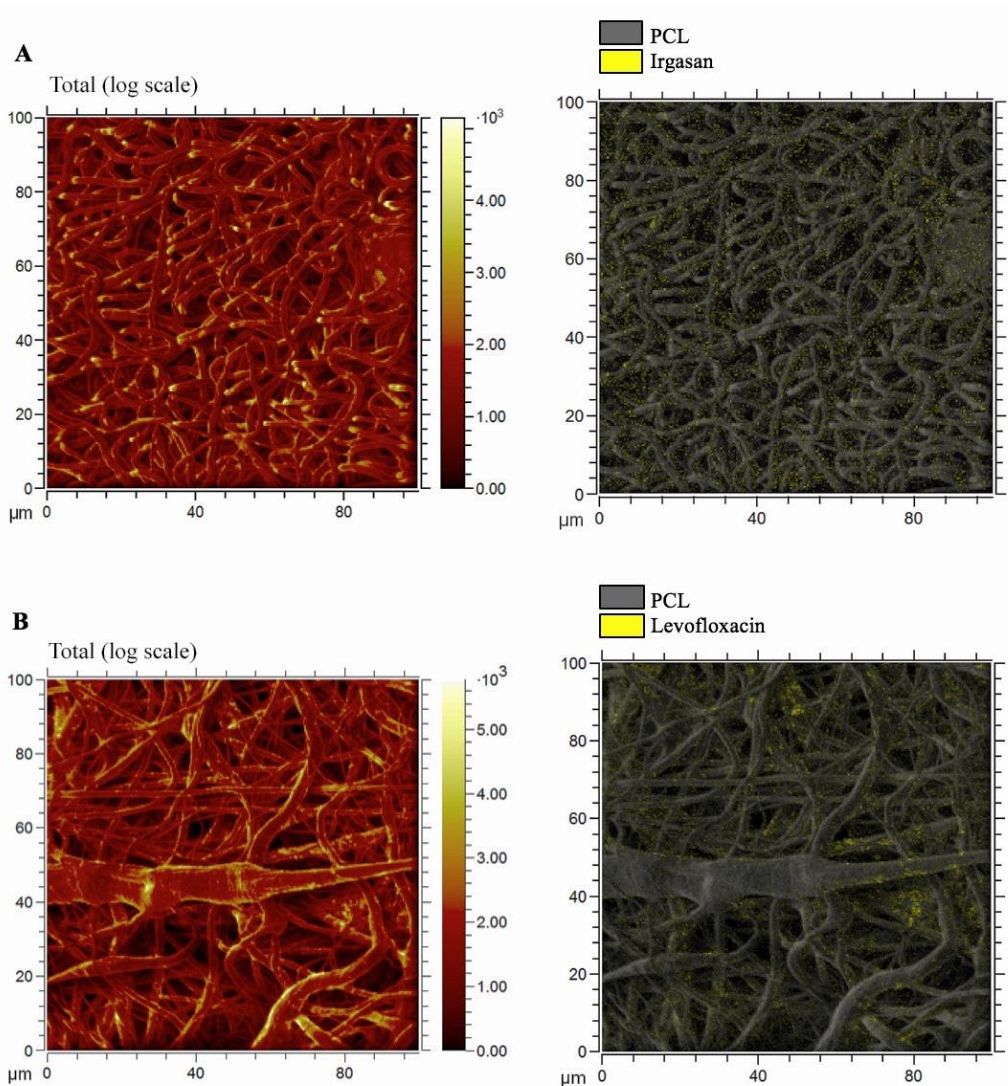
Figure 3.15 – ToF-SIMS images showing localized areas of drug (a) PCL-IRG (b) PCL-LEVO

PLA

Imaging data showed a difference in the distribution of the APIs in the various strands. The compounds of interest are identified by unique characteristic ion peaks; PLA at m/z 71 ($[C_3H_3O_2]^-$) and m/z 89 ($[C_3H_5O_3]^-$), levofloxacin at m/z 360 ($[C_{18}H_{19}FN_3O_4]^-$, $[M-H]^-$) and m/z 316 ($[C_{17}H_{19}FN_3O_2]^-$), and irgasan at m/z 287 ($[C_{12}H_6{}^{35}Cl_3O_2]^-$ $[M-H]^-$), and isotopes m/z 289 ($[C_{12}H_6{}^{35}Cl_2{}^{37}ClO_2]^-$) and m/z 291 ($[C_{12}H_6{}^{35}Cl{}^{37}Cl_2O_2]^-$). The total ion images and the overlays of single ion images for the characteristic peaks

of PLA and the two drugs are reported in Figure 3.16. With regards to the PLA-IRG and PLA-LEVO electrospun scaffolds, by the ion images irgasan appears to be homogeneously distributed throughout the sample, whilst the presence of levofloxacin is concentrated in multiple small regions on the surface of the fibers. This confirms the data obtained with the AFM analysis and with the release study – (see: Results, Fibre Morphology and Results, Drug Efficacy).
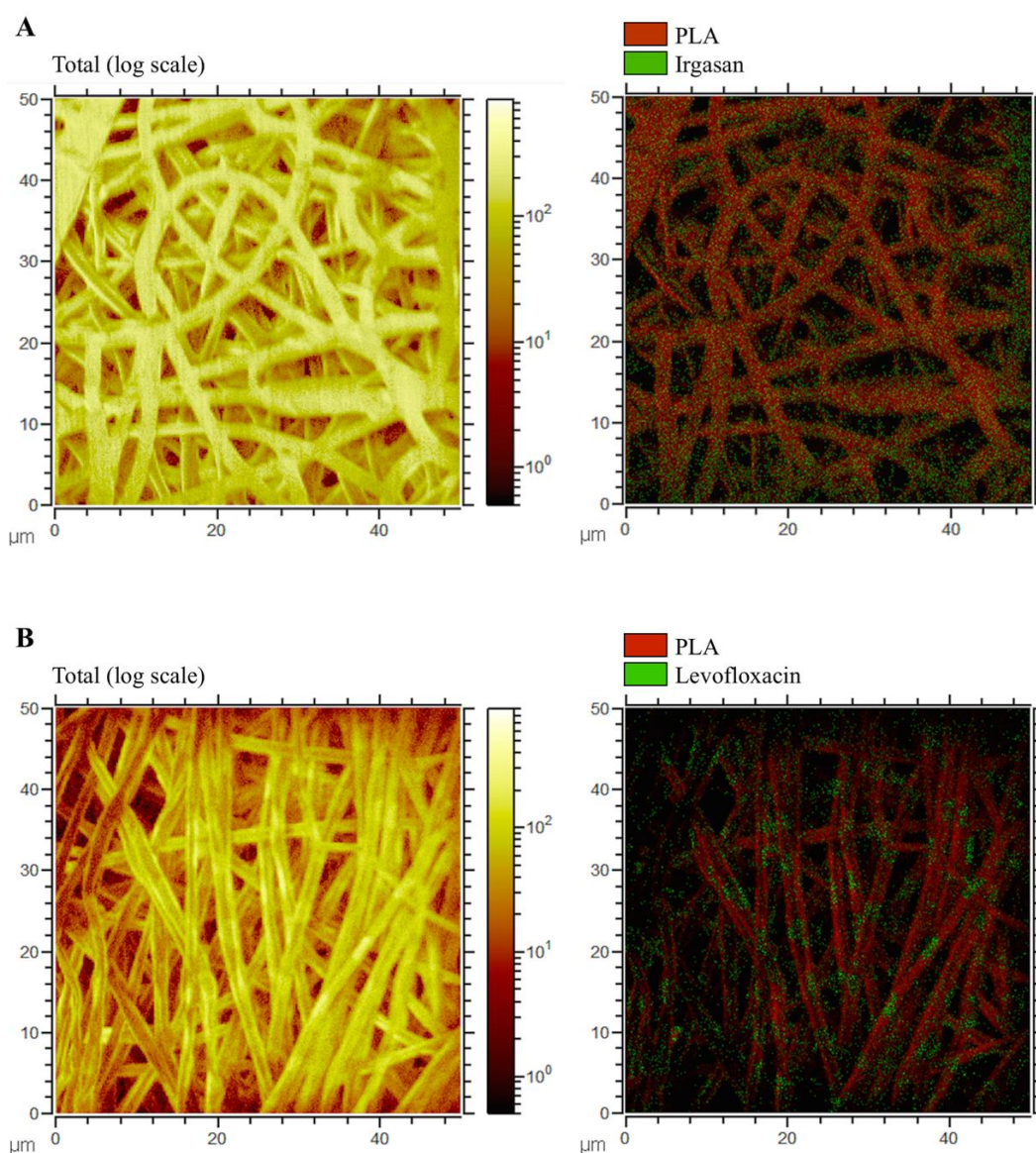
Figure 3.16 – ToF-SIMS images showing localized areas of drug (a) PLA-IRG (b) PLA-LEVO

3.4 Discussion

3.4.1 Rheological Studies

PCL

For each polymeric solution, multiple amplitude sweeps were used in order to correctly identify the linear viscoelastic region (LVR). This was repeated to detect any major variations in the LVR, and for a more accurate shear stress to be used in the frequency sweeps. For each of the samples, elastic modulus (G'), viscous modulus (G'') and shear viscosity (η) was calculated and subsequently analysed. It can be seen in Figure 1 that for all three solutions, the viscosity modulus (from 30 Pa to 80 Pa) is considerably greater than the elastic modulus (0.5 Pa to 6 Pa), which implies that the solutions exhibit significantly less elastic properties. As observed in Figure 3.1c, both polymer-drug-loaded solutions of irgasan and levofloxacin show differences in the shear viscosity (η). The amplitude sweep demonstrated that these drugs caused a reduction in all three of these parameters – this may be caused by the possible transition from semi-dilute to dilute regime, where there are less polymer chain entanglements (Dias et al. 2013). It is also worth noting that the LVR for the drug-loaded solutions was extended; the unloaded PCL solution had a short LVR of between 50 Pa to 100 Pa (shear stress), which then resulted in shear thinning at high shear stresses. These long LVRs are indicative of well-dispersed, stable polymer-drug systems.

The frequency sweep data shown in Figure 2 are indicative of how the drug dispersed in the matrix affected the overall structure. Again, it was observed that loading the polymer solution with drugs had an effect, with measured viscosity in all three samples appearing to be frequency dependent. According to data in both G' and G'' graphs,

G'' was shown to be the dominating effect (G' ranging from seven to 30 Pa, and G'' ranging from 150 to 175 Pa). Long regions of viscoelasticity normally imply that there is a certain degree of stability within the polymer matrix; however, the frequency sweep implies otherwise. It appears that G' and G'' are both frequency dependent, which implies that the system has little internal network and is easily disturbed (Bubel et al. 2014).

PLA

The amplitude sweep testing generally shows that PLA does not have a majorly stable linear viscoelastic region – nor does the addition of IRG or LEVO affect this. The two drugs, however, do affect the viscosity of the solution by increasing the values each time. This behaviour may be explained due to the nature of branch entanglements within PLA – the addition of drug increases the entanglement and leads to an increase in the viscosity (Dorgan et al. 1999). The frequency sweep data shown in are indicative of the structure of the solutions; for PLA-unloaded solution, G'' > G', which shows that the viscous modulus dominant – this means that the solution shows a weakly structured system. With the drug-loaded solutions, G' > G'', which implies that there is interaction between drug and polymeric matrix – this is usually indicative of a well-structured system; however, the amplitude sweep data suggests a potential entanglement of chains, rather than a well-structured system. It may well be the case that the dispersive surface energy of the drug molecules are actively causing drug-polymer interactions (see section 4.4.3) and this can be observed in Figure 3.4, where the elastic modulus value for PLA-LEVO (~1300 Pa) is significantly higher than the elastic modulus value for PLA-IRG (~800 Pa).

3.4.2 Fibre Morphology

PCL

Smooth morphology can be observed in all 3 different scaffolds and at a 12% concentration of polymer, there is no significant beading or any visible signs of either API outside of the fibres. The major differences across the three different scaffolds are the fibre size – the addition of irgasan reduced the average fibre diameter to 1.623 ± 1.9 µm. These fibres appear to be relatively consistent in size compared to other various PCL-fibre studies, 1.1 ± 6.6 µm, 2.7 ± 2.0 µm and 1.83 ± 0.05 µm (Celebioglu et al. 2014; Detta et al. 2010; Del Valle et al. 2011). The morphology of the levofloxacin-loaded fibres appeared to differ from the unloaded and irgasan loaded fibres: whilst there appears to be a smooth morphology, the fibres appear more densely packed with a greater 'curvature' of the fibres. These fibres are also greater in diameter in comparison with the PCL-IRG scaffold, with an average fibre diameter or 2.865 ± 3.0 µm. The PCL-LEVO fibres appear to be much larger in diameter compared with studies by Jalvandi *et al* (Jalvandi et al. 2015) (600 – 800 nm), Puppi and colleagues (Puppi et al. 2011) (219.2 ± 55.1 nm) and Park and colleagues (Park et al. 2012) (232 ± 20.4 nm). This variation in fibre diameter could possibly be attributed to the higher voltage applied to the target plate during the electrospinning process – for PCL and PCL-IRG solutions, the voltage applied varied between 10 – 12 kV whereas the PCL-LEVO solution was ± 18 kV. There is a critical value of applied voltage, and the increase in the diameter with an increase in the applied voltage are attributed to the decrease in the size of the Taylor cone and increase in the jet velocity for the same flow rate (Haider et al. 2015).

Considering the morphology of the fibres at a greater detail and image resolution, the AFM characterisation showed a significant difference between the irgasan-loaded and levofloxacin-loaded fibres. Figure 3.7B shows the smooth morphology of the PCL-IRG scaffold at a 400 nm scale, and it can be clearly seen that there appears to be no signs of API on the surface of the polymer. This suggests that the irgasan is integrated into the polymeric matrix. In contrast, it was found using AFM that within certain areas of the PCL-LEVO scaffold, there appeared to be regions with crystalline API sitting at the surface (Figure 3.7C).

PLA

The fibre diameter for the three samples PLA, PLA-IRG and PLA-LEVO appear to consistent and similar in size; all ranging between $2 - 3$ µm. There a range of different fibre diameters reported that range from 516.2 nm (Wang et al. 2017) to 4.6 µm (Toncheva et al. 2016). The ranges in fibre diameters across those studies and this one can be attributed to the different processing parameters that can affect the electrospinning process: spinning voltage, flow rate, collector distance and concentration of polymer solution (Sukigara et al. 2003; Deitzel et al. 2001). It should be noted the difference in polymer concentrations for the electrospun PCL and PLA samples (12% and 8%, respectively); PLA solutions greater than 8% simply did not work with the electrospinning apparatus, with blockages occurring within the connecting tubing. The addition of IRG and LEVO within the solutions meant modifications of the parameters used during the electrospinning process: similar to the PCL-LEVO solution, the voltage used for PLA-LEVO was variable, with some fibre formation seen at $12 - 15$ kV, however for the fibres shown in Figure 3.6F, a voltage

of ~ 20 kV was used. Generally, uniform fibres are achieved due to the increase of voltage relative to a critical concentration (Zamani et al. 2013) of solution.

Rheology results previously indicated that the addition of LEVO caused an increase in the viscous modulus of both the PCL and PLA solutions; and this change in viscosity may be the reason why a change in voltage is needed. Given that levofloxacin is zwitterionic (it contains both positive and negative charges, in this case a carboxylate and an amine) (Hirano et al. 2006), this data might indicate intramolecular electrostatic interactions, which can affect the chain entanglement behaviour in solutions (Brown et al. 2009). In order for electrospinning to successfully yield fibres, the presence of chain entanglements within the polymer solution are critical (McKee et al. 2004).

AFM images revealed smooth morphology for both PLA and PLA-IRG samples. PLA-LEVO image showed a similar image to the PCL-LEVO sample, where there was no consistency with the morphology, and there appears to be API at the surface of the fibres. This was confirmed through ToF-SIMS analysis in section 3.3.6.

3.4.3 Solid State Characterisation

PCL

Given that both PCL and IRG have similar T_m values of 60 °C it was difficult to determine whether the T_m for IRG was suppressed – this suppression of the endothermic peak at this temperature is indicative of whether the IRG molecules have been incorporated within the polymeric structure (Kayaci et al. 2013). The endothermic peak observed for pure LEVO at $90 - 100$ °C is the dehydration of LEVO (Kitaoka et al. 1995): this curve can be seen (minimally) within the PCL-LEVO curve,

which may suggest there is a presence of free LEVO within this sample. However, no T_m for LEVO is observed for this sample, which would normally be indicative of the drug successfully integrating within the polymer – although it should also be noted that PCL (at a molecular weight of 80,000 g/mol), decomposition products (due to thermal degradation) are detected at around 250 °C and this may affect the results (Unger et al. 2010).

PLA

The DSC results for PLA were far clearer in indicating potential interactions between polymer and drug (in comparison to the DSC results for the various PCL samples). Firstly, for the unloaded PLA samples, we can clearly see both the T_g and T_m values – if there has been successful integration of either IRG or LEVO within the polymeric matrix, a suppression or shift of the T_g should be observed. For the PLA-IRG sample, there is no visible sharp endothermic T_g peak at around 62°C, instead there is a smaller, broader endothermic peak occurring at around 55°C. Given that there is no observable T_m of the IRG at ~ 60°C, and no T_c peak at 90°C, it can be concluded that there is a successful integration of irgasan within the PLA fibre structure. This is confirmed through the XRPD data, as there are no observable crystalline peaks (main peaks at 8° and 25°) – this may be because there is a complexation between PLA and IRG molecules, meaning that guest molecules are separated from each other within the polymeric structure, which does not allow them to form a crystal structure (Celebioglu et al. 2014).

The broad exothermic peak that occurs at just below 60°C in the PLA-LEVO sample is likely to be the same exothermic peak shown for the raw levofloxacin DSC curve –

68

thus implying that there is presence of free drug within the sample. This is confirmed through the unsuppressed T_g and T_c values observed. Levofloxacin crystalline peaks (predominately at 6°, 10° and 26°) can be seen within the XRPD PLA-LEVO data, which is further confirmation that the drug has not fully embedded within the sample.

3.4.4 Surface Characterisation

PCL

The CAG results for the irgasan-loaded fibres indicated an increase in the hydrophobicity of the scaffold in comparison to the unloaded PCL scaffold – the contact angle for PCL-IRG was greater (80° to 110°), with the slope showing a slow uptake of the water droplet over 20 min. This slow nature of absorption potentially indicates that the irgasan may release in a sustained mechanism. This is most likely due to the hydrophobic nature of irgasan combined within the polymeric matrix of PCL, which also has a certain degree of hydrophobicity. The CAG results for the levofloxacin-loaded scaffolds were inconclusive given that hydrophilic nature of levofloxacin – the water droplet applied was absorbed almost immediately; therefore, no data could be obtained. However, this does support the hypothesis that there may be an amount of levofloxacin sitting at the surface of the sample – the rapid absorbance of the water droplet may be the levofloxacin uptake.

PLA

PLA and PLA-IRG samples showed similar behaviour for the water droplet absorption that shows a high degree of hydrophobicity for both samples. The addition of LEVO to PLA caused a decrease in the starting contact angle; however had a similar gradient compared with PLA and PLA-IRG. The hydrophilic nature of LEVO may be causing

the decreased contact angle, and may indicative that this drug is again (similar to the PCL-LEVO sample) at or near the surface of the fibres.

3.4.5 Drug Efficacy of Synthetic Scaffolds

The release of irgasan from the PCL-irgasan scaffold appeared to exhibit sustained release behaviour of the encapsulated drug. The final cumulative drug release was found to be at 50%; although more irgasan will be released beyond 200 hr (equilibrium had not been observed at the 200 hr). The behaviour of the PCL-levofloxacin scaffold was entirely different to the irgasan-loaded scaffold. It exhibited burst release behaviour and the antibiotic was almost entirely lost from the matrix within the first 15 min of measurements. The final cumulative drug release was also found to be at 50%. This burst release behaviour is consistent with the manner in which the drug is associated with the polymer matrix – the previous SEM and AFM were indicative of the presence of levofloxacin on the surface of the fibres in some areas. Similarly, the PLA samples released both IRG and LEVO in the same manner as the PCL samples – with a sustained release of IRG occurring (not reaching equilibrium) over 200 hr, and LEVO exhibiting a burst release behaviour. However, the final drug release % was lower for PLA, with the LEVO releasing around 20%, which is significantly lower than the amount released within the PCL-LEVO sample. It should be noted that the drug release values calculated are based on the theoretical loading amounts – this means that the value of 50% for LEVO-loaded solutions is related to the theoretical amount. It may be the case that a 50% drug release amount is due to LEVO not fully loading into the polymer fibres.

Determining the drug release profiles of the drugs was a crucial part of this study, as divergent behaviours helped to characterise bridging properties indicating the manner in which irgasan and levofloxacin dispersed within the polymer matrices (PCL and PLA). The irgasan released steadily over 200 hours, which would suggest that the drug is being released through molecular diffusion (Yao & Weiyuan 2010). The levofloxacin exhibited a burst release mechanism, although this may be attributed to the mechanism in which levofloxacin functions in most polymers (Park et al. 2012).

The main factors that could be expected to influence the drug release kinetics for the different polymeric samples can be summarised as followed:

- **Material matrix**: this includes the composition, structure and degradation of the polymers; however, both PCL and PLA showed no signs of degradation and both are known to show a high degree of stability.
- **Release medium**: the irgasan was released in a buffer of PBS and sodium dodecyl sulphate (surfactant), therefore it could be suggested either that the surfactant is interacting with the polymer/drug or that it is changing the ionic strength of the buffer (Thongngam & McClements 2005).
- **Drug compounds**: Fu and Kao (Yao & Weiyuan 2010) cite solubility, stability charges and interaction with matrix as major factors with the drug that may affect the drug release kinetics. The results in this study can demonstrate this, given that potential charges of the drug were affecting the electrospinning process, therefore it can be assumed that the charges of irgasan and levofloxacin may be affecting the drug release kinetics.

One of the most important points regarding the drug release results is the difference in hydrophobicity between IRG and LEVO – most cases of sustainable release for drugs within a polymeric matrix occur primarily with hydrophobic small molecule drugs. With LEVO being considered a hydrophilic drug, it is an apparent challenge to attempt to shift the release behaviour from burst to sustained release. Hydrophilic (small molecule) drugs typically have a high solubility with the release media, poor partitioning, and low compatibility with many hydrophobic polymers (Chou et al. 2015).

3.4.6 ToF-SIMS Analysis

The ion images show a homogeneous distribution of irgasan, throughout the electrospun fibres (for both PCL and PLA samples), whilst the levofloxacin appears to be concentrated in several small areas. This was confirmed by 3D imaging, where irgasan characteristic peaks appeared to be homogeneously distributed in the volume (Figure 3.15a). Conversely, levofloxacin had an intense signal localized to small areas and mainly on the surface. The images here are a confirmation of what has been theorised (regarding the positioning of both drugs within the polymeric matrices) within this Chapter.

3.5 Conclusion

The purpose of this Chapter was to fabricate drug-loaded fibres that may potentially be used within a hernia repair context. The good understanding of the relationship between the solution viscosity and the spinning parameters is essential if the technique is to be effective, hence the need to characterise the effect of drug loading on the

rheological behaviour of the spinning solutions. It was observed that the addition of both irgasan and levofloxacin had a direct influence on the rheological behaviour of the solutions; a reduction in elastic modulus, viscous modulus, and shear viscosity occurred, which may cause a reduction in polymer chain entanglements. However, this explanation may not be the only viable one – rheological behaviour of drug-loaded solutions has been widely researched, although further characterisation into the molecular interactions between drug and polymer may give further insight into why the solution behaviour changes significantly.

Atomic force microscopy indicated that crystals, probably of levofloxacin were present on the surface of the polymer fibres, and this was crucial in explaining the behaviour of the drug during *in vivo* release studies and antibacterial activity profile. The presence of levofloxacin at the surface of the polymer was confirmed through contact angle goniometry (immediate absorbance of the water droplet showed the hydrophilic nature of levofloxacin in action), *in vitro* release studies (the drug demonstrated a burst release behaviour), and ToF-SIMS. In the ToF-SIMS study, the molecular weight of levofloxacin was shown at various areas across the fibres and the 3D imaging of the matrix indicated there was a certain degree of drug encapsulation. This experimental Chapter has contrasted the incorporation of two different drugs within an electrospun fibre, and shown that through bridging chemical, mechanical and biological studies, their behaviours can be fully interpreted.

At this stage of the research project, there are a number of points that must be addressed in order to improve on the basic polymer-drug fibres created – in particular, improving the biocompatibility of the scaffolds. It is still important to continually address the

requirements of hernia meshes described in Chapter 2, and biocompatibility is a vital need. Another important area to improve on for these polymeric scaffolds, would be to modify the release behaviour of levofloxacin – for example, the creation of super hydrophobic structures have previously been created that have been successful in controlling the rate at which drug is released (Falde et al. 2015).

Chapter 4: Biofunctionalisation of Synthetic Polymers

4.1 Introduction

Within the field of tissue engineering, there are a number of different applications that can be explored relating to the combination of synthetic and natural polymers, and integration with various active pharmaceutical ingredients. For example, wound closure involves the bringing together of opposing surfaces using glues, staples and/or sutures. The re-joined structure then undergoes a primary hyper-proliferative stage, characterised by clot formation and the recruitment of inflammatory cells (macrophages) into the wound. Secretion of local tissue mediators encourages cell migration and begins the process of scar formation (Hu et al. 2014). Tissue remodelling results in wound contraction and an increase in tensile strength across the lesion, resulting in increased resistance to rupture. During the healing stage, the tissue is open to infection as a pathway into deeper tissue structures has been provided. In supporting healing, the purpose of an added matrix task may be to provide tensile strength, to encourage controlled epithelialisation and new vascular growth and to decrease the formation of bacterial biofilms. The fabrication of scaffolds for wound repair has become important, especially the formation of tissue-specific scaffolds (van Winterswijk & Nout 2007).

For the creation of scaffolds it is essential to mimic the chemical composition, the physical morphology, and the biological functions of the human body (Jiang et al. 2013). Scaffolds can be created using synthetic polymers (e.g. PLGA) or natural

polymers (e.g. chitosan), or a combination of both – the addition of natural polymers can be highly advantageous as these may avoid the stimulation of chronic inflammation, immunological reactions and toxicity (Mano et al. 2007). An example of a natural polymer is *collagen*, which is the most abundant protein in the human body, a key element of the extracellular matrix (ECM), and imparts structural integrity and tensile strength to tissues (Sell et al. 2009). Using collagen in scaffolds has been previously shown to show a high *in vivo* stability and is able to maintain a high biomechanical strength over time (Tillman et al. 2009).

Electrospinning, a fabrication technique used in Chapter 3 for the creation of drug-loaded polymeric scaffolds, is an ideal micro and nanofiber fabrication technique for tissue engineering, as the fibres within the resulting scaffold closely mimic the size and structure of the native extracellular matrix (Tan et al. 2008) – the use of solvent and aqueous based systems are useful for the integration of biological compounds, such as collagen. Previous studies have been shown various practices of electrospinning collagen, including collagen-elastin blends (Buttafoco et al. 2006), collagen-polycaprolactone scaffolds for vascular tissue engineering (Venugopal et al. 2005), and fibrinogen fibres which allows native deposits of collagen during cell growth (McManus et al. 2006). Despite these examples of electrospinning involving collagen, there is an apparent gap in the research concerning the integration of drugs in these electrospun scaffolds. This integration of drugs, such as antibiotics, with polymer-collagen blends may be critical in the future success of human tissue accepting the scaffolds; there are many clinical applications for scaffolds that require controlling growth of bacteria. For example, one of the requirements for controlling intra-abdominal infection is to maintain satisfactory levels of antimicrobial drug level

during drug administration (Solomkin et al. 2010), which means that the sustained release of drugs is critical. Sustained release of drugs with electrospun materials have been previously studied, such as polylactic acid with diclofenac sodium (an anti-inflammatory agent) (Toncheva et al. 2011), metronidazole-loaded polycaprolactone nanofibers (He et al. 2016), and polyvinylidene fluoride with enrofloxacin (an antibiotic) (T. He et al. 2015). Given the range of success there has been with electrospinning polymer with drug, and polymer-collagen blends, the next area of research should be to determine whether we can alter any of the characteristics of scaffolds with the inclusion of collagen, whether it be mechanical, chemical or drug release changes.

The purpose of this Chapter is to examine the physicochemical properties, bacterial response, drug loading and bio-functionalisation of electrospun scaffolds that have been prepared using Type I Collagen with a supporting synthetic polymer. The polymers chosen for this Chapter are again PCL and PLA – PLA in particular has been previously used for other clinical uses such as cell based gene therapy (Papenburg et al. 2009), stents for wound healing (Zhang et al. 2008), and drug delivery of anti-inflammatory drugs in PLA implants (Li et al. 2013). The solutions were modified by the addition of type I collagen. The matrix was loaded and electrospun with two drugs, irgasan and levofloxacin. The electrospun fibres were then characterised through various methods: the morphology of the electrospun fibres was characterised by scanning electron microscope (SEM) and Atomic Force Microscope (AFM), solid state characterisation was performed by x-ray powder diffraction (XRPD) and differential scanning calorimetry (DSC), surface characterisation of the two drugs was investigated by surface energy analysis (SEA) and contact angle goniometry (CAG),

and drug efficacy (e.g. *in vitro* release studies, antibacterial studies and time-of-flight secondary ion mass spectrometry (ToF-SIMS)). The tensile strength of the scaffolds was also measured (for both polymer-drug and polymer-drug-collagen samples) in order to determine any potential differences in mechanical strength. The results from this Chapter should help to determine whether the addition of a biological compound, such as collagen, is useful in modifying various characteristics of electrospun scaffolds for hernia repair.

4.2 Materials & Methods

Polycaprolactone (PCL) and polylactic acid (PLA) were the chosen polymers for this study and was used as purchased from the suppliers (Sigma-Aldrich, *GF45989881*), and the collagen used was type I from calf skin (Sigma-Aldrich, *C9791*). Irgasan (5-Chloro-2-(2,4-dichlorophenoxy)phenol), Triclosan, >97%, (Sigma-Aldrich, *72779*) and levofloxacin ((*S*)-9-fluoro-2,3-dihydro-3-methyl-10-(4-methylpiperazin-1-yl)-7-oxo-7*H*-pyrido[*1,2,3-de*]-1,4-benzoxazine-6-carboxylic acid) purity >98%, (Sigma-Aldrich, *28266*) were obtained commercially. The solvent used for the electrospinning was also commercially purchased from Sigma-Aldrich, specifically 1,1,1,3,3,3-hexafluoro-2-propanol (GC grade >99%).

4.2.1 Preparation of Polymer-Collagen-Drug Solutions

Investigations, previously shown in Chapter 3, of the polymer-drug solutions prepared showed that the optimum w/w concentration for electrospinning was 12% for PCL and 8% for PLA. These particular concentrations were used as previous experimentation revealed that higher concentrations did not result in suitable fibre formation. PCL

(12% w/w) and PLA (8% w/w), were mixed with solvent. Due to the formulations containing collagen type I, both polymers were solubilised in hexafluoropropanol (HFP) with a total polymer (collagen + PLA) concentration of either 12% or 8%. The polymers were blended with collagen containing 1% collagen (M_{PLA} / [$M_{Collagen}$ + M_{PLA}] x 100) (Powell & Boyce 2009). Collagen at a 1% concentration was used as higher concentrations, as when in the range 2% to 10% w/w, mixtures yielded unstable and inconsistent fibre formations.

The solutions were mixed through 30 min in the centrifuge, a further 30 min in a sonicator and a final 1 h with a magnetic stirrer, which resulted in a solution that appeared homogeneous and composed of a single phase. The solution was left overnight, and a further 30 min of sonication was applied the following morning in order to confirm the uniformity of the solution. For the irgasan-loaded solutions, the same method was applied, at a concentration of 1% irgasan w/w. The concentration of the levofloxacin-loaded solutions was adjusted to 0.5% w/w to facilitate accurate measurement of the drug release profile. All the solutions remained clear after preparation. This process was based on the method as described by Hall Barrientos et al. (2016) for solution preparation.

4.2.2 Electrospinning of Polymer-Collagen-Drug Solutions

Various scaffolds were fabricated for each polymeric solution, using an in-house electrospinning apparatus which consisted of a syringe pump (Harvard Apparatus PHD 2000 infusion, US) and two 30kV high-voltage power supplies (Alpha III series, Brandenburg, UK). The polymer solution was loaded into a 5 mL glass syringe and fed through tubing with a metal needle tip attached at the end. The needle was clamped

into place, to allow for a high-voltage supply to run through it – this allowed for an electric field to be created between the needle and the target plate. The syringe was clamped to a pump, which determined the specific injection flow rate of the polymeric solutions. For each of the three solutions (e.g. unloaded, irgasan loaded, and levofloxacin loaded), 3 varying flow rates of 0.5, 1 and 1.5 mL h^{-1} were applied across varying voltages of 2 kV – 5 kV (across the needles) and 10 kV – 18 kV (Hall Barrientos et al. 2016). A 21-gauge needle, at a deposition distance of 8 – 14 cm was used. The process was performed at ambient room temperature (approximately 21°C) with a relative humidity of between 2 – 4 % (electrospinning was not performed is the relative humidity was greater than 5%). The solution was electrospun onto the target that was covered with aluminium foil, in order for the final material to be removed and used for further characterisation.

4.2.3 SEA-IGC

The dispersive surface energy of the raw drug samples was determined by inverse gas chromatography using both a SEA–IGC (Surface Measurement Systems). The samples were packed into 30 cm (3 mm inside diameter) silanised glass columns, plugged at either end by silanised glass wool. Various dispersive probes were used; undecane, decane, nonane, octane, heptane, and hexane were injected at a range of fractional surface coverage in order to determine the concentration free dispersive surface energy (Gamble et al. 2012).

4.2.4 IR Spectroscopy

Infrared spectroscopy analyses of the electrospun samples (for all variations of polymer-drug and polymer-collagen-drug) were performed using a Tensor II Bench ATR-IR. Spectra were recorded from 4000 to 400 cm^{-1}; the number of scans set at 32 at a resolution of 1 cm^{-1}. The spectra were analysed using the specific OPUS software associated with the equipment.

4.2.5 Mathematical Analysis of Fibre Diameters

Statistical comparisons of samples were conducted using SPSS 20.0 software package (SPSS Inc., Chicago IL, USA). Descriptive statistics, analysis of variance, Scheffé post hoc test and Kolgomorov-Smirnov test were performed using 50 individual fibre diameters of each samples obtained from the morphological analysis.

4.2.6 Tensile Testing

In order to test the mechanical strength of the electrospun fibres (PCL, PCL-IRG, PCL-LEVO, PCL-collagen, PCL-collagen-IRG, PCL-collagen-LEVO, PLA, PLA-IRG, PLA-LEVO, PLA-collagen, PLA-collagen-IRG and PLA-collagen-LEVO), scaffolds were cut into rectangular samples (3 x 1 cm). Macro-tensile measurements were tested using an Instron ElectroPuls E3000 (3 kN). Samples were mounted within the holders at a distance of 1 cm, and the tensile testing was performed at a rate of 5 mm/min at a temperature of 26°C.

4.3 Results

4.3.1 Fibre Morphology

The addition of collagen to PCL caused a decrease of average fibre diameter from 2.02 µm to 782 nm – however the coefficient of variance increasing from 22.3% to 68.2%. One-way ANOVA (Scheffé test) confirmed significance with this comparison (PCL to PCL-Collagen), and also a significant difference in means between PCL-IRG/PCL-Collagen-IRG (1.6 µm to 893 nm, 24.3% to 33.6% coefficient of variance) and PCL-LEVO/PCL-Collagen/LEVO (2.87 µm to 1.52 µm, 57.9% to 70.7% coefficient of variance). Overall, PCL exhibited the lowest coefficient of variance at 22.3%.
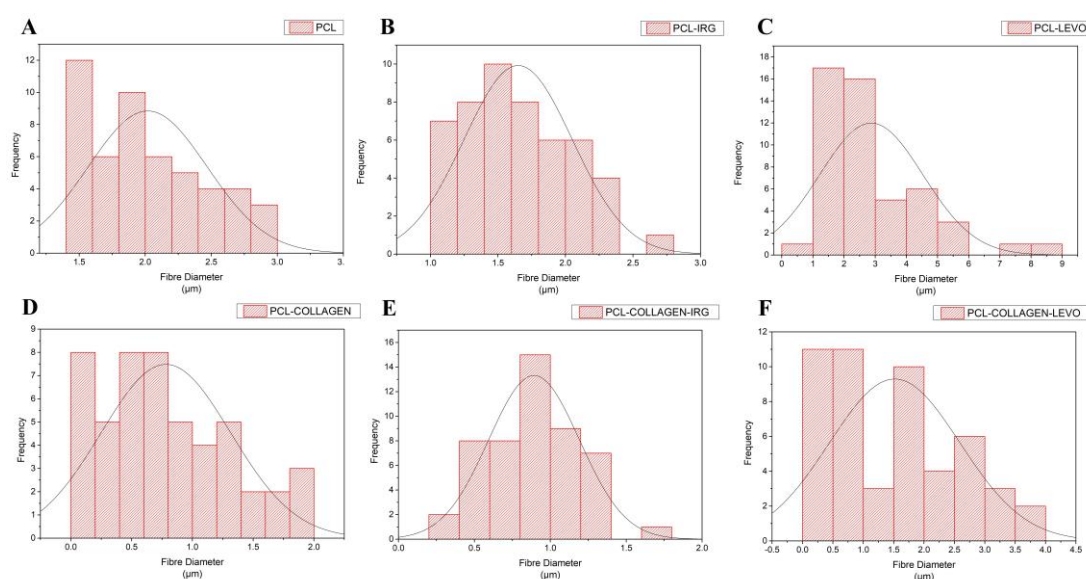
Figure 4.1 – Histograms of varying fibre diameters (a) PCL (b) PCL-IRG, (c) PCL-LEVO (d) PCL-collagen (e) PCL-collagen-IRG (f) PCL-collagen-LEVO

A one-way between-groups analysis of variance (ANOVA) indicated that there are significant differences ($p < 0.05$) between the investigated formulations. Applying Scheffé post-hoc comparison, significant differences were confirmed between samples

except for PLA compared with PLA-IRG and PLA-Collagen compared with PLA-Collagen-IRG. The latter was also corroborated by the overlap between the obtained confidence intervals; whilst in case of the other samples the confidence intervals are separated from each other. Except for PLA-Collagen-LEVO, 99.7 % of the measured fibre diameters fall between the range of mean $\pm$ 3 SD, and similarities of the mean and median values suggest that these samples are normally distributed (Figure 4.2).
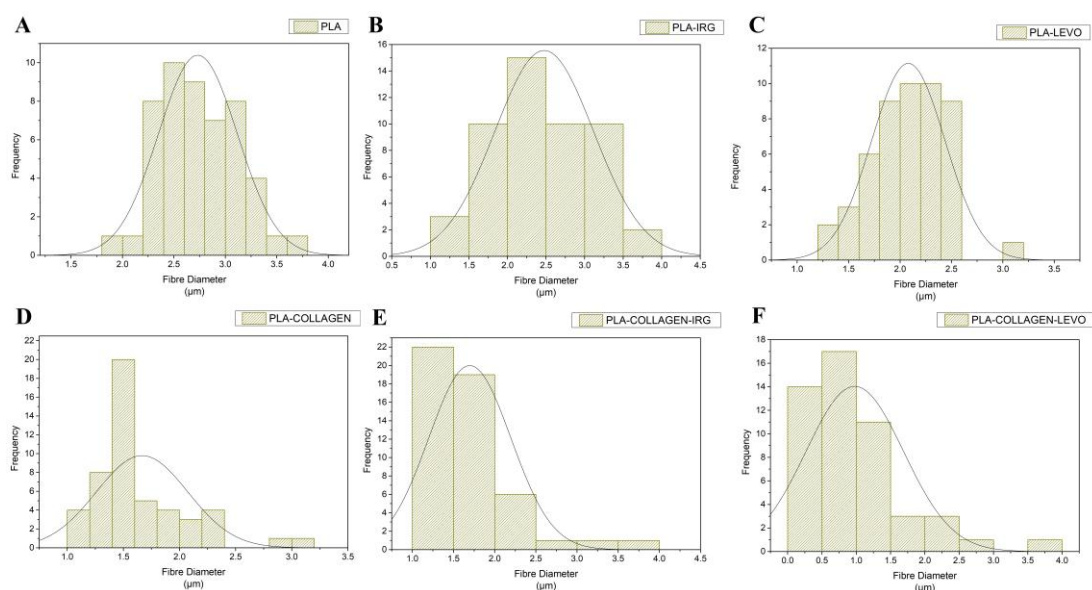
Figure 4.2 – Histograms of varying fibre diameters (a) PLA (b) PLA-IRG, (c) PLA-LEVO (d) PLA-collagen (e) PLA-collagen-IRG (f) PLA-collagen-LEVO

Fibre diameter histograms were assayed using Kolgomorov-Smirnov test ($p<0.05$) of equality of distributions, which indicated that there is no significant difference, when PLA compared with PLA-IRG; and PLA-Collagen compared with PLA-Collagen-IRG. On the other hand, distributions of PLA/PLA-IRG; PLA-Collagen/PLA-Collagen-IRG; PLA-LEVO; PLA-Collagen-LEVO were significantly different when compared with each other. It must be noted that PLA-Collagen-LEVO exhibited the

highest coefficient of variation (72.7 %), whilst PLA-LEVO had the lowest value (17.2 %) (Appendix B).
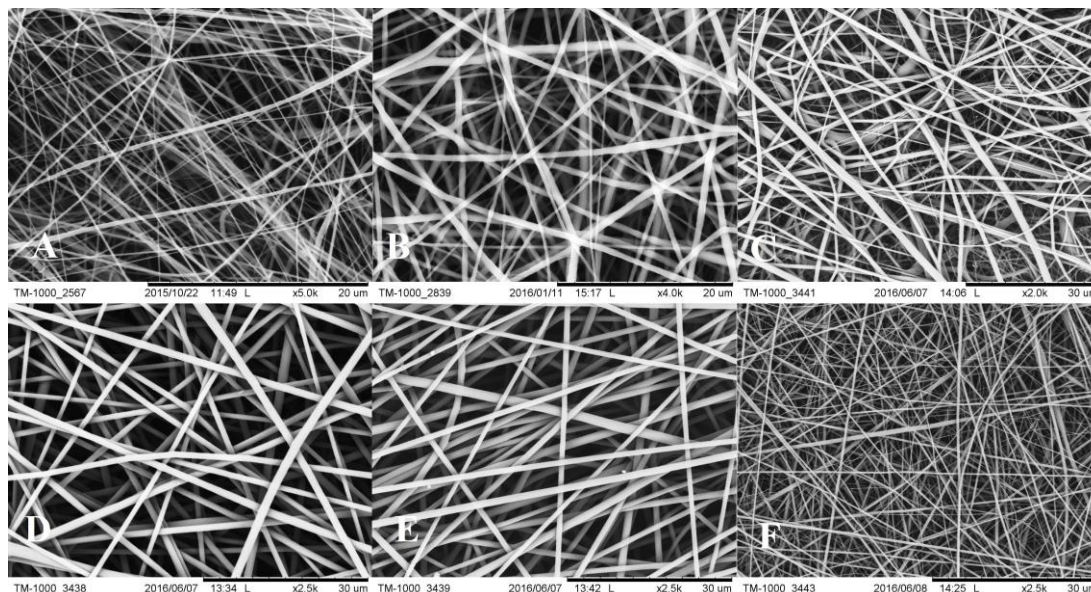
Figure 4.3 – SEM images of PCL and PLA fibres. (a) PCL-collagen (b) PCL-collagen-IRG (c) PCL-collagen-LEVO (d) PLA-collagen (e) PLA-collagen-IRG (f) PLA-collagen-LEVO

The SEM images (Figure 4.3) demonstrated a range of morphologies across both polymer-drug and polymer-collagen-drug electrospun scaffolds. Images revealed a significant change in fibre morphology for PCL-Collagen (Figure 4.3a), showing visibly thinner fibres. The addition of IRG appeared to create thicker fibres with a smooth morphology, however closely resembled a similar structure of fibres compared with the PCL-Collagen sample. The PLA-Collagen scaffolds (Figure 4.3d – 4.3f) showed a significant change in fibre morphology when compared with the original PLA samples – there is less tortuosity to the fibres and a visible reduction in fibre thickness. The addition of LEVO to the PLA-Collagen fibres caused a thinner, more fibrous network (but a wider distribution of fibre diameter).

The AFM images (Figure 4.4) show the morphology of the fibres at a greater detail and resolution. Presence of collagen can be observed within the PCL-Collagen sample (Figure 4.4a), with what appears to be small fibres moving horizontally across the fibre surface. The surface morphology for the PLA-collagen-drug scaffolds (Figure 4.4d – 4.4f) showed the presence of collagen "wrapping" the polymeric fibres in a helical manner. This morphology was consistent throughout, which may highlight a helical coating of the collagen through the fabricated scaffolds. There appeared to be no presence of drug on the surface of these fibres.
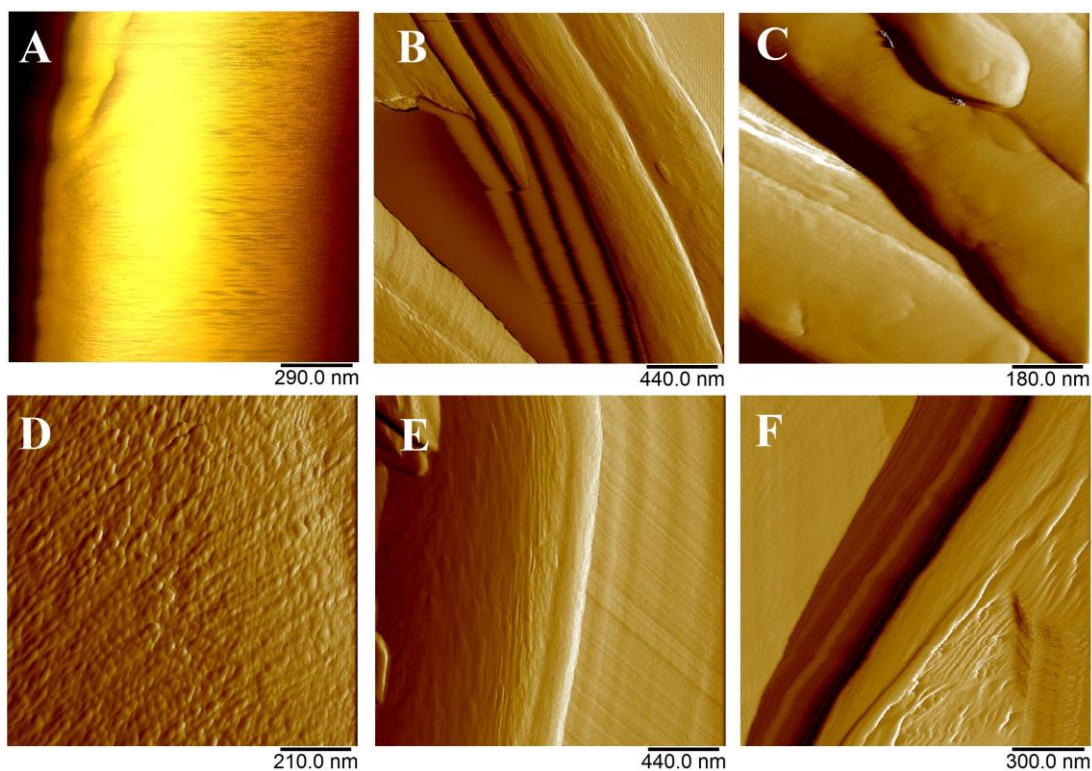
Figure 4.4 – AFM images of PCL and PLA fibres. (a) PCL-collagen (b) PCL-collagen-IRG (c) PCL-collagen-LEVO (d) PLA-collagen (e) PLA-collagen-IRG (f) PLA-collagen-LEVO

4.3.2 Solid State Characterisation

PCL

IR Spectra for PCL and PCL-collagen with IRG and LEVO is shown in Figure 4.5. Initial IR spectra was taken for IRG and LEVO before sampling the drug-loaded PCL samples. It can be observed that for IRG, there is a peak occurring at ~3250 cm^{-1} which is typically the O-H stretching, and a range of peaks ranging from ~1600 – 1400 cm^{-1}, that corresponds to the C-C stretching of the benzene rings of IRG (structure of IRG shown in Chapter 2) (Celebioglu et al. 2014). The IR spectra for LEVO indicates main peaks for the –COOH (carboxylic acid) functional group at 3240 cm^{-1} (stretching and bonding), stretching vibration for C=O at ~1650 cm^{-1} and ~780 cm^{-1} for the C-F peak (Mouzam et al. 2011). For the drug-loaded PCL samples, prominent peaks at ~3000 cm^{-1} and ~2900 cm^{-1} are representative of asymmetric and symmetric CH$_2$ stretching, and at ~1700 cm^{-1} there is a strong peak that is indicative of C=O (carbonyl) stretching (Elzein et al. 2004).
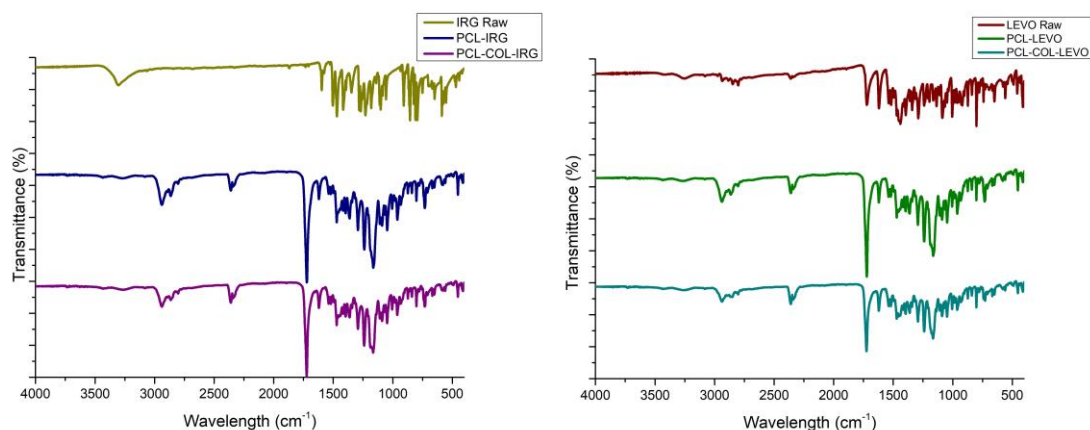
Figure 4.5 – IR spectra results (a) IRG, PCL-IRG, PCL-collagen-IRG (b) LEVO, PCL-LEVO, PCL-collagen-LEVO

Examination of the raw collagen (Figure 4.6) used within the electrospinning process revealed a thermal event at ~65°C, an endothermic peak at ~130°C, and a final exothermic peak at ~190°C. The DSC data shown for the PCL-Collagen samples, in Figure 4.7, shows a change in the sharpness of the exothermic reaction occurring at ~ 65°C. PCL-Collagen-IRG and PCL-Collagen-LEVO samples exhibited similar behaviour to PCL-drug samples, with a T_m of 60°C. XRPD data of PCL-Collagen samples were inconclusive in displaying potential interactions between PCL and collagen due to the high noise from the polymeric sample.
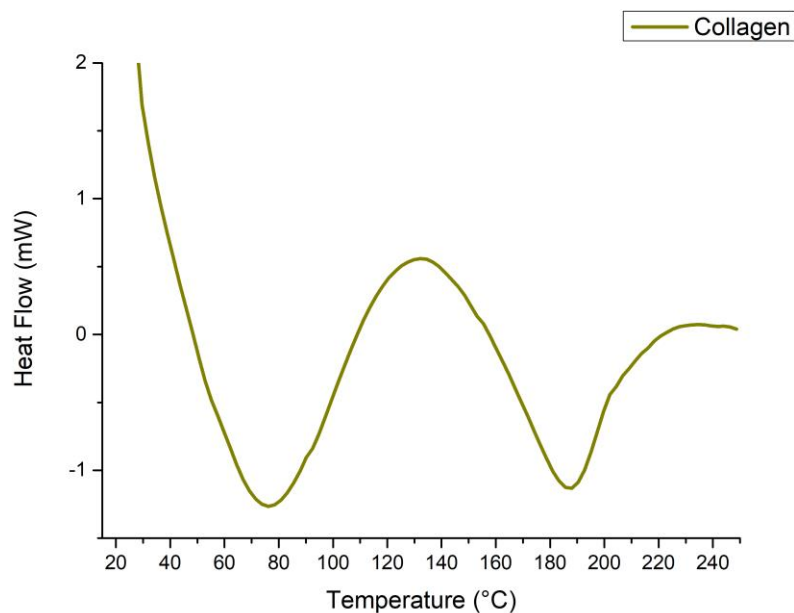
Figure 4.6 – DSC thermogram of raw collagen
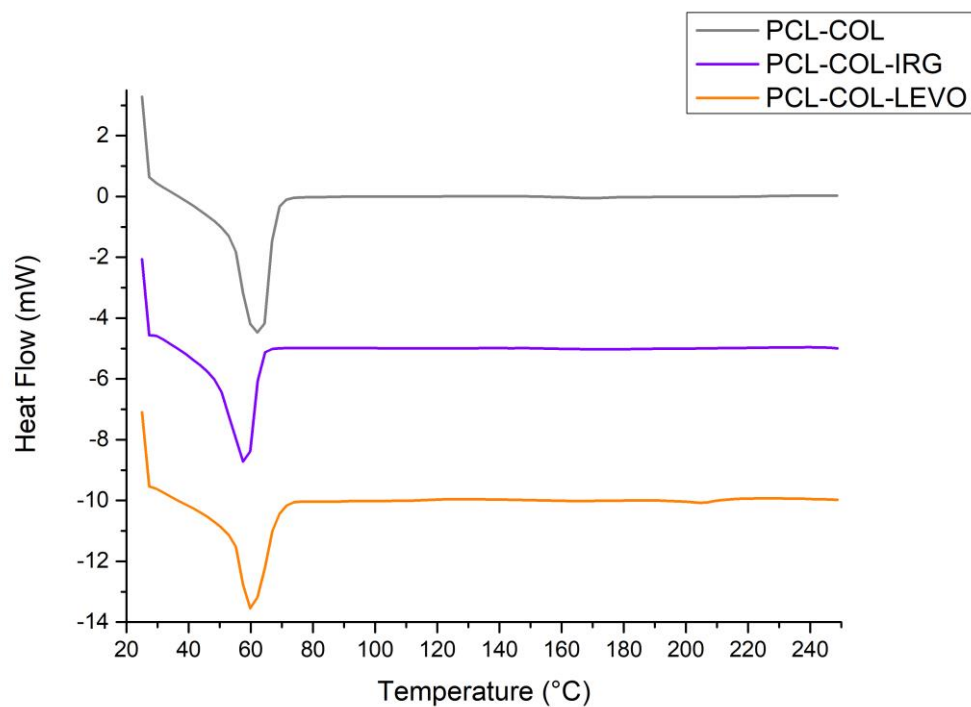
Figure 4.7 – DSC thermograms of PCL-collagen, PCL-collagen-IRG and PCL-collagen-LEVO

PLA

IR Spectra for drug-loaded scaffolds of PLA and PLA-collagen are shown in Figure 4.8. The spectrum for PLA shows strong peaks at ~1750 cm^{-1} and 1200 – 1100 cm^{-1}, which are indicative of C=O stretching and O-C=O stretching. There are also polymeric peaks for PLA occurring at ~2350 – 2250 cm^{-1} and ~3000 – 2750 cm^{-1}, which are characteristic of CH$_3$ stretching and C=O stretching overtones (Orozco et al. 2009).
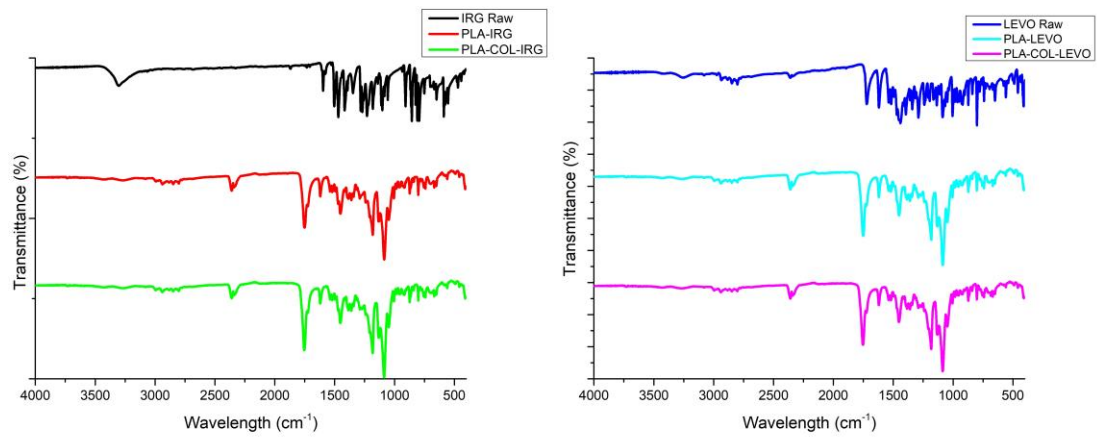
Figure 4.8 – IR spectra results (a) IRG, PLA-IRG, PLA-collagen-IRG (b) LEVO, PLA-LEVO, PLA-collagen-LEVO

The graphs in Figure 4.9 indicate the various DSC isotherms for PLA-Collagen, PLA-Collagen-IRG, and PLA-Collagen-LEVO fibres. For most of the samples, the glass transition temperature is observed below 60°C, the crystallisation temperature (T_c,), an endothermic peak, is observed around 115°C and the melting point, an exothermic peak, is observed at ~145°C.
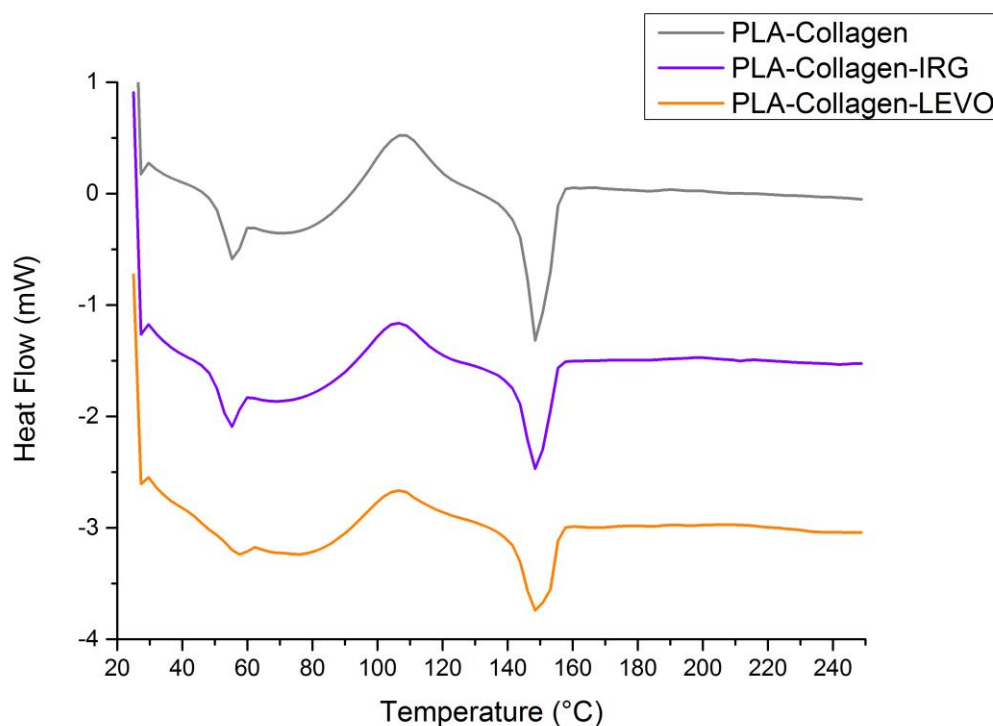
Figure 4.9 – DSC thermograms for PLA-collagen, PLA-collagen-IRG and PLA-collagen-LEVO

XRPD data shown in Figure 4.10 and 4.11 indicate that PLA fibres are semi-crystalline, indicated by broad region, followed by a sharp peak at ~17°. It can be observed in Figure 4.8 that the addition of IRG causes an increase in the crystallinity of the polymer-drug sample, due to the sharp polymer peak at ~17°. There are no significant peaks arising within the PLA-IRG graph related to the IRG intensity. The PLA-collagen-IRG graph indicates that the sample is in an amorphous state, due to the very broad peak observed from ~5° to ~25°. The graphs relating to the PLA-LEVO sample (Figure 4.11) show two significant peaks at ~7° (relating to levofloxacin) and ~17° (relating to PLA). Again, the addition of collagen to these samples resulted in a broad amorphous peak ranging from ~5° to ~25°.
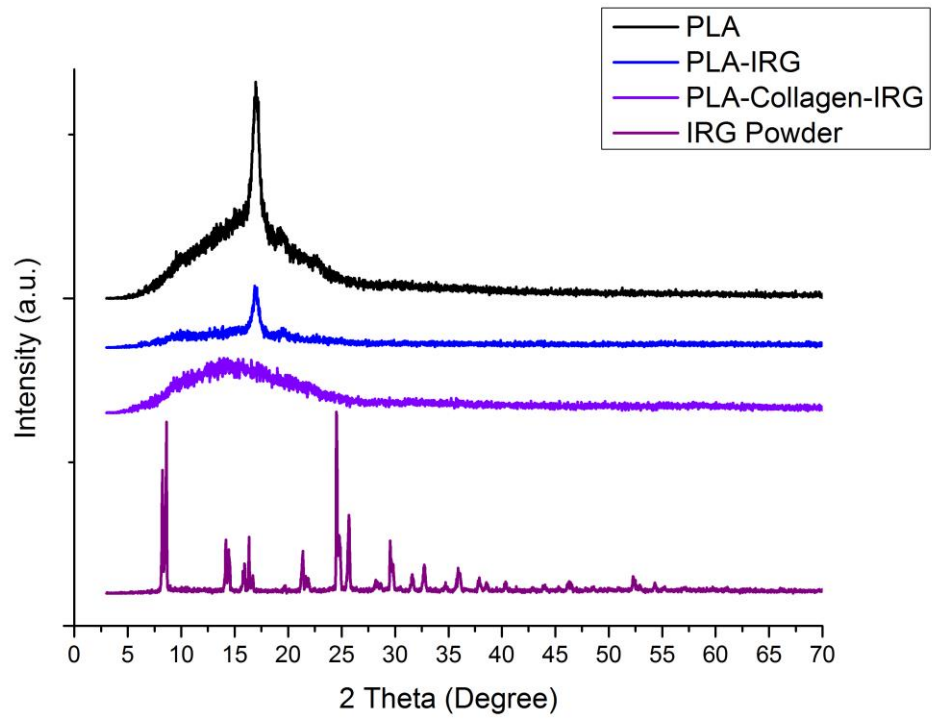
Figure 4.10 – XRPD curves for PLA, PLA-IRG, PLA-collagen-IRG and IRG powder
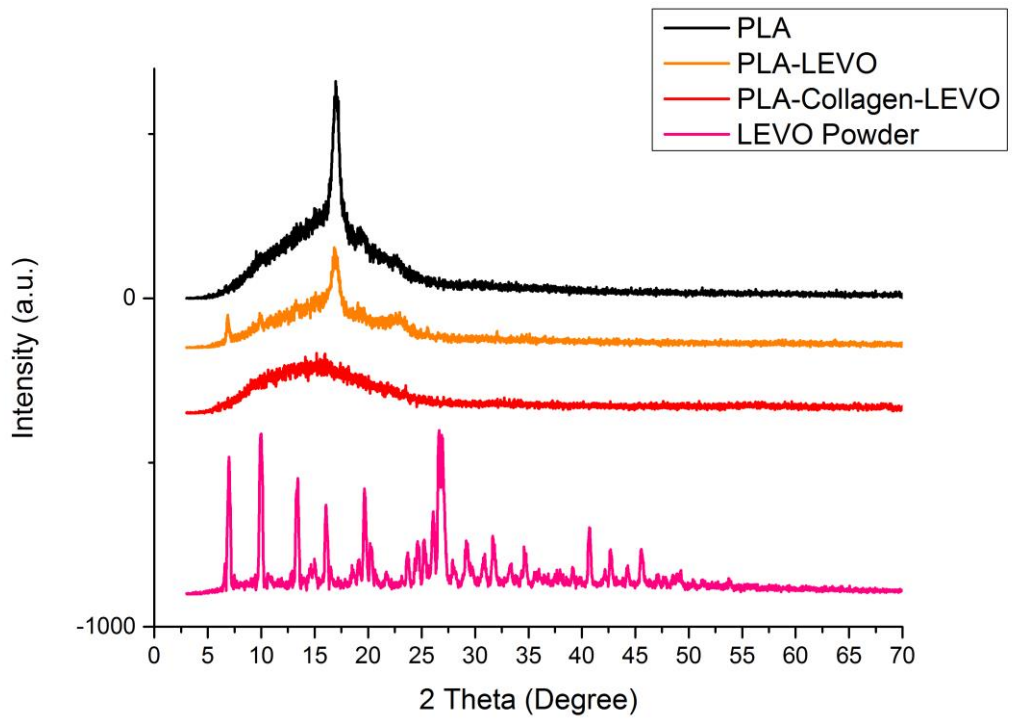
Figure 4.11 – XRPD curves for PLA, PLA-LEVO, PLA-collagen-LEVO and LEVO powder

4.3.3 Surface Analysis

The dispersive surface energy of powder irgasan was measured at 37.32 mJ/m^2, and a BET specific surface area of 0.0103 m^2/g. Levofloxacin had a higher dispersive surface energy of 47.34 mJ/m^2 and a BET specific surface area of 0.0481 m^2/g (table 4.1).

Table 4.1 – Table displaying dispersive surface energy data, density and surface area values for IRG and LEVO

	Disp. Surf. En. (mJ/m^2)					
	Stz & Max	Stz & Com	DnG & Max	DnG & Com	Density (g/cm^3)	Surface Area (m^2/g)
Irgasan	37.32	23.2	38.2	23.54	1.48	0.0103
Levofloxacin	47.34	48.23	48.43	49.33	1.49	0.0481

PCL contact angle data is shown in Figure 4.12 – it can be observed that the PCL-Collagen has increased in hydrophobicity, increasing from a starting angle of ~ 80° (PCL) to ~ 130°. PCL-Collagen-IRG had a similar starting contact angle with PCL-IRG (~ 110°), however showed a smaller slope in gradient, which is representative of a slower uptake of the water droplet. PCL-Collagen-LEVO exhibited a similar behaviour to PCL-LEVO, with a rapid uptake of water occurring within the first 4 min.
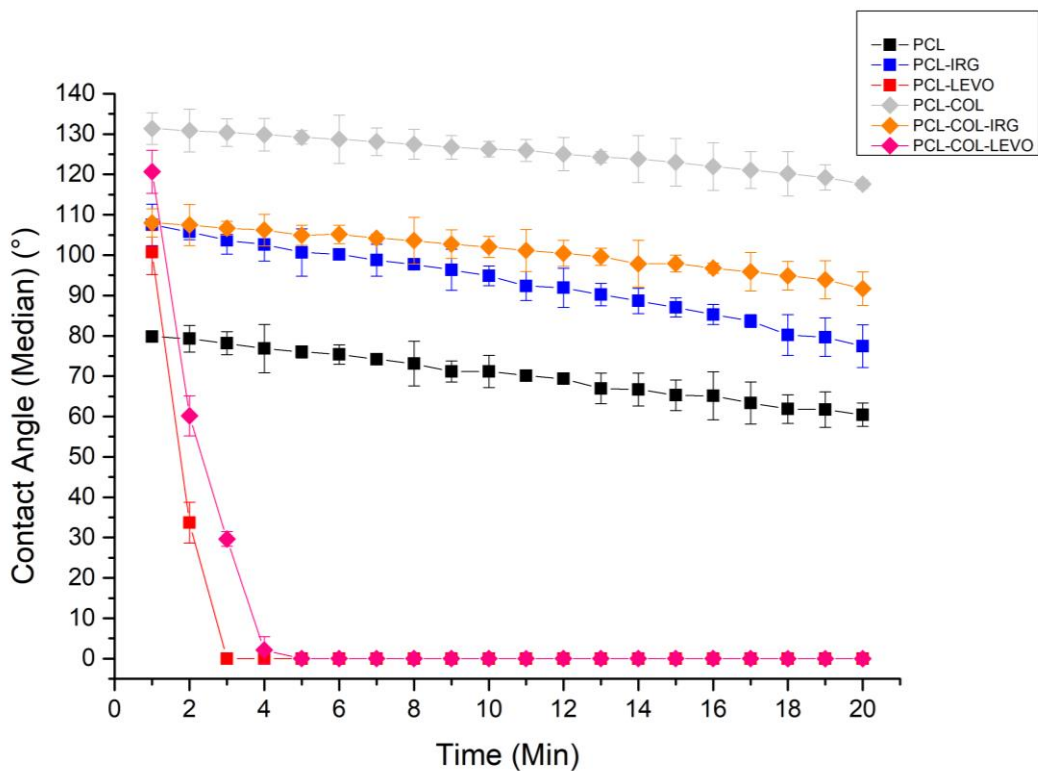
Figure 4.12 – CAG graph showing the contact angle median values versus time for PCL, PCL-IRG, PCL-LEVO, PCL-collagen, PCL-collagen-IRG and PCL-collagen-LEVO (*n=3*)

The contact angle measurements shown in Figure 4.13 highlight the differences across PLA-drug and PLA-collagen-drug combinations; PLA-LEVO had a lower overall starting and finishing contact angle (108° to 50°, respectively), compared with the PLA and PLA-IRG (120° to 80°, respectively). The samples containing collagen had a greater starting contact angle (130°) and final contact angle reading (120°).
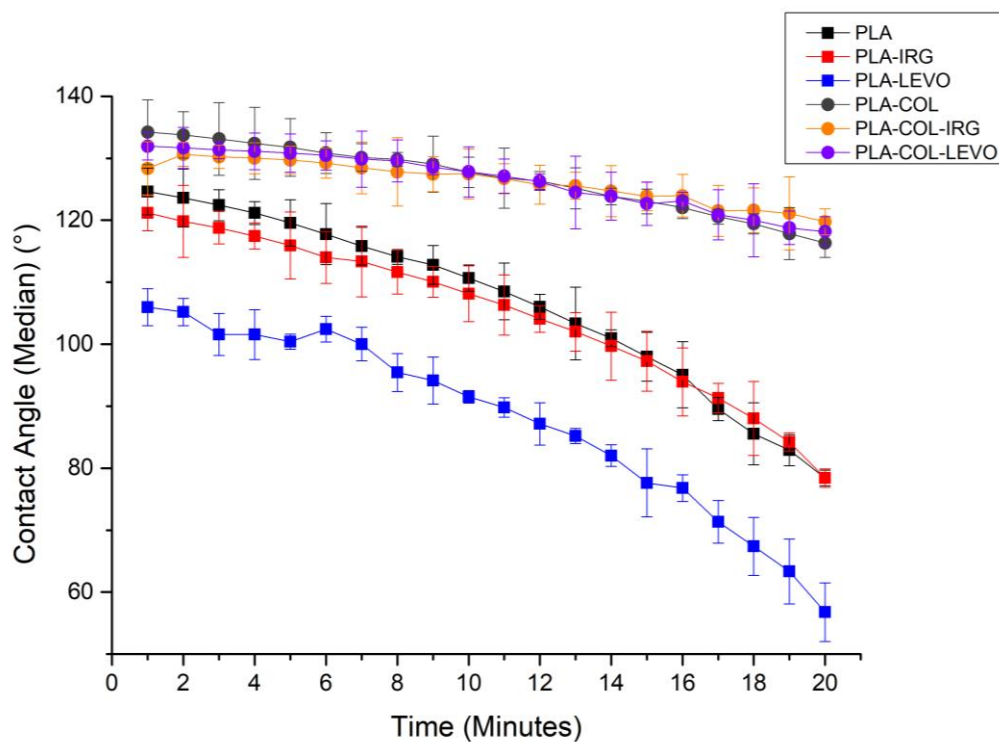
Figure 4.13 – CAG graph showing the contact angle median values versus time for PLA, PLA-IRG, PLA-LEVO, PLA-collagen, PLA-collagen-IRG and PLA-collagen-LEVO (*n=3*)

4.3.4 Drug Efficacy of Collagen-Polymer Solutions

The cumulative drug release profiles are presented in Figure 4.14; both PCL-collagen-IRG and PLA-collagen-IRG samples exhibited sustained release behaviour over 192 h, with a final release of ~35% and ~40%. PCL-collagen-LEVO exhibited burst release behaviour, releasing ~10% within the first 24 h of measurement. PLA-collagen-LEVO showed a significantly low release percentage initially, however it appeared to exhibit sustained release behaviour, with a final cumulative release of 25%.
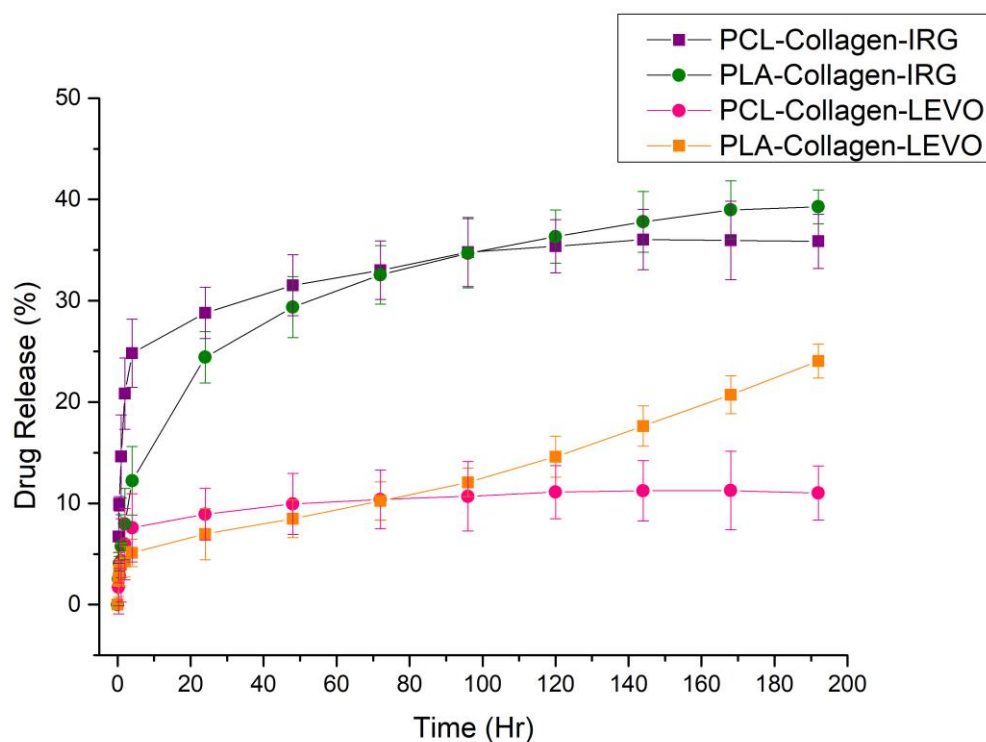
Figure 4.14 – *In vitro* release rate data for PCL-collagen-IRG, PCL-collagen-LEVO, PLA-collagen-IRG and PLA-collagen-LEVO (*n=6*)

4.3.5 ToF-SIMS

The diagnostic peaks for both the APIs in the PLA-collagen-API samples presented normalized intensities which are 2 to 3 times lower than the corresponding peaks in the PLA-API samples, making it difficult to comment on their distribution. The reduced signal could be caused by matrix effects, an artefact of ionization. Here, it is possible that the presence of collagen in the system suppressed the ionization of the APIs. Alternatively, it could suggest a lower concentration of the APIs present on the surface of the PLA-Collagen fibres compared to the PLA ones, and could be interpreted as a better embedding of the APIs into the strands.
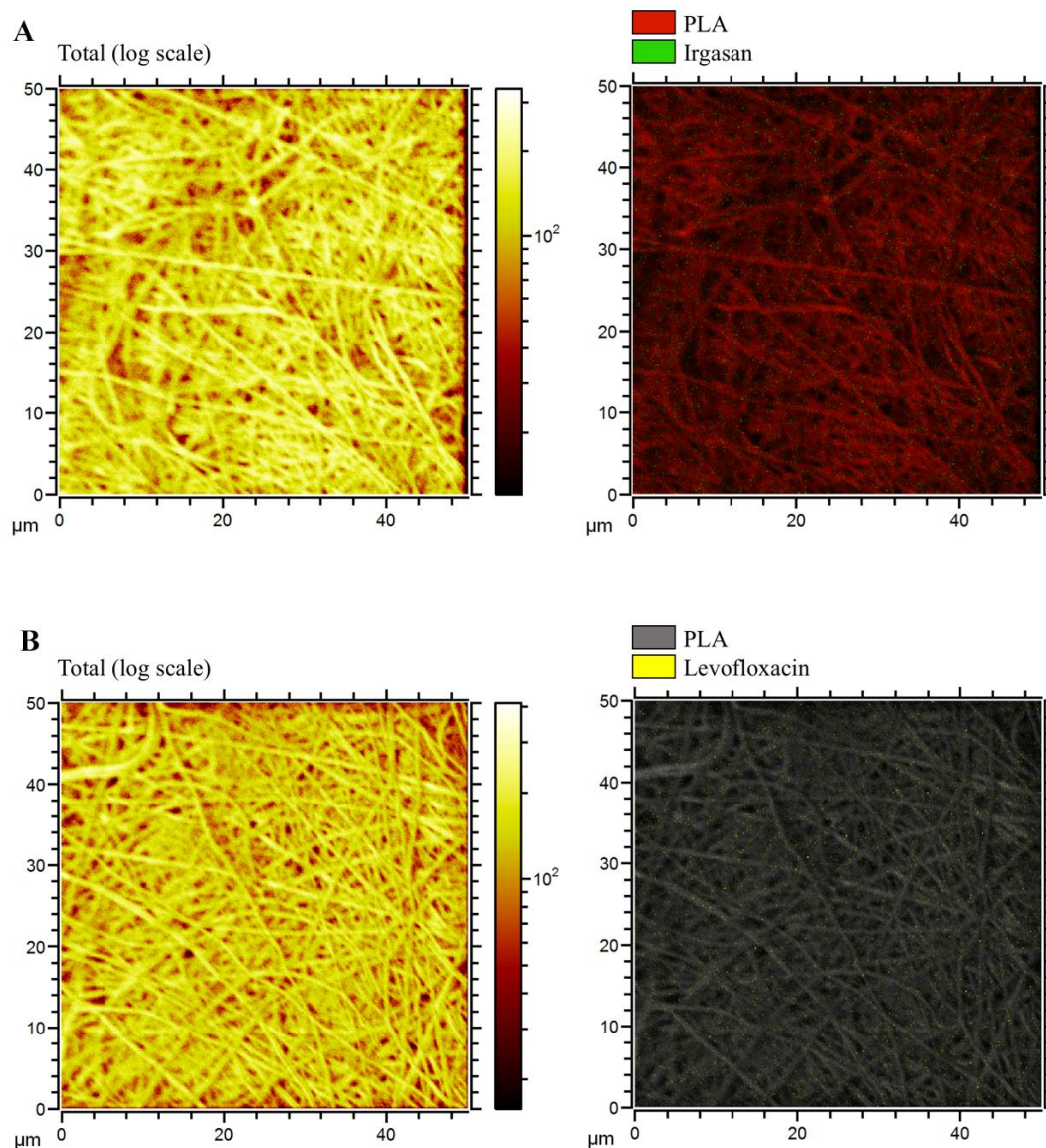
Figure 4.15 – ToF-SIMS images of drug distribution (a) PLA-collagen-IRG (b) PLA-collagen-LEVO

4.3.6 Tensile Testing

For samples without collagen, the addition of both IRG and LEVO caused a decreased in the tensile strength (PCL = 12.06 ± 0.24 MPa, PCL-IRG = 3.25 ± 0.21 MPa, PCL-LEVO = 3.33 ± 0.94 MPa) and a decrease in the elasticity (PCL = 17.5 ± 0.24 MPa, PCL-IRG = 13.01 ± 0.13 MPa, PCL-LEVO = 6.88 ± 0.76 MPa). For samples that contained collagen, the tensile strength was the same for PCL-collagen and PCL-

collagen-LEVO (7.86 ± 0.92 MPa and 7.81 ± 0.33 MPa); with PCL-collagen-IRG, the lowest of all PCL samples at 1.91 ± 0.40 MPa. PCL-collagen-LEVO showed an increase in elasticity compared with PCL-collagen (4.02 ± 0.25 MPa to 12.88 ± 0.11 MPa).
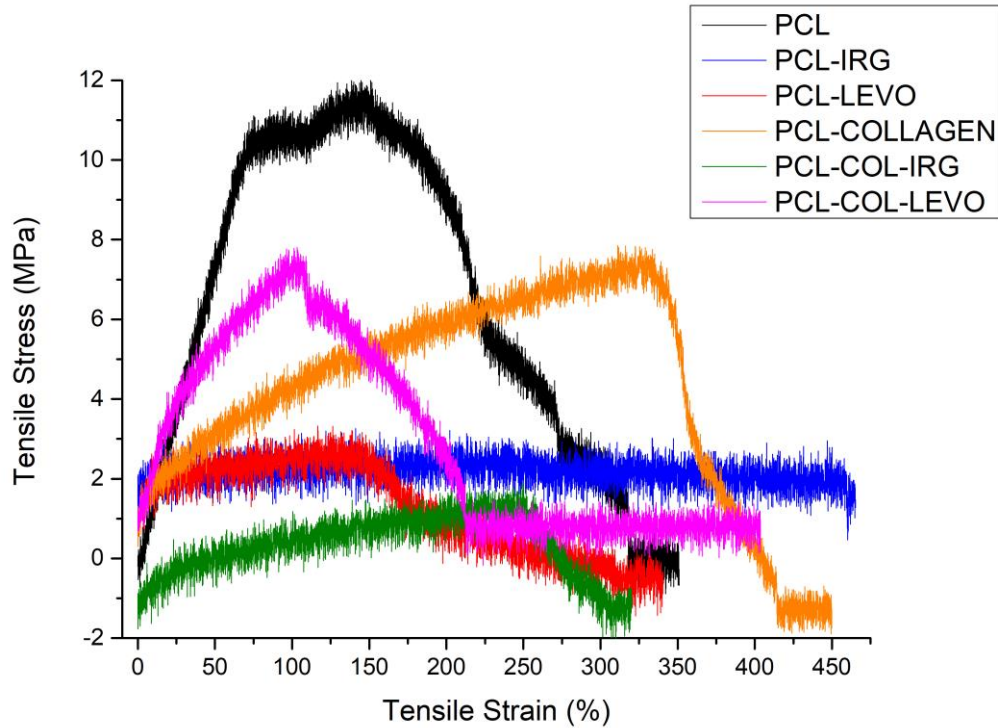
Figure 4.16 – Stress-strain curve for PCL, PCL-IRG, PCL-LEVO, PCL-collagen, PCL-collagen-IRG and PCL-collagen-LEVO

PLA samples without collagen showed an increase in tensile strength between PLA and PLA-LEVO (2.32 ± 0.49 MPa to 4.82 ± 0.64 MPa). PLA-IRG demonstrated the lowest tensile strength of 1.21 ± 0.18 MPa. It was observed that the elasticity increased with the addition of IRG and LEVO (PLA = 20.21 ± 0.66 MPa, PLA-IRG = 37.1 ± 0.35 MPa, PLA-LEVO 49.18 ± 0.19 MPa). PLA samples containing collagen showed an increased tensile strength (compared with PLA only samples): PLA-collagen = 5.6

± 0.77 MPa, PLA-collagen-IRG = 7.13 ± 0.53 MPa, and PLA-collagen-LEVO = 5.23

± 0.44 MPa. However, it appears that the elasticity of the samples decreases due to the

addition of IRG and LEVO (PLA-collagen = 91.04 ± 0.87 MPa, PLA-collagen-IRG =

66.3 ± 0.34 MPa, and PLA-collagen-LEVO = 31.51 ± 0.24 MPa) [a full table of

mechanical property values can be found in Appendix C].
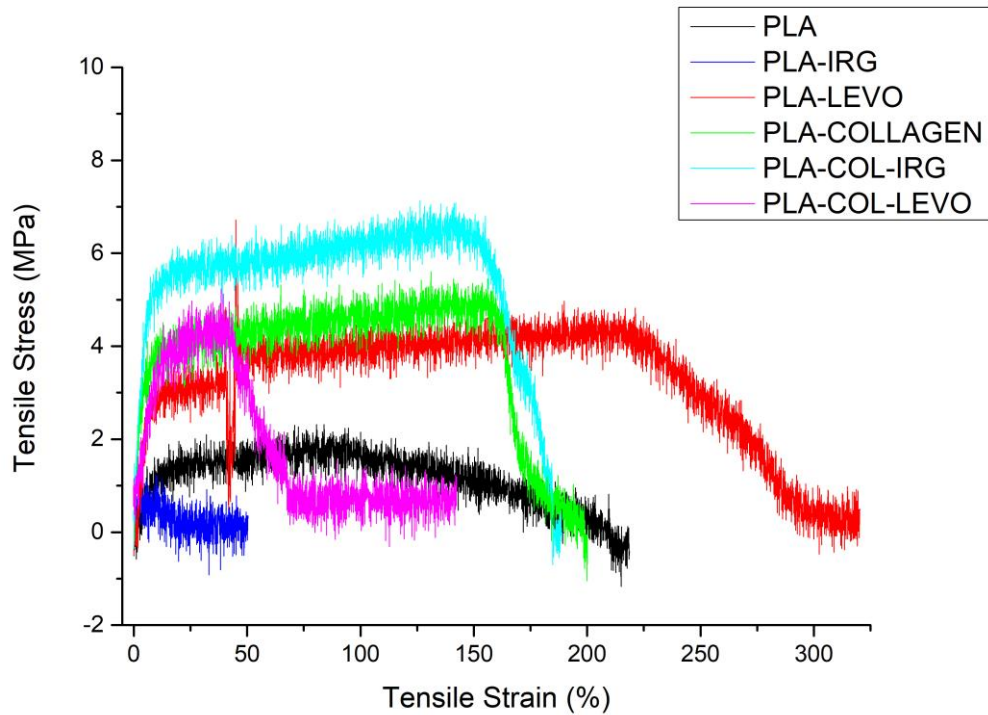
Figure 4.17 – Stress-strain curve for PLA, PLA-IRG, PLA-LEVO, PLA-collagen, PLA-collagen-IRG
and PLA-collagen-LEVO

4.4 Discussion

4.4.1 Fibre Morphology

It is clear that the addition of Type I collagen to PCL caused a significant difference

to the fibre morphology, the fibres for PCL-collagen appearing (and confirmed through

fibre diameter analysis) to yield the smallest fibres (782 nm). The addition of IRG and LEVO caused an increase in fibre diameter, and this may be due to an increase of the solution viscosity (the addition of IRG and LEVO to PCL solutions previously indicated this in Chapter 3) (Chakrapani et al. 2013). Compared with other PCL-collagen studies, the fibres produced here are fairly similar, with some studies demonstrating fibre diameters of 700 nm, 500 nm and 750 nm (Hartman et al. 2011; Badrossamay et al. 2014; Powell & Boyce 2009). The addition of LEVO caused the highest coefficient of variance amongst the PCL fibres, which suggests that this drug is similarly affecting the electrospinning process (similar to PCL-LEVO, Chapter 3) – it can therefore be inferred that there are issues regarding the specific interaction (or lack thereof) between PCL and LEVO, given that different solvents (chloroform/DMF and HFP) were used for the different formulations.

Although there is seemingly an interaction between the PCL and collagen, the AFM images did not reveal the same type of collagen banding observed for the PLA-collagen samples. However, there is evidence of what could possibly be collagen, moving horizontally across the polymer fibre. Given that there is evidence of an interaction between PCL and collagen (section 4.42) this may be the case, although they appear to be far smaller than typical collagen banding of 67 nm (Matthews et al. 2002).

The differences in fibre form between PLA-drug and PLA-collagen-drug samples can be clearly seen in Figure 4.3, where the addition of collagen has created smaller diameters of the fibres. This is due to the nature of collagen fibre formation, which usually form nanofibres of around 100 nm (Matthews et al. 2002). Although, the fibres

created in this study are significantly bigger than other studies (e.g. average collagen fibres diameters = ~400 nm (Buttafoco et al. 2006)) this may be largely due to the blend of PLA and collagen – with PLA-drug solutions producing fibres with a diameter greater than 2 µm. Fibre formation may also be more effective with collagen, due to the HFP solvent; the low boiling point (58.2 ºC) of this solvent allows for a quicker evaporation during the electrospinning process, which in turn means that the fibres are being deposited in a dry state. HFP is also a denaturing organic solvent, and therefore the interaction between solvent and collagen may cause change in the structure of the proteins (Guo et al. 2013). When compared to polycaprolactone fibres electrospun in similar conditions, the addition of levofloxacin increased the overall average fibre diameter (PCL = ~1.83 µm (Del Valle et al. 2011) PCL-LEVO = ~2.8 µm (shown in Chapter 3)).

It was also observed that the addition of levofloxacin within both PLA and PLA-collagen blends resulted in a decreased average fibre diameter; this can be linked to the rheological behaviour of the solutions where levofloxacin altered the viscosity of the solution, which normally results in a change in fibre size (Song et al. 2012). There also appears to be evidence of levofloxacin appearing at the surface of the fibres for the PLA-LEVO sample, however this may be expected for this particular drug due to the high dispersive surface energy (see Results: Surface Analysis). If the drug has a high surface energy, this affects the viscosity of the solution, which in turn alters the surface tension.

The AFM images of the PLA-collagen blends revealed a helical pattern of collagen around the fibres – the fibrils of collagen exhibit a repeating, nano-banding pattern.

Collagen naturally forms a coiled structure, and the underlying alpha chains within the collagen fibrils could be responsible for the repeating banding pattern observed (Barnes et al. 2007). This may be useful within a tissue engineering context, given that this repeat banding is thought to expose a binding site in the native collagen fibril that enhances cell adhesion and migration (Sell et al. 2009).

4.4.2 Solid State Characterisation

IR spectra were taken in order to characterise the functional groups for the polymers and drugs used in this study. IR spectra were taken for the raw collagen sample, however due to the nature of this material the results were inconclusive. However, from literature the typical bands for collagen are N-H stretching (3068 cm^{-1}, for Amide A), C=O stretching ($1700 - 1600 \text{ cm}^{-1}$, for Amide B) and N-H deformation ($1550 - 1500 \text{ cm}^{-1}$) for Amide I (Venugopal et al. 2005). These bands were difficult to observe within the IR data due to both IRG and LEVO having strong bands at similar wavelengths.

The DSC data was vital in understanding any potential chemical interactions between the drug and polymer. With the PLA-IRG plot, it shows that there is no visible exothermic reaction (T_c) occurring after the initial glass transition phase, and also no indication of the T_m of the raw IRG drug at around 60 °C – this can interpreted as the IRG being fully integrated within the polymeric structure (Kayaci et al. 2013). The T_c values recorded were greater in the samples containing collagen which may be attributed to dehydration of the collagen (Bozec & Odlyha 2011). This may be indicative of the collagen successfully embedding or interacting with the polymer. A reduction in the T_g at around 60 °C of the PLA-Collagen-LEVO can be observed,

which again may indicate that there is no presence of free LEVO particle in this sample – this is perhaps why a sustained release behaviour is observed in section 4.4 (drug efficacy).

The data presented by the DSC was effectively confirmed through the XRPD data. The PLA-IRG sample can be seen to remain in a near semi-crystalline form (slight broad peak, followed by sharp crystalline PLA peak), with no IRG peaks. It can be concluded from this that the IRG is fully embedded within the polymeric network. Similarly, no IRG peaks were visible within the PLA-collagen-IRG graph; however, the broad peak does indicate that the material is in an amorphous form. The PLA-LEVO graph showed a peak, indicating that the drug is still in crystalline form and is not incorporated uniformly into the polymeric network. A similar amorphous peak was observed in the PLA-collagen-LEVO peak, which may indicate a better encapsulation of drug.

4.4.3 Surface Analysis

Understanding the surface energy of the drug molecules was an important part of this study, since it has successfully helped to understand the reasons behind particular behaviour relating to fibre morphology and overall drug encapsulation. The surface energy analysis of the two drugs indicated a higher dispersive surface energy for levofloxacin compared with irgasan. Given these two drugs are both originally found in a crystalline form, and that polylactic acid is naturally semi-crystalline, there may be an increased possibility of the two drugs integrating into the polymeric matrix. The two drugs may require a higher energy in order to disperse properly within the PLA polymeric structure. With irgasan having a lower dispersive surface energy and a

hydrophobic nature, there may be a reduced energy requirement for this drug to properly disperse within a solvent solution. If levofloxacin has a higher dispersive surface energy, then the transfer of energy between LEVO and solvent will be insufficient to overcome the drug-drug attractions. Therefore, not all the levofloxacin molecules in solution will be surrounded by solvent molecules and dispersed fully into solution (Shah et al. 2014). At equilibrium, hydrophobic molecules preferentially partition into the organic phase, typically due to a high log P value (Vorng et al. 2016) - the log P of levofloxacin is 1.27 (Drugbank 2008) and the log P of Irgasan is 4.76 (Anon 2008). Based on the positive values on the log P, both drugs are hydrophobic and Irgasan is more hydrophobic than LEVO. With both drugs and PLA exhibiting a hydrophobic nature, this suggests that hydrophobic interactions might occur between the materials. If the hydrophobic interactions are a dominant, this should be more advantageous in increasing encapsulation efficiency (Jeyanthi et al. 1997).

The change in contract angle may reflect the encapsulation of both drugs within the polymer matrix. It can be clearly seen in Figure 6 that the contact angle was lowest for the PLA-LEVO sample. This can be attributed to the lower hydrophobic nature of levofloxacin, the high dispersive surface energy and the probability of the drug on the surface of the fibres (see Results: Fibre Morphology, AFM). With the PLA-collagen-drug samples, the contact angles are greater, implying that the samples are more hydrophobic. These results differ from the contact angle measurements in other studies, in particular collagen is found to have previously increased the hydrophilicity of PLA samples (Ahmed et al. 2015). It may be the case that the collagen fibrils have interacted within the polylactic acid based nanofibre. This strong hydrophobic connection may be linked to the better integration of both irgasan and levofloxacin.

4.4.4 Drug Efficacy of Polymer-Collagen Solutions

The release profiles of both irgasan and levofloxacin are similar to the results in a previous study using *polycaprolactone* (Hall Barrientos et al. 2016). However, the final cumulative release percentages with Polylactic acid appear to be lower (Final PCL scaffolds drug release ~50%, PLA scaffolds ~20% to 40%). This may suggest a poorer drug encapsulation with PLA, which may be due to the fact that PLA is more hydrophilic than PCL (Patrício et al. 2013). The hydrophobic interactions between PLA and IRG may potentially be the cause of the sustained release behaviour *in vitro*, and the lower hydrophobic nature of LEVO may be an even further reduction in a strong polymer-drug interaction. As mentioned in the surface analysis section, the higher dispersive surface energy may cause this weak interaction between PLA and LEVO; AFM images indicated the possible presence of drug at the surface of the fibres. This presence of drug at the surface would result in a rapid uptake of water, and therefore be the reason behind the burst release behaviour observed *in vitro*. The addition of type I collagen to the polymer-drug samples resulted in a difference in release behaviour with LEVO – this drug released in a sustained release time profile, implying that collagen may be directly affecting the release of the drug. Literature evidence suggests that the hydrophilic, carboxyl functional groups in the polymer could be interact with basic functions expressed by the collagen (Cheng & Teoh 2004) which in turn results in a change in the hydrophobicity of the fibre, which may result in the sustained release time profile for the levofloxacin with the PLA-collagen sample.

4.4.5 ToF-SIMS Analysis

The ability to visualise the distribution of the APIs on the sample surface contributed to gain a better understanding about the degree of drug encapsulation and in general about the interactions between the drugs and the fibres. This result concurs with the suggested explanation concerning the release behaviour and is consistent with the results from the other techniques described in this Chapter. However, the results of PCL-collagen samples were not viable due to the level of noise observed in the results.

4.4.6 Mechanical Properties of Fibres

Similar to the rheological results in Chapter 3, the addition of IRG or LEVO appears to affect the mechanical characteristics of the polymeric samples. In particular, both PCL and PLA samples loaded with IRG generally demonstrated the lowest tensile strengths. This change in mechanical strength may be due to polymer-drug interactions, and generally higher drug loading (IRG at 1%, and LEVO at 0.5%) equates to a greater decrease in mechanical properties (Chou & Woodrow 2017). For the PCL-collagen samples there appeared to be no increase in either tensile strength or elasticity, however increases were observed in PLA-collagen samples. This may be attributed to the polymer-collagen (demonstrated in section 4.4.2) interaction occurring in PLA-collagen samples – XRPD results showed that PLA-collagen samples were amorphous in structure, and amorphous polymers generally deform in an elastic manner (Anon 2017).

4.5 Conclusion

It can be seen that the inclusion of type I collagen significantly altered various characteristics of electrospun polymer-drug scaffolds. The addition of collagen caused an overall decrease in fibre morphology and average fibre diameter across both sets of drugs, irgasan and levofloxacin, with nanofibers forming in the PLA-collagen-LEVO samples. AFM images revealed collagen fibril banding on the surface of the fibres, which suggest there is an interaction between the polymer-drug and collagen. There were also changes in the solid-state characteristics of the samples, given that the DSC results indicate an increase in amorphousness of the polymer-drug-collagen samples, and this was confirmed through typically broad peaks in the XRPD results. Most interestingly, the surface energies of the scaffolds were modified with an increase in the hydrophobicity of the polymer-collagen-drug noted. In particular, the PLA-collagen-LEVO sample showed a high deal of hydrophobicity, which was unusual given the low hydrophobic nature of LEVO – this could potentially be attributed to the strong hydrophobic interactions between the PLA and the hydrophobic banding in collagen fibrils, resulting in better encapsulation of the drug. Finally, the drug release profiles of the samples appear to change due to the inclusion of collagen, most significantly demonstrating the shift of the burst release behaviour in PLA-LEVO to sustained release behaviour within PLA-collagen-LEVO samples. This study is important in demonstrating that the modification of electrospun scaffolds can be achieved by incorporating natural polymers, such as collagen – and this modification may be useful in the compatibility and utilisation of tissue engineered structures within the human body.

Chapter 5: Biological Performance of Electrospun Fibres

5.1 Introduction

The two previous Chapters have been important in showing that the fabrication of drug-loaded scaffolds can be achieved using the process of electrospinning. However, despite the various characterisation methods one can perform on these scaffolds, there is a significant importance in understanding and measuring the biological response. In particular, ideal scaffolds for tissue engineering should be biocompatible, biodegradable, promote cell adhesion, proliferation and maintain the metabolic activity of cells (Sivashankari & Prabaharan 2016). With the use of materials such as PCL, PLA and collagen sufficiently satisfying the biocompatible and biodegradable requirement, measuring the adhesion, proliferation and metabolic activity of cells remains the final, but crucial, aspect of this project. Another important biological requirement is efficiently supressing the possibility of bacterial infections at the site of scaffold implant. Controlling the bacterial infection is a vital pre-requisite to any potential cell growth, given that the cells will not proliferate or function in the presence of bacteria such as *Staphylococcus aureus* or *Escherichia coli* (Wang et al. 2010).

S. aureus is a gram-positive bacterium that is commonly found in nasal passages, skin, and mucous membranes (Lowy 1998). This is a major cause of infection of wounds (in particular nosocomial bloodstream infections), especially in surgical procedures that involve medical device implants (Steinberg et al. 1996). Currently, within hernia mesh repair, 68% of infection complications are attributed to the *S. aureus* infections

– any infections related to hernia repair will unfortunately increase the recurrence rates of hernia, meaning that inhibiting the growth of this bacterium will give the patient a better chance of recovery (Iannitti et al. 2008). *E. coli* is another bacterium that can have detrimental effects on the recovery of wounds – it is the most common pathogen found in the hernia sac (Yang et al. 2015). This bacterium tends to develop in fluid collections at the site of mesh implant – if this is found at the site of implant, typically drainage of the fluid and a course of antibiotics are administered (e.g. ceftriaxone and ampicillin) (Aguilar et al. 2010). However, if both *S. aureus* and *E. coli* can be controlled without further administration of antibiotics (which would in turn reduce the possibility of antibiotic resistance), invasive drainage procedures, or overall removal of hernia mesh, then there is a heightened chance of optimum patient recovery, and a better chance of tissue re-growth at a cellular level.

The proliferation of cells relating to the healing of wounds is also important within a hernia repair context. Typically, wound healing can be divided into four main steps:

1. Haemostasis (0 – 7 hours)
2. Inflammation (1 – 3 days)
3. Proliferation (4 – 21 days)
4. Remodelling (21 days – 1 year) (Reinke & Sorg 2012)

The proliferation period here is arguably one of the most important phases given that there is a focus on restoring the tissue network – this can be easily disrupted through any potential infection. Another important aspect of the proliferation stage is the formation of the ECM: proper formation of the ECM will help with cell adhesion and regulate growth, movement and differentiation of the cells growing within it (Barker

2011). One of the main cited benefits of constructing electrospun scaffolds is the similarity between the fibrous polymer networks with ECM networks – therefore if electrospun scaffolds can mimic the ECM successfully, it may help promote cell adhesion, growth, movement and differentiation.

Recently, studies involving the testing of cellular response against electrospun scaffolds have been conducted – testing cell migration of breast cancer cells (MDA-MB-231) against PCL scaffolds (Nelson et al. 2014), rat periodontal ligament cells against PLGA scaffolds (Shang et al. 2010), human umbilical vein endothelial cell (HUVEC) against PCL-collagen scaffolds (Whited & Rylander 2014), and human mesenchymal stems cells against PLA scaffolds (McCullen et al. 2007). In particular, some of these studies showed evidence that cells typically form confluent monolayers on electrospun scaffolds, fibre orientation affects cell alignment, and cells prefer to grow on aligned fibres (cells showed greater attachment to specifically aligned fibres in comparison to randomly oriented scaffolds). Though the studies mentioned successfully demonstrated a range of cellular behaviour on electrospun scaffolds, there is perhaps a lack of research specifically into the cellular response against drug-loaded electrospun scaffolds – it may be the case that cell behaviour may be limited due to the cytotoxicity of drug within the polymeric scaffolds.

For this Chapter, the primary goals were to demonstrate successful inhibition of *S aureus* and *E. coli* bacteria and successful adhesion, growth and proliferation of smooth muscles cells on the various scaffolds (PCL-drug, PCL-collagen-drug, PLA-drug and PLA-collagen-drug variations). The antibacterial efficiency of the scaffolds was measured using a bacterial inhibition assay; cell proliferation was measured with

a cell adhesion assay (with subsequent fluorescent and SEM imaging) and cell viability using resazurin and 5-bromo-2'-deoxyuridine (BrdU) assays. The results from this Chapter reflect a number of factors discovered in Chapters 3 and 4, such as the importance of hydrophobicity/hydrophilicity of the scaffolds, drug release rates, drug concentrations and fibre morphology.

5.2 Antibacterial Efficacy of Electrospun Scaffolds

5.2.1 Materials & Methods

5.2.1.1 Antibacterial Study Procedure

The antibacterial efficacy of the drug loaded electrospun scaffolds were tested against *Escherichia coli* (*E. coli*) 8739 and *Staphylococcus aureus* (*S. aureus*) 29213. *S. aureus* is Gram positive, *E. coli* is Gram negative and both bacteria are common causes of nosocomial infections. Both irgasan and levofloxacin should have antibacterial effects. For this study, an agar diffusion method was used. Luria-Bertani (LB) agar was prepared from a formulation of 5 g tryptone, 2.5 g yeast extract, 5 g NaCl in 475 ml of deionized water. The LB agar was autoclaved and poured into 20ml plates. The *E. coli* and *S. aureus* were grown overnight in 5 ml of LB Broth, with both bacteria inoculated from a single colony. 150 µL of the *E. coli* and *S. aureus* cultures were spread onto six different plates of LB agar. Three plates consisted of spread *E. coli*, including a scaffold free plate, which acted as a control – the other 2 plates, were divided into 4 sections, with 1 section containing an unloaded PCL scaffold, and the other 3 containing PCL-irgasan and PCL-levofloxacin scaffolds. This procedure was repeated for three plates of spread *S. aureus*. The plates were incubated for 24 h, and

subsequently examined. Diameters of the zones of growth inhibition were measured, and these data compared across the drugs and bacterial strains. This method was based on the method described by Davachi *et al* (Davachi et al. 2016).

5.2.3 Results

5.2.3.1 PCL Samples Results

A full of list of inhibition zone measurements can be seen in table 5.1. For PCL scaffolds (Figure 5.1), both PCL-LEVO and PCL-collagen-LEVO showed the largest inhibition zones for both *E. coli* and *S. aureus* at approximately 2.6 – 2.8 cm. IRG-loaded scaffolds showed the smallest inhibition zones against *E. coli* at between 0.5 – 0.7 cm. For all samples, no re-growth of either bacterium can be observed over 48 hr.

Table 5.1 – Inhibition zone measurements (cm) for *E. coli* and *S. aureus* against PCL-IRG, PCL-LEVO, PCL-collagen-IRG, PCL-collagen-LEVO, PLA-IRG, PLA-LEVO, PLA-collagen-IRG and PLA-collagen-LEVO (*n=3*)

	Inhibition Zone (cm) *E.coli*	Inhibition Zone (cm) *S.aureus*
PCL-IRG	0.7 ± 0.5	1.8 ± 0.5
PCL-LEVO	2.6 ± 0.0	2.6 ± 0.1
PCL-COL-IRG	0.5 ± 0.2	2.5 ± 0.3
PCL-COL-LEVO	2.7 ± 0.1	2.8 ± 0.3
PLA-IRG	1.0 ± 0.3	1.0 ± 0.2
PLA-LEVO	2.1 ± 0.2	2.0 ± 0.2
PLA-COL-IRG	1.1 ± 0.1	1.1 ± 0.0
PLA-COL-LEVO	1.0 ± 0.1	0.4 ± 0.1
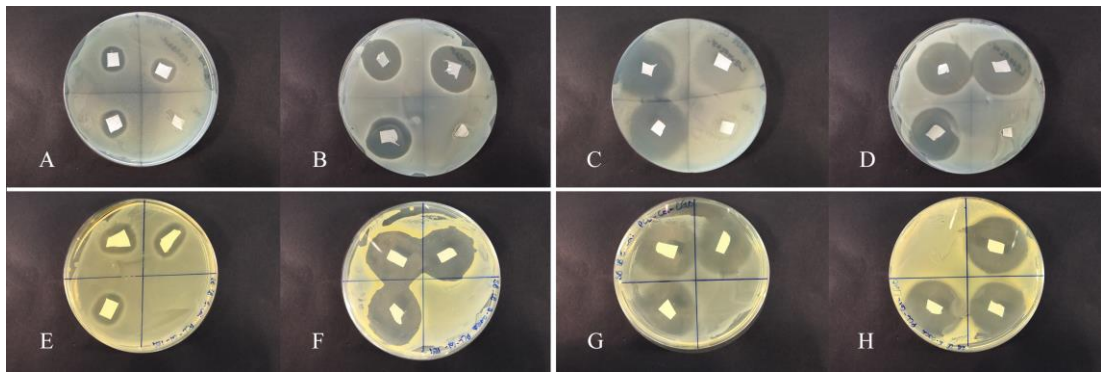
Figure 5.1 – Antibacterial study images for *E. coli* and *S. aureus* against (a) PCL-IRG and *E. coli* (b) PCL-IRG and *S. aureus* (c) PCL-LEVO and *E. coli* (d) PCL-LEVO and *S. aureus* (e) PCL-collagen-IRG and *E. coli* (f) PCL-collagen-IRG and *S. aureus* (g) PCL-collagen-LEVO and *E. coli* (h) PCL-collagen-LEVO and *S. aureus*

5.2.3.2 PLA Samples Results

Antibacterial measurements were taken at 24 h and 48 h (Figure 5.2, 48 h only) – it can be seen that the PLA-drug samples have a high efficacy at controlling the growth of both E. coli and S. aureus. In particular, PLA-LEVO (2.1 cm; table 5.1) had a higher average inhibition zone than PLA-IRG (1.0 cm; table 5.1). PLA-collagen-IRG resisted both strains of bacteria in a similar manner to the PLA-IRG sample (average inhibition zone = 1.1 cm). Finally, the PLA-collagen-LEVO sample showed an average inhibition zone to E. coli of 1.0 cm; however white spores of bacteria were re-forming near the sample (Figure 5.3). This sample also had a smaller efficacy with inhibiting the growth of S. aureus, demonstrating an average inhibition zone of 0.4 cm.
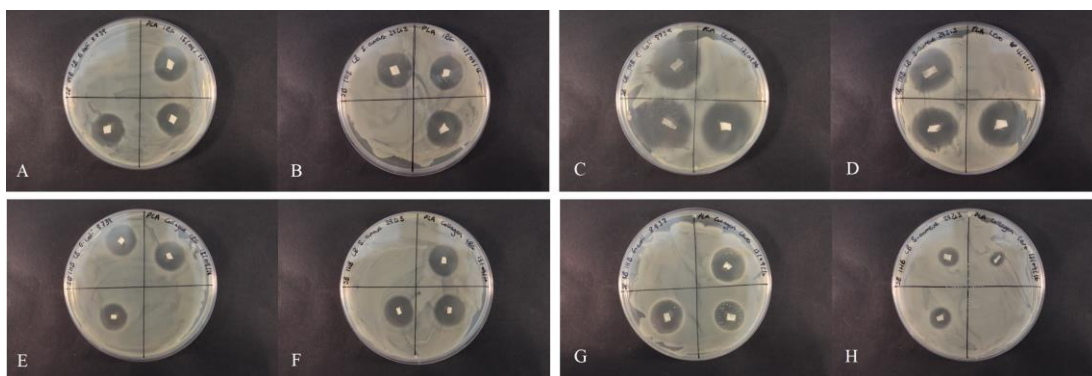
Figure 5.2 – Antibacterial study images for *E. coli* and *S. aureus* at 48 hr against (a) PLA-IRG and *E. coli* (b) PLA-IRG and *S. aureus* (c) PLA-LEVO and *E. coli* (d) PLA-LEVO and *S. aureus* (e) PLA-collagen-IRG and *E. coli* (f) PLA-collagen-IRG and *S. aureus* (g) PLA-collagen-LEVO and *E. coli* (h) PLA-collagen-LEVO and *S. aureus*

5.2.4 Discussion

The antibacterial efficacy of both irgasan and levofloxacin-loaded scaffolds were tested against strains of *E. coli* and *S. aureus*, with the efficacy specifically determined by visual zones of inhibition on the agar plate. The PCL-IRG scaffold showed signs of some activity, albeit weak, against *E. coli* with an average inhibition zone diameter of 0.7 ± 0.5 cm. However, the PCL-IRG loaded scaffold was particularly successful inhibiting the growth of *S. aureus* with an average inhibition zone diameter of 1.8 ± 0.5 cm. There was a higher-level efficacy observed within the PCL-levofloxacin cultures of both *E. coli* and *S. aureus*. The addition of collagen to the PCL-IRG sample created little difference against the efficacy of *E. coli* growth – however, there appeared to be an increase inhibition of *S. aureus* (increase from 1.8 to 2.5 cm). This increase in inhibition efficacy could possibly be attributed to the difference in drug release rate for PCL-IRG and PCL-collagen-IRG, with PCL-collagen-IRG showing a quicker (but still sustained) release of IRG (at 48 hr, PCL-IRG ~28% cumulative release and PCL-collagen-IRG ~32%). The antibacterial studies have shown that there

113

is a high efficacy of bacteria inhibition in both irgasan and irgasan-collagen loaded scaffolds across *E. coli* and *S. aureus* bacteria.

The levofloxacin-loaded scaffolds generally demonstrated larger values of inhibition zones, for both bacteria – this should be the case, given that levofloxacin is a broad-spectrum antibiotic, active against both gram positive and gram-negative bacterium. The irgasan-loaded scaffold showed stronger inhibition to the *S. aureus* bacteria; however, this should not be viewed as a negative result. *S. aureus* is a gram-positive bacterium that is commonly found on the skin, therefore is a major cause of nosocomial wound infection (Sisirak et al. 2010). The hydrophobic natures of irgasan and PCL, and potential stronger interactions between drug and polymer are likely to aid the sustained release from the fibres – this sustained release can be observed in the previous *in vitro* drug release study, and observed in the reduced inhibition of *E. Coli* (Celebioglu et al. 2014).
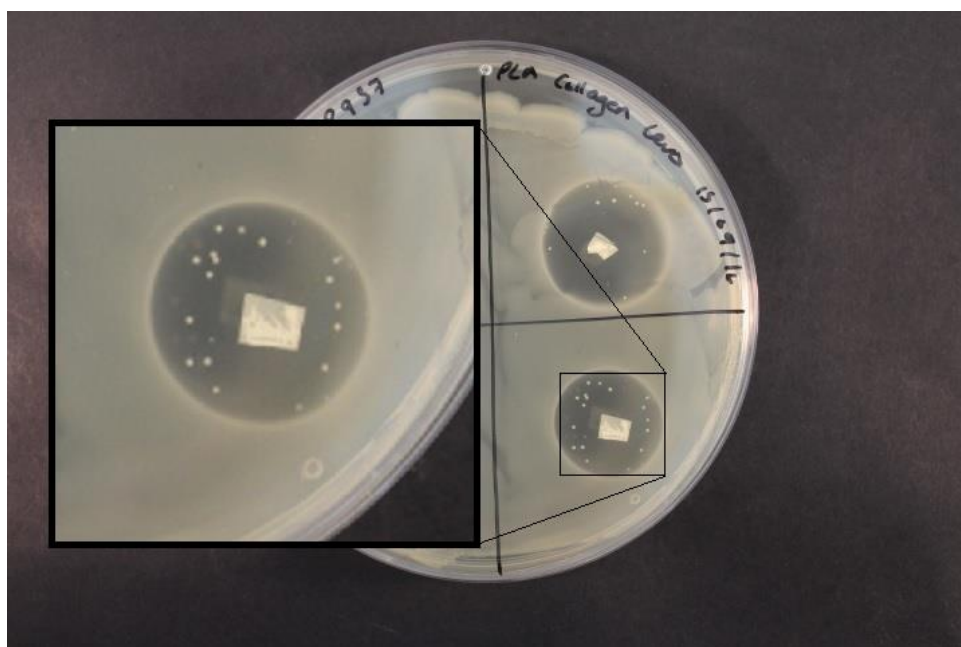
Figure 5.3 – Image detailing the re-growth of *E. coli* on a PLA-collagen-LEVO scaffold

The antibacterial studies were extremely useful in proving that the drug release profiles were consistent, and still effective in inhibiting the growth of E. coli and S. aureus. The larger zones of inhibition can be seen in the PLA-LEVO sample, which exhibits burst release behaviour. The smaller inhibition zones for PLA-IRG and PLA-collagen-IRG were indicative of the sustained release profiles. The sustained release profile of PLA-collagen-LEVO was also confirmed, given that there were small areas of bacterial re-growth (Figure 5.3) – this can be attributed to the low cumulative release percentage at 48 h of the study (at 48 h, < 10% of the drug had been released).

5.3 *In-Vitro* Cellular Studies

5.3.1 Materials & Methods

5.3.1.1 Cell Adhesion & Proliferation

For this Chapter, rat aortic smooth muscle cells (RAOSMCs) were used as the main cell type to test against the electrospun scaffolds. This cell type was grown in an incubator under 5% CO_2 using Dulbecco's Modified Eagle Medium: Nutrient Mixture F-12 9 (DMEM/F-12) media, with an addition of 10% foetal calf serum (FCS) and 1% penicillin/streptomycin. Third passage cells were grown to approximately 70% - 80% confluence in T75 flasks, subsequently trypsinized, and re-suspended in the growth medium in a centrifuge for 5 minutes at 10,000 RPM. Cells were seeded at a density of ~ 5.6 x 10^4 cells/100 μl for RAOSMCs.

Cell adhesion was monitored in 24-well plate dishes with cells seeded directly onto electrospun scaffolds. Square electrospun scaffolds (1 cm x 1 cm) were pre-wet with media and placed in tissue culture plates. Cells (at the previously mentioned density)

in a volume of 100 μl were seeded directly onto each scaffold, incubated at 37ºC for 4 hours in order for the cells to adhere to the surface. Each well was then filled with 2 ml of growth medium.

Initially, the ROASMCs were left for 3 days to judge the adhesion of cells on the scaffold surface, and then ROASMCs were tested for proliferation within 14 days of seeding. In this case, media was replaced every 3 days, and scaffolds were removed at 3, 7 and 14 days in order to image cells on the scaffold (using fluorescent microscopy). Adhesion and proliferation were determined through the staining of dead cells using propidium iodide (PI) – a red-fluorescent nuclear and chromosome counterstain. This process involved lifting the scaffolds from the wells, washing with PBS buffer, and fixing the cells using 5% paraformaldehyde. Samples were then placed in 1 ml of PBS buffer, and 10 μl of PI solution was added and left in dark storage for approximately 30 min. Samples were then placed on a coverslip then subsequently imaged on a Nikon Eclipse E600 Epiflurorescent Upright Microscope, at wavelengths of 495 nm (FITC) and 532 nm (TRITC). Cells were then counted using ImageJ software: images were converted to greyscale, image threshold was altered to display a black and white image highlighting the cell nuclei, a watershed function is then applied to separate cells that were grouped close together, and a particle analyser was run at a measurement of minimum 100-120 pixels and a circularity range of 0.00 – 1.00.

5.3.1.2 Cell Viability

In order to measure the cell viability against the levels of drug used in the electrospun scaffolds, a resazurin assay was performed. Cells (RAOSMCs) were grown in 1% FCS, 10% FCS, 1% addition of IRG, 0.5% addition of LEVO, and DMSO, at a density

of 3 x 10^4 cells/100 µl (in 24-well plates) for 3 days. The resazurin reagent was then added to each well, incubated at 37°C for 4 hours, then subsequently tested for fluorescence using a fluorometer at 560_{Ex} nm and 590_{Em} nm.

Ranges of drug concentrations (IRG = 1%, 0.1%, 0.01%, LEVO = 1%, 0.5%, 0.1%) were then tested against the growth of cells (RAOSMCs). A 5-bromo-2'-deoxyuridine (BrdU) assay was used to test the proliferation of cells. Cells were grown at a density of 3.6 x 10^4 cells/100 µl (in 96-well plates) for 3 days. After 3 days, a fixing/denaturing solution was added and left for 30 minutes. This solution was then removed and replaced with a detection antibody solution for 1 hour. The solution was then washed using a wash buffer, and replaced with HRP-conjugated secondary antibody solution (left for 30 min). Finally, a TMB substrate was added and incubated for 30 min at room temperature (21°C). The absorbance was then measured using a Molecular Device M5 Plate Reader at 450 nm.

5.3.2 Results

5.3.2.1 Cell Adhesion & Proliferation

Initial 3-day studies of RAOSMC growth against all PCL and PLA variations can be seen in Figures 5.4 and 5.5. The fluorescent images in Figure 5.4 indicate there is no adhesion of cells on the PCL or PCL-collagen scaffolds, and there appears to presence of a bacterial infection (bacteria unknown). RAOSMC adhesion was found to be minimal within both PCL-IRG and PCL-collagen-IRG samples, with a cell density of approximately ~1600 cells/cm^2 and ~500 cells/cm^2. PCL-LEVO, however, showed a

cell adhesion density of approximately ~14,000 cells/cm^2 and ~7,500 cells/cm^2 for PCL-collagen-LEVO.
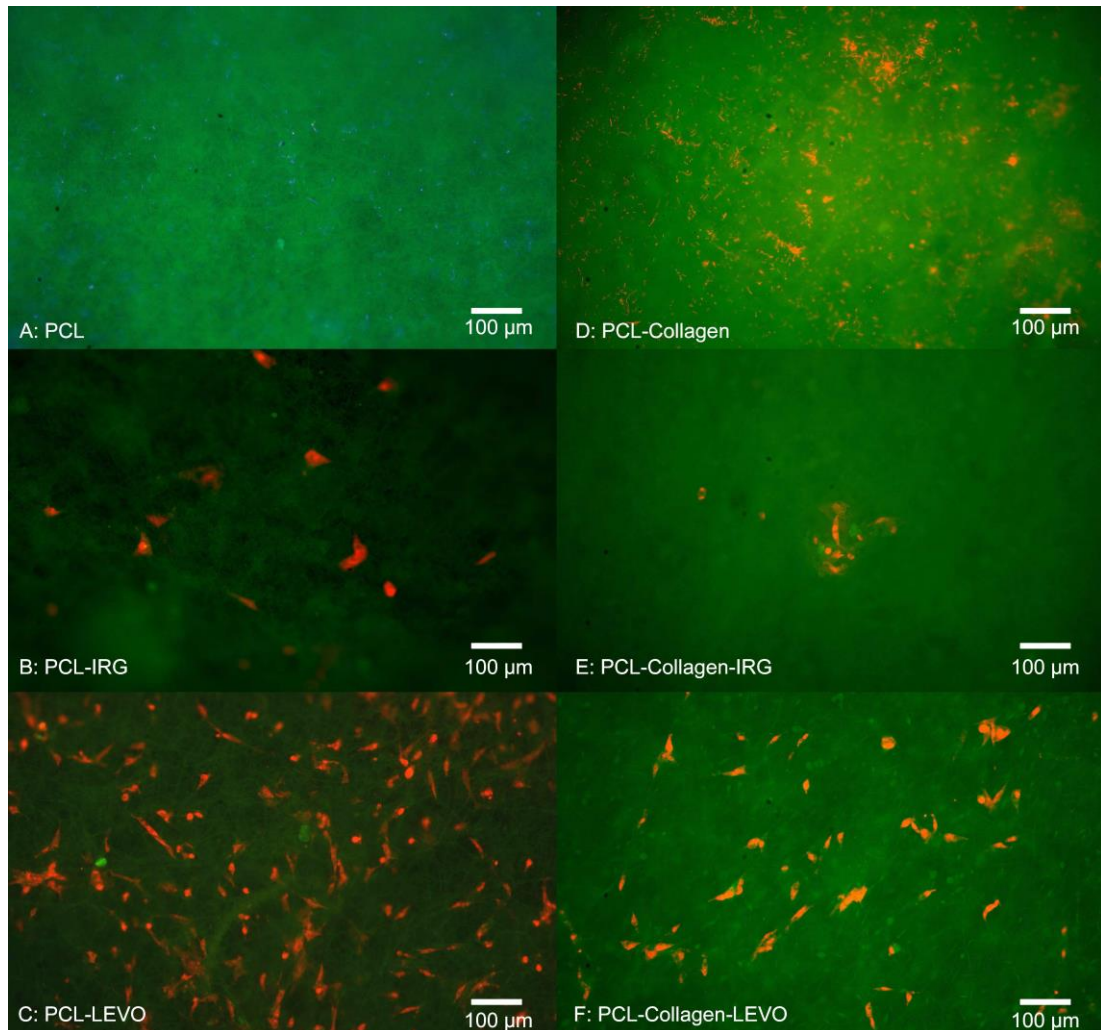
Figure 5.4 – Fluorescent image of cell adhesion assay for RAOSMCs after 3 days (a) PCL (b) PCL-IRG (c) PCL-LEVO (d) PCL-collagen (e) PCL-collagen-IRG (f) PCL-collagen-LEVO

Figure 5.5 indicates that there was no apparent cell adhesion of RAOSMCs against the PLA, PLA-collagen and PLA-collagen-IRG scaffolds, with only a bacterial infection appearing in each case. There was no cell adhesion measured for the PLA-IRG scaffold, however no bacterial infection was observed. Cell adhesion was observed for

PLA-LEVO and PLA-collagen-LEVO scaffolds, with a cell count of approximately ~11,000 cells/cm^2 and 2,000 cells/cm^2, respectively.
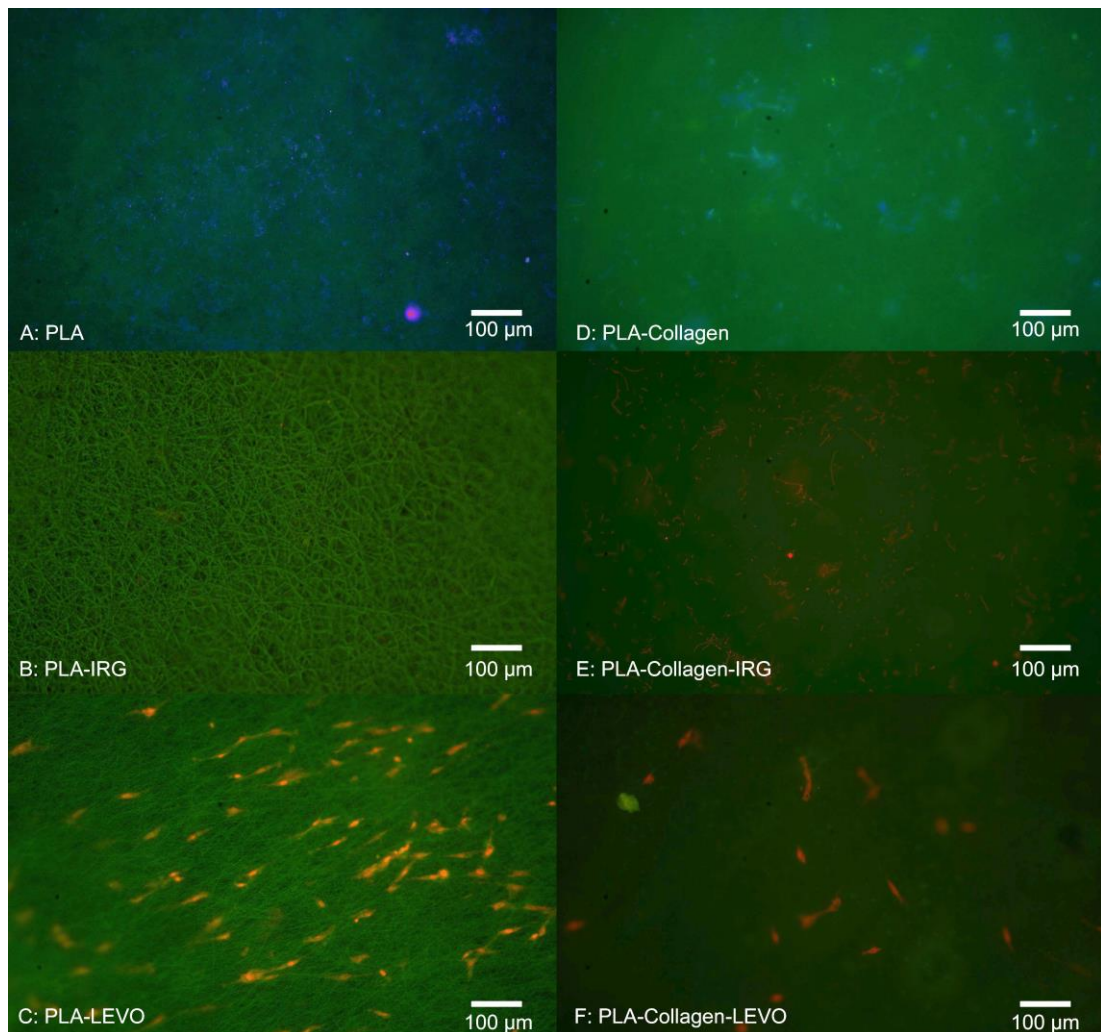
Figure 5.5 – Fluorescent image of cell adhesion assay for RAOSMCs after 3 days (a) PLA (b) PLA-IRG (c) PLA-LEVO (d) PLA-collagen (e) PLA-collagen-IRG (f) PLA-collagen-LEVO

A 14-day study was conducted on PCL-LEVO and PLA-LEVO combinations due to the highest measurement of proliferative cells in the previous 3-day study. The results from this 14-day study can be seen in Figures 5.6 and 5.7. PCL-LEVO showed a cell count across 3, 7 and 14 days of 6,800, 140,000 and 98,000 cells/cm^2. PCL-collagen-scaffold had a cell count of 1,500, 180,000 and 130,000 cells/cm^2.
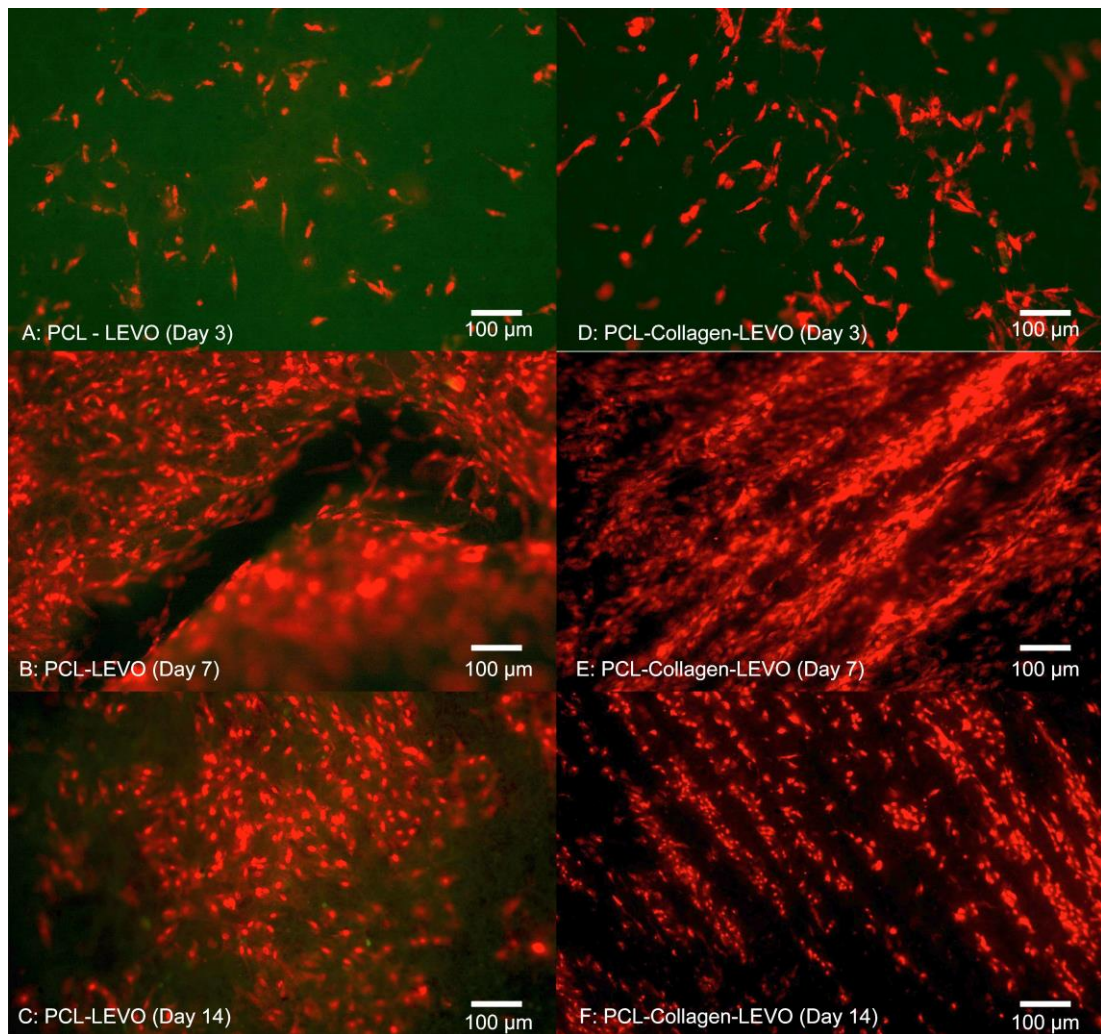
Figure 5.6 – Fluorescent image of cell proliferation of RAOSMCs (a) PCL-LEVO after 3 days (b) PCL-LEVO after 7 days (c) PCL-LEVO after 14 days (d) PCL-collagen-LEVO after 3 days (e) PCL-collagen-LEVO after 7 days (f) PCL-collagen-LEVO after 14 days

Similar to the results of the 3-day study with PCL-LEVO/PCL-collagen-LEVO, greater proliferation was measured against the PLA-LEVO and PLA-collagen-LEVO scaffolds, therefore the 14-day study was tested against the mentioned scaffolds. PLA-LEVO scaffolds showed an average cell count of 7,800, 128,000 and 119,000 cells/cm^2 at 3, 7 and 14 days. PLA-collagen-LEVO scaffolds showed an average cell count at 12,800, 168,000 and 0 cells/cm^2 (a bacterial infection was observed after 14 days).
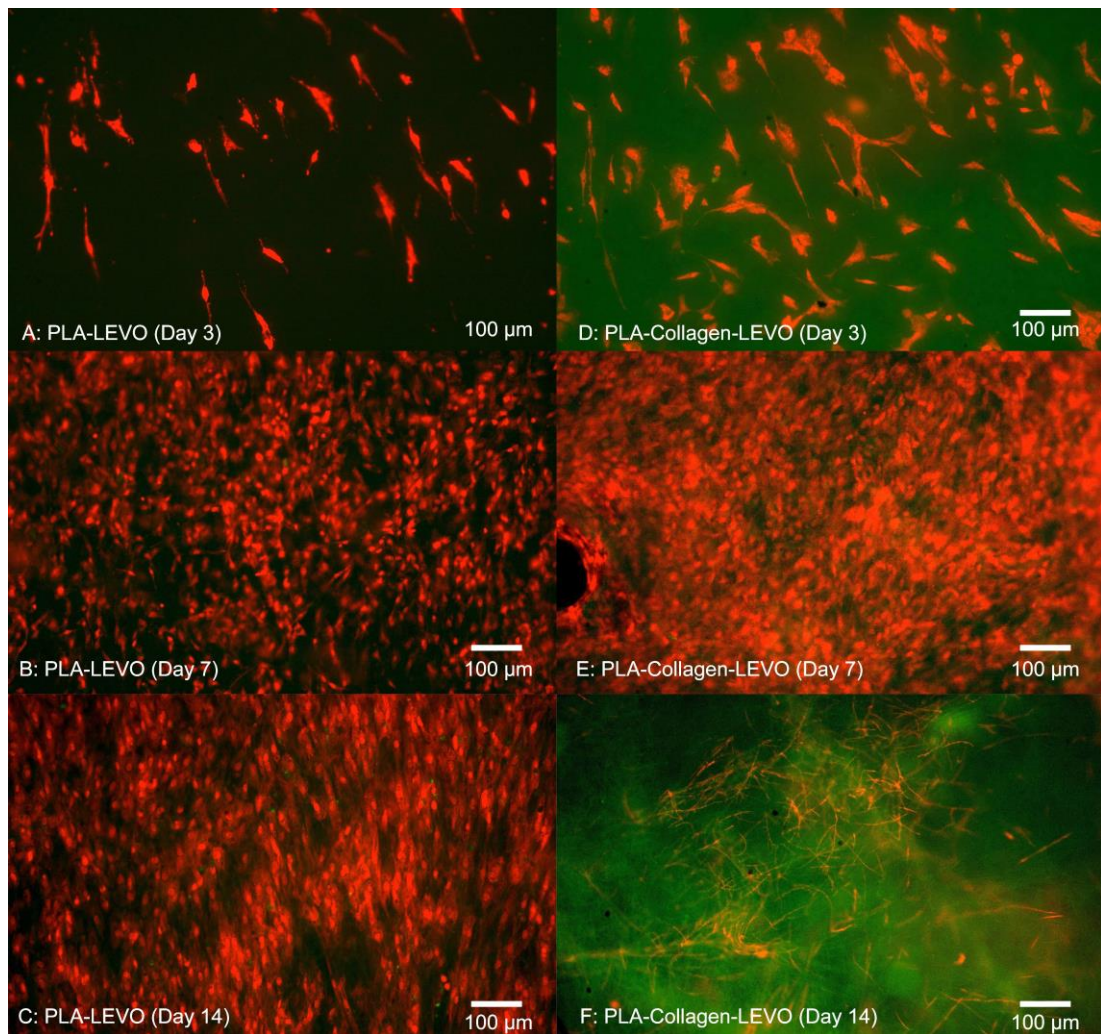
Figure 5.7 – Fluorescent image of cell proliferation of RAOSMCs (a) PLA-LEVO after 3 days (b) PLA-LEVO after 7 days (c) PLA-LEVO after 14 days (d) PLA-collagen-LEVO after 3 days (e) PLA-collagen-LEVO after 7 days (f) PLA-collagen-LEVO after 14 days

5.3.2.2 Cell Viability

Data relating the absorbance of resorufin from the resazurin assay can be seen in Figure 5.8. Results indicated an increase in metabolic activity of approximately 24% (in relation to the background growth) with the addition of 10% FCS, a 90% decrease with an IRG concentration of 1%, a 4% increase with a LEVO concentration of 0.5%m and a decrease of 27% with DMSO.
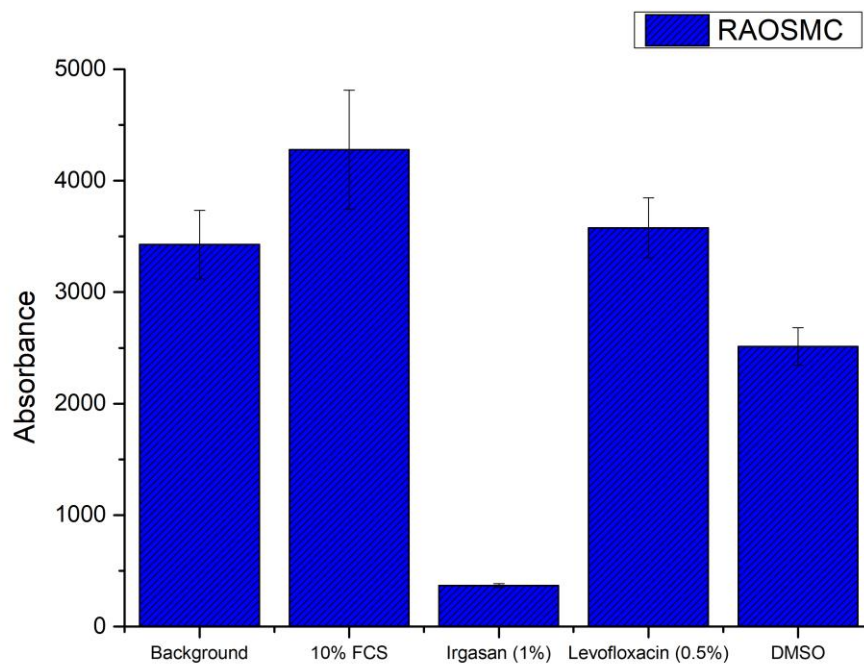
Figure 5.8 – Absorbance data with standard error bars (*n=3*) for resazurin assay against background, 10% FCS, 1% IRG, 0.5% LEVO and DMSO concentration

BrdU data is shown in Figure 5.9. In comparison with the background, a high cell proliferation is observed with the addition of 10% FCS. For the range of IRG concentrations, cell proliferation increased for 0.01% and 0.1% concentrations, and a decrease in proliferation for 1% concentration. LEVO concentrations generally showed a higher proliferation compared with the background, with cell proliferation reducing as the concentration increased from 0.1% to 1%. No change in proliferation was observed with a concentration of DMSO.
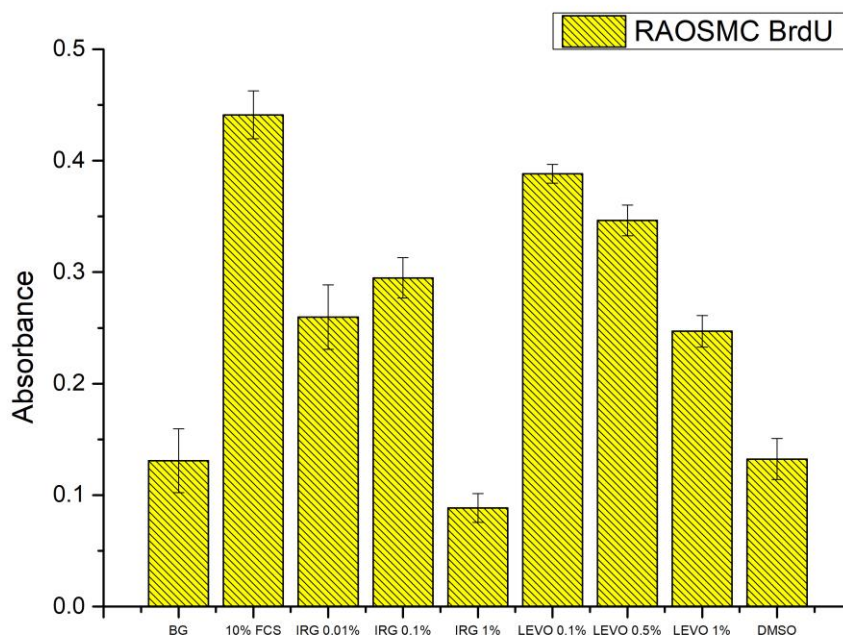
Figure 5.9 – Absorbance data with standard error bars (*n=3*) for BrdU assay against background, 10% FCS, 0.01% IRG, 0.1% IRG, 1% IRG, 0.1% LEVO, 0.5% LEVO, 1% LEVO and DMSO concentration

5.3.2 Discussion

Understanding the behaviour of smooth muscle cell growth against scaffolds is vital, given the importance of SMCs within the development of tissue re-growth. Initial 3-day studies of RAOSMCs against the various scaffold combinations proved extremely useful in determining which scaffolds exhibited the greatest efficacy in allowing cells to adhere. Bacterial infections were mainly observed in the scaffolds that did not contain any antibacterial drug or agent – media was initially administered with a mixture of penicillin and streptomycin. However, the media was not changed for the duration of the 3 days, meaning there is a chance the bacteria became resistant to the antibiotics within the media. Typically, bacterial cells have been shown to invade endothelial and smooth muscle cells, and bacterial persistence is largely due to

usurping of intracellular trafficking to avoid lysis (Kozarov 2012). The addition of IRG across both PCL and PLA samples yielded poor adhesion of RAOSMCs. This may be largely due to the high hydrophobicity of IRG in combination with two types of polymers that are generally hydrophobic in nature – hydrophobicity typically hinders cell adhesion and proliferation (M. He et al. 2015).

There appeared to be a greater attachment of cells on LEVO-loaded scaffolds that did not contain type I collagen – in the case of the PCL-LEVO and PCL-collagen-LEVO samples, both have the same hydrophilic characteristics. However, the difference in cell adhesions cannot be attributed to this. It is more likely the cells are interacting in regards the variance in fibre diameters for the two scaffolds or the release of levofloxacin inhibiting bacteria that may be affecting the adhesion. With regards to the cell attachment against fibre diameter, it should be the case that scaffolds (in particular PCL scaffolds) with smaller diameters (such as PCL-collagen-LEVO, with an average fibre diameter of 1.5 µm) will have better attachment of cells, due to the increase in specific surface area (Chen et al. 2007). This was not the case, however, and therefore the decrease in cell attachment for the PCL-collagen-LEVO scaffold may be down to factors that include drug release rate (there is a higher release % of drug from the PCL-LEVO scaffolds compared with the PCL-collagen-LEVO scaffold, and an increase in bacterial resistance may help with cell adhesion), or simply that the number of cell seeded onto the scaffolds were lower. PLA-LEVO and PLA-collagen-LEVO scaffolds showed a lower cell adhesion count – this lower cell adhesion may have attributed to the high hydrophobicity (water contact angles ~ 108° for PLA-LEVO and ~ 132° water contact angle), and smaller fibre diameter for the PLA-collagen-LEVO. Although smaller fibre diameter was previously stated that it can encourage cell attachment,

having fibres that range between 100 – 300 nm (of which there are some measured in the PLA-collagen-LEVO scaffold) will not have a significant impact in the promotion of cell adhesion (Whited & Rylander 2014).

One explanation that the RAOSMCs are adhering and proliferating across the LEVO-loaded scaffolds (for both PCL and PLA) may be due to the varying surface charges. It has been shown in various studies that the most suitable conditions for cell adhesion and proliferation occur when there is presence of negative ions (Ishikawa et al. 2007). In particular, it was highlighted in Chapter 4 (section 4.3.2) within the IR spectrometry a strong peak relating to a carboxylic (-COOH) functional group found predominately in the levofloxacin compound – this functional group has a negative charge, with hydrophilic properties, and interacts almost exclusively with fibronectin (Schmidt et al. 2009). This interaction with fibronectin (which is typically found within the extra cellular matrix of cultured cells) is important, because if the fibronectin protein is adsorbed onto the scaffold surface, this allows for the anchoring of fibronectin to the cell (Ruoslahti 1984) – in this case allowing the RAOSMC to adhere to the scaffold surface.
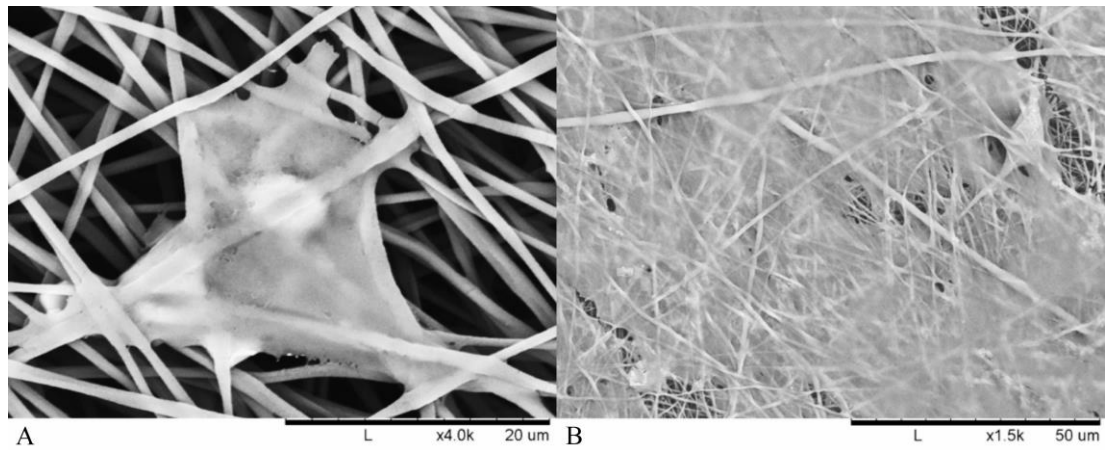
Figure 5.10 – SEM images of adhered RAOSMC in polymer fibres (a) 20 μm image at 3 days (b) 50 μm image at 14 days

Cell adhesion within the fibrous scaffolds can be seen in Figure 5.10. The structure of the cell takes shape according the fibrous network it is surrounded by, extending in multiple directions according to whatever direction a fibre oriented. This is due to cells and nuclei becoming elongated in order to adapt to the fibre structure, with the cell contracting in order to accommodate within the fibrous network of the electrospun scaffolds (Qin et al. 2015). A high confluence of cell proliferation can be seen in Figure 5.10B, suggesting that initial success in cell adhesion allows the smooth muscle to proliferate over 14 days.

Examining the cell proliferation of RAOSMCs over 14 days was useful in demonstrating the efficacy of the scaffolds within a biological environment. It can be clearly seen that the cells have a high level of proliferation and confluence at 7 days (across PCL and PLA scaffolds), followed by a decrease in proliferation at 14 days for most scaffolds. This decrease may be explained due to the inhibition that is typically experienced when cell proliferation is at a high confluence (Chen et al. 2010). This particular cell line (RAOSMCs) also stops growing, and cells die after confluency

(Masuda et al. 1999). Despite a reduced number of cell adhesions observed in scaffolds containing collagen, this does not affect the cell proliferation from 7 to 14 days – it was explained in Chapter 4 that there is a possibility of the hydrophobic bands (from collagen fibrils) being drawn to the surface of the fibres, therefore it may be the case that any cell-collagen interactions occurring may be delayed due to hydrophobic forces.

It can also be observed that the smooth muscle cells are growing in 'lines' on the PCL-collagen-LEVO scaffold. This may be due to the fibre orientation of the sample, as fibres can be oriented in one direction simply by stretching the scaffold in one direction – it may be the case that the samples were stretched during the setup process (samples had to be removed from their aluminium backings, with PCL-collagen-LEVO demonstrating high adhesion to the aluminium). However, this is an important factor as cells will typically elongate and grow along a particular direction of aligned fibres (Gnavi et al. 2015).

Cell viability studies were useful in determining whether the levels of drug loaded into the scaffolds had any potential toxic or inhibitory effects on the growth of RAOSMCs. It is clear from the results that the concentration of IRG used (1%) is not beneficial for the growth of RAOSMCs, and is completely inhibitory. It is reported that IRG has an EC_{50} value of approximately 0.0012 mg/ml (Gao et al. 2015) – given that the 1% concentration used in the resazurin assay was 0.57 mg/ml (475 times higher than the EC_{50} value), it can be concluded that the reason for poor cell adhesion and proliferation on IRG-loaded scaffolds is due to this high concentration of drug used. The BrdU assays were useful in demonstrating the varying IRG concentrations directly against

the proliferation of smooth muscle cells – with 0.1% and 0.01% concentrations showing a greater proliferation against the background, but very short of the proliferation observed with 10% FCS. Similarly, this may due to the 0.1% and 0.01% concentrations being greater than the previously mentioned EC_{50} value. It should also be noted that IRG has a mode of action where the drug can break through membranes and demonstrate inhibitory effects, such as blocking of lipid biosynthesis (von der Ohe et al. 2012), which may be another plausible explanation as to why there was poor cell adhesion and proliferation.

It was observed that the concentration of LEVO (0.5%) used in the initial resazurin study did not significantly increase nor decrease the metabolic activity in relation to the background. At this stage, it would be safe to judge that the concentration of LEVO used is not detrimental to the growth and proliferation of RAOSMCs. Further evidence of this is shown in the BrdU results, indicating that an increase in concentration (to 1%) of LEVO decreases the proliferation of cells, and that a decrease in concentration (to 0.1%) causes an increase in cell proliferation. This may be linked to the quoted EC_{50} value of 0.0074 mg/ml (Robinson et al. 2005) – 0.1% of LEVO used was 0.024 mg/ml which is closer to the EC_{90} value.

5.4 Conclusion

Examining the biological response to polymeric scaffolds has proven extremely useful in determining whether they have potential use for further development within the hernia repair field. One of the main goals set out in this project was to ensure that potential bacterial infections could be controlled or inhibited, to an extent where it would begin to help reduce chain reaction events as a result of normal mesh insertion

(chronic infection, which typically results in chronic inflammation and chronic pain). Antibacterial studies indicated that both scaffolds containing irgasan and levofloxacin successfully inhibited the growth of *E.coli* and *S. aureus*, with various measured zones of inhibition reflecting the different drug release profiles measured in Chapters 3 and 4. However, it should come as no surprise that both these drugs demonstrate an effective response to bacteria, given that these are two drugs are still widely used in surgical environments to control infection – it is evident that there should be a shift to treating infection efficiently and directly at the site of mesh insertion, and this efficacy is possible through drug-loaded polymeric scaffolds.

Concerning the response of smooth muscle cells against the various scaffolds, a number of important outcomes can be taken from the results and discussion. Firstly, the use of irgasan within the polymeric scaffolds proved to be detrimental to the adhesion and proliferation of cells – this was due to the concentration of IRG used being far greater than the EC_{50} value quoted in various publications, which meant that it was toxic to the cells growing in culture. Secondly, levofloxacin-loaded scaffolds showed the greatest number of cell adhesions and subsequent proliferation over 14 days – this could be explained to the hydrophilic nature of the drug (cells have a preference to grow in hydrophilic conditions), however a very high hydrophobicity of the PLA-collagen-LEVO scaffold was measured in Chapter 4. A more plausible explanation may be that the negatively carboxylic acid group found in LEVO is attracting positively charged fibronectins, which in turn is attracting the cell to adhere to the adsorbed proteins on the surface of the scaffold. Overall, the biological studies examined in this Chapter are useful as preliminary data for potential further studies into more complex aspects of cell behaviour: for example, understanding the behaviour

of fibroblasts against electrospun scaffolds will help understand potential scar formation at site of insertion (reducing scar tissue formation will help prevent mesh adhesion), and measuring inflammatory factors such as transforming growth factor beta 1 (TGF-β1) and interleukin 6 (IL-6).

Chapter 6: Final Discussion & Conclusions

6.1 Final Discussion

In Chapter 1, a number of different research questions were asked in relation to the research that was conducted in this project. They were questions that fundamental to help address various needs and requirements for a new-generation of hernia meshes that are optimal for the patient. **Can a different material within hernia repair be used?** It has been shown in the experimental Chapters that materials such as polycaprolactone, polylactic acid and collagen are viable materials with regards to their physicochemical characteristics: the two polymers readily interact with collagen in a positive manner (e.g. creating smaller fibres, helping alter the release rate of drugs), they allow for drugs such as irgasan and levofloxacin to be readily embedded within their polymeric matrices, and still retains mechanical strength that is still more than enough for abdominal requirements (hernia meshes should be able to withstand up to 0.026 MPa of pressure (Brown & Finch 2010)). The materials used are by no means new entities; however, they should be given serious consideration for potential use in hernia mesh repair.

Can a new-generation drug-loaded mesh that is bio-available to the surrounding tissues be created? A cellular response using smooth muscle cells was reported, with an emphasis on successful cell adhesion and proliferation against polymeric scaffolds loaded with the levofloxacin antibiotic. This data is only preliminary in regards to understand how they would affect the surrounding tissues of hernia repair; therefore, measured responses against cells such as fibroblasts would begin to give a better

indication of the bioavailability of the drug-loaded scaffolds. A long-term goal that would create better accuracy of tissue response would be to test the various scaffolds with *in vivo* animal testing (e.g. rat or rabbit models).
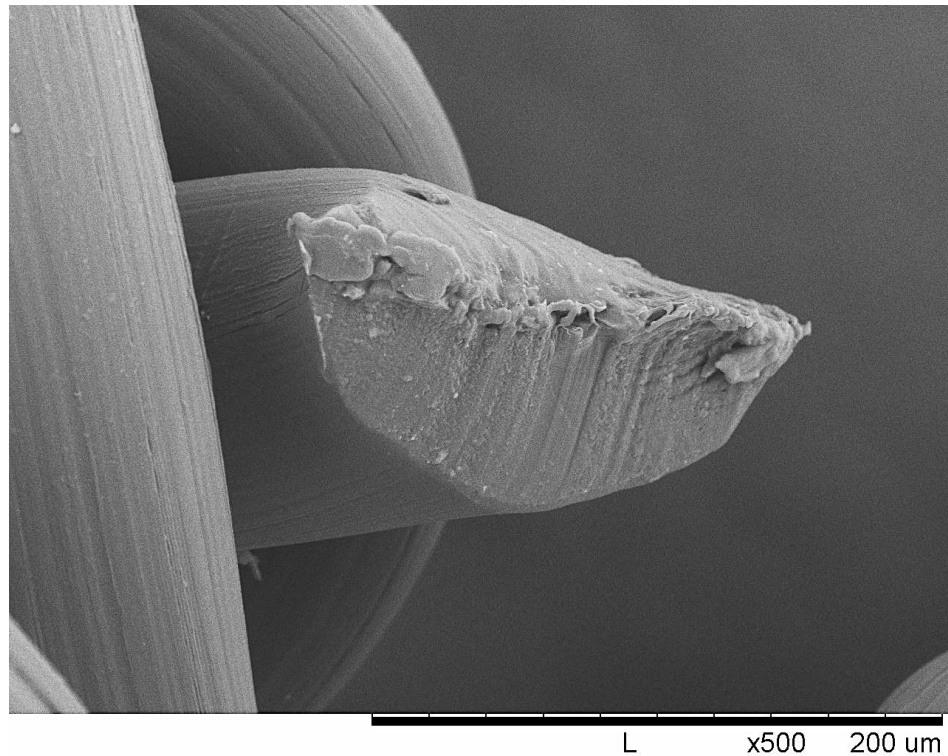
Figure 6.1 – SEM image of polypropylene mesh edges cut

Can a mesh that fulfils the patients' needs, whilst reducing the negative side effects associated with polypropylene mesh repair be created? The use of both irgasan and levofloxacin were initially chosen in order to try to tackle the issue of chronic infection – both drugs were embedded into the polymeric scaffolds, and showed successful inhibition of bacterial growth that is commonly found in surgical environments. The reduction of chronic infection is intrinsically connected with chronic inflammation and pain, so perhaps this new type of drug-loaded mesh is a step in right direction to help alleviate some of the side effects experience by patients.

Recently, there has been substantial press coverage of the side effects caused by hernia mesh insertion (Collinson 2017), and the problems associated are still largely blamed on the material choice of polypropylene. One examination (Figure 6.1) of a polypropylene mesh revealed that when cut, sharp edges are formed around the entirety of the mesh – these sharp edges will contribute towards inflammation, weakening and erosion of the viscera (Aggarwal et al. 2016). One distinct advantage of electrospun scaffolds (compared with polypropylene meshes) is that there are no sharp edges formed, regardless of whether they are cut to a particular size or not. At this stage of research, it is too early and perhaps too challenging to attempt to address all the various patients' needs, however, addressing one of the major issues (chronic infection) shows promise for further research in this area.

Electrospinning was the primary method of fabrication for the scaffolds in this project, and a broad range of characterisation techniques allowed for a deep understanding about the efficacy of the scaffolds in many different areas. There were a number of advantages that became apparent as analysis was performed throughout the project. Firstly, it is a quick and easy method of fabrication: sample solutions could be made with relative ease, and with enough preparation, scaffolds can fabricate within a few hours and ready for characterisation. This allowed for various formulations to be made quickly, and subsequent analysis determined what formulation was best suited to successful fibre formation. From an experimental point of view, the process of electrospinning is cost effective given that only 5 ml of solution is injected for each experiment, meaning that very low quantities of materials can be used to successfully create viable samples for analysis. Another advantage is that a variety of synthetic and natural materials can be used to create scaffolds, given they have the correct solubility

against various solvents. The studies in previous Chapters have demonstrated the ease in which both PCL and PLA can be broken down using cheap solvents such as chloroform and DMF, and using different solvents with these materials may actually yield different morphological characteristics of the fibres produced. The fibrous network created through the process of electrospinning also appeared to be advantageous with regards to attracting cell adhesion and a high proliferation.

Despite the number of advantages identified, there are still a number of drawbacks for electrospinning that perhaps prevent the process from being used commercially. There is likely to be difficulty with scaling-up this manufacturing process to a level where electrospun meshes could be mass-produced – the main difficulty being the low rate of production due to the slow feeding rate of solutions (Li et al. 2006), with increasing the feed rate of solutions resulting in poor fibre formation. Another distinct disadvantage of electrospinning is the use of harmful solvents – solvents commonly used to prepare solutions are toxic and harmful to the environment (Jiang et al. 2016). However, there a number of new studies into the use of 'green' electrospinning using water-soluble polymers and benign solvents, which may help rectify this issue (Agarwal & Greiner 2011; Liverani et al. 2017). Overall, electrospinning produces materials that are useful in meeting particular goals that are required for hernia mesh repair, although it may be a technique that remains for laboratory use only.

The two drugs examined in this project were carefully selected in relation to how relevant they are within surgical environments. Although triclosan (irgasan) is not administered to patients in the same manner that antibiotics are, they are still used within surgical products to reduce surgical-site infections. It is clear, however, from

the results in Chapter 5 that using an appropriate dosage of this drug is vital to promote the fine balance between controlling infection and allowing cells (such as smooth muscle cells) to grow and proliferate in an optimum environment. Currently, triclosan-coated sutures show a significant effect in the inhibition of bacteria within surgical environments (Z. X. Wang et al. 2013), however it must be noted that there is now a growing concern regarding the use of triclosan related to antibacterial resistance (Webber et al. 2017). A number of other concerns related to dermal carcinogenicity, potential hormonal effects and photo-toxicity have been expressed by the Food & Drug Administration (FDA) – it appears that the long-term use of this drug is set to decline, and the relevance of this drug for use within surgical products may become obsolete.

The use of levofloxacin within scaffolds has a far greater relevance (in comparison to the irgasan used) to the treatment of bacterial infections within hernia repair, given its predominant use in conjunction with other antibiotics such as ciprofloxacin and cefazolin (Mehrabi Bahar et al. 2015). However, issues including antibacterial resistance for levofloxacin are now a reality (Boveneind-Vrubleuskaya et al. 2017). It has been recently shown that the prophylactic administration of levofloxacin to prevent infections at the site of mesh has no significant effect (J. Wang et al. 2013), and that infection can be prevented through the targeted antibiotic use at the tissue site (Dohmen 2008). The manner in which levofloxacin has behaved with various electrospun polymers in previous Chapters, means that there is a possibility of reducing the need for prophylactic treatment (which may be causing an increase in antibiotic resistance). Other antibiotics such as ciprofloxacin and cefazolin can be implemented within the electrospinning process (Baskakova et al. 2016; Maleki et al.

2016), however their tissue response with relation to hernia repair must be assessed to determine suitability for further study.

Despite the level of negative media coverage currently happening, directed to the use of polypropylene meshes, these types of meshes are still widely used. New studies regarding this have shown that the complication rate of hernia mesh insertion is at 0.6% (Kelly 2017) – however, there is an inevitable degree of reluctance from patients now, given that the media coverage regarding mesh insertion is global. Despite the procedure currently being the most effective and common way to treat hernias, a focus on developing new techniques and materials is essential in order to allow for patients concerns to be alleviated. For example, first use of a hybrid synthetic/biologic mesh has been conducted (although the mesh is still using polypropylene) which has proven to be safe and effective (Bittner et al. 2017), and also use of a fibrin glue to fixate the mesh in order to reduce chronic pain from the use of transfascial sutures (Weltz et al. 2017). New techniques have also been proposed, with a new surgical approach for large incisional hernias through the use of a double layered mesh (mixture of film and filament) (Munegato et al. 2017), and the use of a self-gripping mesh to reduce the need of sutures (Molegraaf et al. 2017). The hernia mesh market has yet to venture into the use of electrospun scaffolds within surgical environments, however there is still plenty of research being undertaken into this possibility (Ackermann et al. 2017).

6.2 Conclusions

The work conducted in this project has demonstrated a wide variety of conclusions, which ultimately contribute towards furthering the research and development of materials for use within hernia repair:

- Various complications from the use of polypropylene meshes for hernia repair have been identified – chronic infection, chronic inflammation and chronic pain. It is vital that in order to develop a new-generation of meshes, that these factors are addressed ultimately to help with patient recovery and comfort.

- The process of electrospinning is a useful tool for the rapid fabrication of a scaffold – integrating drugs such as irgasan or levofloxacin into the polymeric matrices is simple, and will affect different physicochemical aspects of the scaffold.

- Biofunctionalisation of the scaffolds using type I collagen appeared to alter scaffold characteristics – the introduction of collagen to polymer showed an alteration in the release rate of drug, a change in the hydrophobicity/hydrophilicity of the scaffold surfaces, a decrease in fibre diameter and a shift in polymer structure from semi-crystalline to amorphous.

- Cell adhesion and proliferation was found to be prominent in scaffolds containing levofloxacin – cells may be attracted to the hydrophilic, negatively charged carboxylic acid functional group. Poor cell adhesion was observed in scaffolds containing irgasan, however cell viability assays revealed that the concentration used was harmful to the cells in culture.

6.3 Future Work

Although a number of useful outcomes were achieved in this project, there is still more research that can be conducted to further this line of work. Firstly, other fabrication methods can be explored – hot-melt extrusion (for the creation of filaments), 3D

printing, or melt spinning. Exploring these fabrication techniques will allow examination of whether the polymers and drugs used in this study will behave and interact in the same manner and also will open the used of more polymers that can't be used by electrospinning. A comparison of these techniques may help decide which fabrication method is suited to hernia mesh development and benefit the patients.

Examination of other synthetic and natural materials is another area that must be performed. Synthetic materials such as polyethylene glycol (PEG), polylactic-co-glycolic acid (PLGA) and polyvinylidene fluoride (PVDF) are materials that have been previously used in electrospinning, that have the potential to be drug-loaded and tested for feasibility within the hernia repair field. Natural materials such as fibrin and elastin are some alternatives to collagen that may be useful in mimicking the extracellular matrix of tissue. Similarly, other drugs (in particular, antibiotics that are commonly used for gastrointestinal infections) should be explored to determine whether they behave in the same manner as levofloxacin did in this study – ciprofloxacin, cefazolin and doxycycline are examples of relevant drugs.

Finally, an expansion into *in vitro* studies related to cellular activity against the drug-loaded scaffolds is essential. Biological responses of cells such as fibroblasts, endothelial and mesothelial cells will give a detailed insight into the efficacy of the electrospun scaffolds. Given that the scaffolds have already been measured for their antibacterial efficacy, the next logical step is to understand the inflammatory response – this can be achieved by measuring the release of inflammatory-inducing proteins such as TBG-beta, IL6 and IL10. Testing the scaffolds in animal models (e.g. rabbits)

will also show how the surrounding tissue will react, which will be incremental in determining whether electrospun scaffolds are viable for surgical use.

References

Ackermann, M. et al., 2017. Collagen-inducing biologization of prosthetic material for hernia repair: Polypropylene meshes coated with polyP/collagen. *Journal of Biomedical Materials Research Part B: Applied Biomaterials*, pp.1–13.

Agarwal, S. & Greiner, A., 2011. On the way to clean and safe electrospinning-green electrospinning: Emulsion and suspension electrospinning. *Polymers for Advanced Technologies*, 22(3), pp.372–378.

Aggarwal, S. et al., 2016. Laparoscopic management of mesh erosion into small bowel and urinary bladder following total extra-peritoneal repair of inguinal hernia. *J Minim Access Surg.*, 12(1), pp.79–82.

Aguilar, B. et al., 2010. Conservative management of mesh-site infection in hernia repair surgery-a case series. *Journal of Laparoendoscopic & Advanced Surgical Techniques*, 20(3), pp.249–252.

Aguirre-Chagala, Y.E. et al., 2017. Physicochemical properties of polycaprolactone/collagen/elastin nanofibers fabricated by electrospinning. *Materials Science and Engineering C*, 76, pp.897–907.

Ahmed, M. et al., 2015. A combinatorial approach towards the design of nanofibrous scaffolds for chondrogenesis. *Scientific Reports*, 5, pp.1–12.

Akolekar, D. et al., 2008. Comparison of recurrence with lightweight composite polypropylene mesh and heavyweight mesh in laparoscopic totally extraperitoneal inguinal hernia repair: An audit of 1,232 repairs. *Hernia*, 12(1),

pp.39–43.

Anon, 2017. Chapter 16. Polymers. Characteristics, Applications and Processing.

Anon, 2008. Nomination profile triclosan supporting information for toxicological evaluation by the national toxicology program. *U.S. Food & Drug Administration*.

Athanasiou, K.A., Niederauer, G.G. & Agrawal, C.M., 1996. Sterilization, toxicity, biocompatibility and clinical applications of polylactic acid/polyglycolic acid copolymers. *Biomaterials*, 17(2), pp.93–102.

Azimi, B. et al., 2014. Poly (ε-caprolactone) Fiber: An overview. *Journal of Engineered Fibers and Fabrics*, 9(3), pp.74–90.

Badrossamay, M.R. et al., 2014. Engineering hybrid polymer-protein super-aligned nanofibers via rotary jet spinning. *Biomaterials*, 35(10), pp.3188–3197.

Balouiri, M., Sadiki, M. & Ibnsouda, S.K., 2016. Methods for in vitro evaluating antimicrobial activity: A review. *Journal of Pharmaceutical Analysis*, 6(2), pp.71–79.

Barker, T.H., 2011. The role of ECM proteins and protein fragments in guiding cell behavior in regenerative medicine. *Biomaterials*, 32(18), pp.4211–4214.

Barnes, C.P. et al., 2007. Cross-linking electrospun type II collagen tissue engineering scaffolds with carbodiimide in ethanol. *Tissue engineering*, 13(7), pp.1593–605.

Baskakova, A. et al., 2016. Electrospun formulations of acyclovir, ciprofloxacin and cyanocobalamin for ocular drug delivery. *International Journal of Pharmaceutics*, 502(1–2), pp.208–218.

Bendavid, R. et al., 2014. Mesh-related SIN syndrome. A surreptitious irreversible neuralgia and its morphologic background in the etiology of post-herniorrhaphy Pain. *International Journal of Clinical Medicine*, 5(5), pp.799–810.

Bhavsar, M.D. & Amiji, M.M., 2008. Development of novel biodegradable polymeric nanoparticles-in-microsphere formulation for local plasmid DNA delivery in the gastrointestinal tract. *AAPS PharmSciTech*, 9(1), pp.288–94.

Bikiaris, D.N. et al., 2007. Miscibility and enzymatic degradation studies of poly(ε-caprolactone)/poly(propylene succinate) blends. *European Polymer Journal*, 43(6), pp.2491–2503.

Bilsel, Y. & Abci, I., 2012. The search for ideal hernia repair; mesh materials and types. *International Journal of Surgery*, 10(6), pp.317–321.

Bittner, J.G. et al., 2017. First human use of hybrid synthetic/biologic mesh in ventral hernia repair: a multicenter trial. *Surgical Endoscopy*.

Boveneind-Vrubleuskaya, N.V. et al., 2017. Pharmacokinetics of levofloxacin in multidrug- and extensively drug-resistant tuberculosis patients. *Antimicrobial Agents and Chemotherapy*, 61(8).

Bozec, L. & Odlyha, M., 2011. Thermal denaturation studies of collagen by microthermal analysis and atomic force microscopy. *Biophysical Journal*,

101(1), pp.228–236.

Brown, C.N. & Finch, J.G., 2010. Which mesh for hernia repair? *Annals of the Royal College of Surgeons of England*, 92(4), pp.272–278.

Brown, R.H. et al., 2009. Electrospinning zwitterion-containing nanoscale acrylic fibers. *Polymer*, 50(20), pp.4781–4787.

Bubel, K. et al., 2014. Solvent-free aqueous dispersions of block copolyesters for electrospinning of biodegradable nonwoven mats for biomedical applications. *Macromolecular Materials and Engineering*, pp.1445–1454.

Bugay, D.E., 2001. Characterization of the solid-state: Spectroscopic techniques. *Advanced Drug Delivery Reviews*, 48(1), pp.43–65.

Buttafoco, L. et al., 2006. Electrospinning of collagen and elastin for tissue engineering applications. *Biomaterials*, 27(5), pp.724–734.

Celebioglu, A. et al., 2014. Antibacterial electrospun nanofibers from triclosan/cyclodextrin inclusion complexes. *Colloids and Surfaces B: Biointerfaces*, 116, pp.612–619.

Cha, Y. & Pitt, C.G., 1988. A one-week subdermal delivery system for l-methadone based on biodegradable microcapsules. *Journal of Controlled Release*, 7, pp.69–78.

Chakrapani, V.Y. et al., 2013. Electrospinning of type I collagen and PCL nanofibers using acetic acid. *Polymers and Polymer Composites*, 21(7), pp.449–456.

Charulatha, V. & Rajaram, A., 2003. Influence of different crosslinking treatments on the physical properties of collagen membranes. *Biomaterials*, 24(5), pp.759–767.

Chen, M. et al., 2007. Role of fiber diameter in adhesion and proliferation of NIH 3T3 fibroblast on electrospun polycaprolactone scaffolds. *Tissue Engineering*, 13(3), pp.579–587.

Chen, Z.G. et al., 2010. Electrospun collagen-chitosan nanofiber: A biomimetic extracellular matrix for endothelial cell and smooth muscle cell. *Acta Biomaterialia*, 6(2), pp.372–382.

Cheng, Z. & Teoh, S.H., 2004. Surface modification of ultra thin poly (epsilon-caprolactone) films using acrylic acid and collagen. *Biomaterials*, 25(11), pp.1991–2001.

Cheow, W.S., Chang, M.W. & Hadinoto, K., 2010. Antibacterial efficacy of inhalable levofloxacin-loaded polymeric nanoparticles against E. coli biofilm cells: The effect of antibiotic release profile. *Pharmaceutical Research*, 27(8), pp.1597–1609.

Choi, J.S. et al., 2008. The influence of electrospun aligned poly(caprolactone)/collagen nanofiber meshes on the formation of self-aligned skeletal muscle myotubes. *Biomaterials*, 29(19), pp.2899–2906.

Chou, S.-F., Carson, D. & Woodrow, K.A., 2015. Current strategies for sustaining drug release from electrospun nanofibers. *Journal of Controlled Release*, 220, pp.584–591.

Chou, S.F. & Woodrow, K.A., 2017. Relationships between mechanical properties and drug release from electrospun fibers of PCL and PLGA blends. *Journal of the Mechanical Behavior of Biomedical Materials*, 65(September 2016), pp.724–733.

Collinson, A., 2017. NHS hernia mesh repairs "leaving patients in chronic pain." *BBC News*.

Dabbas, N. et al., 2011. Frequency of abdominal wall hernias: is classical teaching out of date? *JRSM Short Reports*, 2(1), p.5.

Davachi, S.M. et al., 2016. Investigating composite systems based on poly l-lactide and poly l-lactide/triclosan nanoparticles for tissue engineering and medical applications. *Materials Science and Engineering C*, 58, pp.294–309.

Deeba, S. et al., 2009. Laparoscopic approach to incarcerated and strangulated inguinal hernias. *JSLS : Journal of the Society of Laparoendoscopic Surgeons*, 13(3), pp.327–31.

Deitzel, J.. et al., 2001. The effect of processing variables on the morphology of electrospun nanofibers and textiles. *Polymer*, 42(1), pp.261–272.

Detta, N. et al., 2010. Melt electrospinning of polycaprolactone and its blends with poly(ethylene glycol). *Polymer International*, 59(11), pp.1558–1562.

Devlin, H., 2017. More than 800 women sue NHS and manufacturers over vaginal mesh implants. *The Guardian*.

Dias, J.R., Antunes, F.E. & Bártolo, P.J., 2013. Influence of the rheological

behaviour in electrospun PCL nano fibres production for tissue engineering application. *Chemical engineering transactons*, 32(2011), pp.1015–1020.

Djagny, K.B., Wang, Z. & Xu, S., 2001. Gelatin: A valuable protein for food and pharmaceutical industries: Review. *Critical Reviews in Food Science and Nutrition*, 41(6), pp.481–492.

Dohmen, P.M., 2008. Antibiotic resistance in common pathogens reinforces the need to minimise surgical site infections. *Journal of Hospital Infection*, 70(SUPPL. 2), pp.15–20.

Domingos, M. et al., 2009. Polycaprolactone scaffolds fabricated via bioextrusion for tissue engineering applications. *International Journal of Biomaterials*, 2009, p.239643.

Dorgan, J.R., Williams, J.S. & Lewis, D.N., 1999. Melt rheology of poly(lactic acid): Entanglement and chain architecture effects. *Journal of Rheology*, 43(5), p.1141.

Drugbank, 2008. Levofloxacin. *Tuberculosis*, 88(2), pp.119–21.

Duan, K., Xiao, D. & Weng, J., 2013. Triclosan-loaded PLGA microspheres-porous titanium composite coating. , pp.1–6.

Dulnik, J. et al., 2016. Biodegradation of bicomponent PCL/gelatin and PCL/collagen nanofibers electrospun from alternative solvent system. *Polymer Degradation and Stability*, 130, pp.10–21.

Dunphy, S.E. et al., 2014. Hydrogels for lung tissue engineering: Biomechanical

properties of thin collagen-elastin constructs. *Journal of the Mechanical Behavior of Biomedical Materials*, 38, pp.251–259.

Earle, D.B., 2010. Biomaterials in hernia repair.

Ebersole, G.C. et al., 2012. Development of novel electrospun absorbable polycaprolactone (PCL) scaffolds for hernia repair applications. *Surgical Endoscopy and Other Interventional Techniques*, 26(10), pp.2717–2728.

Elzein, T. et al., 2004. FTIR study of polycaprolactone chain organization at interfaces. *Journal of Colloid and Interface Science*, 273(2), pp.381–387.

Falde, E.J. et al., 2015. Layered superhydrophobic meshes for controlled drug release. *Journal of Controlled Release : Official Journal of the Controlled Release Society*, 214, pp.23–29.

FDA, 2017. Hernia surgical mesh implants. *U.S. Food & Drug Administration*.

Foraida, Z.I. et al., 2017. Elastin-PLGA hybrid electrospun nanofiber scaffolds for salivary epithelial cell self-organization and polarization. *Acta Biomaterialia*, 62, pp.116–127.

Förstemann, T. et al., 2011. Forces and deformations of the abdominal wall-A mechanical and geometrical approach to the linea alba. *Journal of Biomechanics*, 44(4), pp.600–606.

Franklin, J.E. et al., 2004. Laparoscopic ventral and incisional hernia repair: An 11-year experience. *Hernia*, 8(1), pp.23–27.

Franz, M.G., 2008. The biology of hernia formation. *Surgical Clinics of North America*, 88(1), pp.1–15.

Gamble, J.F. et al., 2012. Surface energy analysis as a tool to probe the surface energy characteristics of micronized materials - A comparison with inverse gas chromatography. *International Journal of Pharmaceutics*, 422(1–2), pp.238–244.

Gao, L. et al., 2015. Effects of triclosan and triclocarban on the growth inhibition, cell viability, genotoxicity and multixenobiotic resistance responses of Tetrahymena thermophila. *Chemosphere*, 139, pp.434–440.

Gaoming, J., Xuhong, M. & Dajun, L., 2005. Process of warp knitting mesh for hernia repair and its mechanical properties. *Fibres and Textiles in Eastern Europe*, 13(3), pp.44–46.

Gbureck, U. et al., 2007. Low temperature direct 3D printed bioceramics and biocomposites as drug release matrices. *Journal of Controlled Release*, 122(2), pp.173–180.

Geisse, N.A., 2009. AFM and combined optical techniques. *Materials Today*, 12(7–8), pp.40–45.

Gnavi, S. et al., 2015. The effect of electrospun gelatin fibers alignment on schwann cell and axon behavior and organization in the perspective of artificial nerve design. *International Journal of Molecular Sciences*, 16(6), pp.12925–12942.

Goldstein, A.S. & Thayer, P.S., 2016. Fabrication of complex biomaterial scaffolds

for soft tissue engineering by electrospinning. In A. Grumezescu, ed. *Nanobiomaterials in Soft Tissue Engineering*. Amsterdam: William Andrew, pp. 299–330.

Grevious, M.A. et al., 2006. Structural and functional anatomy of the abdominal wall. *Clinics in Plastic Surgery*, 33(2), pp.169–179.

Gunatillake, P., Mayadunne, R. & Adhikari, R., 2006. *Recent Developments in Biodegradable Synthetic Polymers*,

Guo, C., Zhou, L. & Lv, J., 2013. Effects of expandable graphite and modified ammonium polyphosphate on the flame-retardant and mechanical properties of wood flour-polypropylene composites. *Polymers and Polymer Composites*, 21(7), pp.449–456.

Haider, A., Haider, S. & Kang, I.K., 2015. A comprehensive review summarizing the effect of electrospinning parameters and potential applications of nanofibers in biomedical and biotechnology. *Arabian Journal of Chemistry*.

Hall Barrientos, I.J. et al., 2016. Fabrication and characterisation of drug-loaded electrospun polymeric nanofibers for controlled release in hernia repair. *International Journal of Pharmaceutics*, 517(1–2), pp.329–337.

Hamer-Hodges, D.W. & Scott, N.B., 1985. Surgeon's workshop. Replacement of an abdominal wall defect using expanded PTFE sheet (Gore-tex). *Journal of the Royal College of Surgeons of Edinburgh*, 30(1), pp.65–7.

Hartman, O. et al., 2011. Biofunctionalization of electrospun PCL-based scaffolds

with perlecan domain IV peptide to create a 3-D pharmacokinetic cancer model. *Biomaterials*, 31(21), pp.5700–5718.

Hassler, K.R. & Baltazar-Ford, K.S., 2017. Hernia, inguinal repair, open. *StatPearls [Internet]*.

Hayashi, T., 1994. Biodegradable polymers for biomedical uses. *Progress in Polymer Science*, 19(4), pp.663–702.

He, M. et al., 2016. Fabrication of metronidazole loaded poly (ε-caprolactone)/zein core/shell nanofiber membranes via coaxial electrospinning for guided tissue regeneration. *Journal of Colloid and Interface Science*.

He, M. et al., 2015. Fibrous guided tissue regeneration membrane loaded with anti-inflammatory agent prepared by coaxial electrospinning for the purpose of controlled release. *Applied Surface Science*, 335, pp.121–129.

He, T. et al., 2015. Electrospinning polyvinylidene fluoride fibrous membranes containing anti-bacterial drugs used as wound dressing. *Colloids and Surfaces B: Biointerfaces*, 130, pp.278–286.

Hirano, T. et al., 2006. Mechanism of the inhibitory effect of zwitterionic drugs (levofloxacin and grepafloxacin) on carnitine transporter (OCTN2) in Caco-2 cells. *Biochimica et Biophysica Acta - Biomembranes*, 1758(11), pp.1743–1750.

Holländer, J. et al., 2016. Three-Dimensional Printed PCL-Based Implantable Prototypes of Medical Devices for Controlled Drug Delivery. *Journal of Pharmaceutical J*, 105.

Hu, M.S. et al., 2014. Tissue engineering and regenerative repair in wound healing. *Annals of Biomedical Engineering*, 42(7), pp.1494–507.

Huang, W. et al., 2007. Levofloxacin implants with predefined microstructure fabricated by three-dimensional printing technique. *International Journal of Pharmaceutics*, 339(1–2), pp.33–38.

Iannitti, D.A. et al., 2008. Technique and Outcomes of Abdominal Incisional Hernia Repair Using a Synthetic Composite Mesh: A Report of 455 Cases. *Journal of the American College of Surgeons*, 206(1), pp.83–88.

Ishikawa, J. et al., 2007. Ion implantation of negative ions for cell growth manipulation and nervous system repair. *Surface and Coatings Technology*, 201(19–20 SPEC. ISS.), pp.8083–8090.

Jackson, J.K. et al., 2002. The encapsulation of ribozymes in biodegradable polymeric matrices. *International Journal of Pharmaceutics*, 243(1–2), pp.43–55.

Jain, A. & Jain, S.K., 2008. PEGylation: an approach for drug delivery. A review. *Crit Rev Ther Drug Carrier Syst.*, 25(5), pp.403–447.

Jalvandi, J. et al., 2015. Release and antimicrobial activity of levofloxacin from composite mats of poly(e-caprolactone) and mesoporous silica nanoparticles fabricated by core-shell electrospinning. *Journal of Materials Science*, 50(24), pp.7967–7974.

Jamshidian, M. et al., 2010. Poly-Lactic Acid: Production, applications,

nanocomposites, and release studies. *Comprehensive Reviews in Food Science and Food Safety*, 9(5), pp.552–571.

Jeyanthi, R. et al., 1997. Effect of processing parameters on the properties of peptide-containing PLGA microspheres. *Journal of Microencapsulation*, 14(2), pp.163–174.

Jiang, Q. et al., 2013. Water-stable electrospun collagen fibers from a non-toxic solvent and crosslinking system. *Journal of Biomedical Materials Research - Part A*, 101 A(5), pp.1237–1247.

Jiang, S. et al., 2016. Polyimide Nanofibers by "green" Electrospinning via Aqueous Solution for Filtration Applications. *ACS Sustainable Chemistry and Engineering*, 4(9), pp.4797–4804.

Jones, D.S. et al., 2002. Poly(ε-caprolactone) and poly(ε-caprolactone)-polyvinylpyrrolidone-iodine blends as ureteral biomaterials: Characterisation of mechanical and surface properties, degradation and resistance to encrustation in vitro. *Biomaterials*, 23(23), pp.4449–4458.

De Jong, W.H. & Borm, P.J., 2008. Drug delivery and nanoparticles : Applications and hazards. *International Journal of Nanomedicine*, 3(2), pp.133–149.

Kabay, G. et al., 2016. Biocatalytic protein membranes fabricated by electrospinning. *Reactive and Functional Polymers*, 103, pp.26–32.

Kaurav, H. & Kapoor, D.N., 2017. Implantable systems for drug delivery to the brain. *Therapeutic Delivery*, 8(12), pp.1097–1107.

Kawaguchi, M. et al., 2015. Transitional mesh repair for large incisional hernia in the elderly. *International Journal of Surgery Case Reports*, 7, pp.70–74.

Kayaci, F. et al., 2013. Antibacterial electrospun poly(lactic acid) (PLA) nano fi brous webs incorporating triclosan/cyclodextrin inclusion complexes. *J. Agric. Food Chem*, 61, p.3901−3908.

Kelly, S., 2017. Mesh abdominal wall hernia surgery is safe and effective-the harm New Zealand media has done. *The New Zealand Medical Journal*, 130(1463), pp.54–57.

Kim, K. et al., 2004. Incorporation and controlled release of a hydrophilic antibiotic using poly(lactide-co-glycolide)-based electrospun nanofibrous scaffolds. *Journal of Controlled Release*, 98(1), pp.47–56.

Kingsworth, A. & LeBlanc, K., 2003. Hernias: inguinal and incisional. *The Lancet*, 362(9395), pp.1561–1571.

Kitaoka, H. et al., 1995. Effect of dehydration on the formation of levofloxacin pseudopolymorphs. *CHem. Pharm. Bull.*, 43(4), pp.649–653.

Klosterhalfen, B., Junge, K. & Klinge, U., 2005. The lightweight and large porous mesh concept for hernia repair. *Expert Rev Med Devices*, 2(1), pp.103–17.

Koju, R. et al., 2017. Transabdominal pre-peritoneal mesh repair versus Lichtenstein's hernioplasty. , 15(2), pp.135–140.

Kozarov, E., 2012. Bacterial invasion of vascular cell types: vascular infectology and atherogenesis. *Future cardiology*, 8(1), pp.123–38.

Lamprou, D.A. et al., 2010. Self-assembled structures of alkanethiols on gold-coated cantilever tips and substrates for atomic force microscopy: Molecular organisation and conditions for reproducible deposition. *Applied Surface Science*, 256(6), pp.1961–1968.

Lamprou, D.A., Venkatpurwar, V. & Kumar, M.N.V.R., 2013. Atomic force microscopy images label-free, drug encapsulated nanoparticles in vivo and detects difference in tissue mechanical properties of treated and untreated: A tip for nanotoxicology. *PLoS ONE*, 8(5), pp.8–12.

Lee, J. et al., 2008. The effect of gelatin incorporation into electrospun poly(l-lactide-co-ε-caprolactone) fibers on mechanical properties and cytocompatibility. *Biomaterials*, 29(12), pp.1872–1879.

Lee, R.E. et al., 2016. Thermoforming of polylactic acid foam sheets: crystallization behaviors and thermal stability. *Industrial and Engineering Chemistry Research*, 55(3), pp.560–567.

Leszczak, V. et al., 2014. Nanostructured biomaterials from electrospun demineralized bone matrix: A survey of processing and crosslinking strategies. *ACS Applied Materials and Interfaces*, 6(12), pp.9328–9337.

Li, D. et al., 2013. PLA/F68/Dexamethasone implants prepared by hot-melt extrusion for controlled release of anti-inflammatory drug to implantable medical devices: I. Preparation, characterization and hydrolytic degradation study. *International Journal of Pharmaceutics*, 441(1–2), pp.365–372.

Li, L., Frey, M. & Green, T., 2006. Modification of air filter media with nylon-6

nanofibers. *Journal of Engineered Fibers and Fabrics*, 1(1).

Liverani, L. et al., 2017. Incorporation of bioactive glass nanoparticles in electrospun PCL/chitosan fibers by using benign solvents. *Bioactive Materials*, pp.1–9.

Lodish, H., Berk, A. & Zipursky, S.L., 2000. Collagen: The fibrous proteins of the matrix. In *Molecular Cell Biology*. New York: W. H. Freeman.

Lowy, F., 1998. Staphylococcus aureus infections. *New England Journal of Medicine*, 339, pp.520–532.

Lukasiewicz, A. & Drewa, T., 2014. Synthetic implants in hernia surgery. *Advances in Clinical and Experimental Medicine*, 23(1), pp.135–142.

Maleki, H. et al., 2016. Drug release behavior of electrospun twisted yarns as implantable medical devices. *Biofabrication*, 8(3), p.35019.

Maleque, M. et al., 2012. Development and validation of a simple UV spectrophotometric method for the determination of levofloxacin both in bulk and marketed dosage formulations. *Journal of Pharmaceutical Analysis*, 2(6), pp.454–457.

Mano, J.F. et al., 2007. Natural origin biodegradable systems in tissue engineering and regenerative medicine: present status and some moving trends. *Journal of the Royal Society, Interface / the Royal Society*, 4(17), pp.999–1030.

Masuda, T. et al., 1999. Growing and differentiating characterization of aortic smooth muscle cell line, p53LMAC01 obtained from p53 knock out mice. *Molecular and cellular biochemistry*, 190(1–2), pp.99–104.

Matabola, K.P. & Moutloali, R.M., 2013. The influence of electrospinning

parameters on the morphology and diameter of poly(vinyledene fluoride)

nanofibers- Effect of sodium chloride. *Journal of Materials Science*, 48(16),

pp.5475–5482.

Matthews, J.A. et al., 2002. Electrospinning of Collagen Nanofibers.

Biomacromolecules, 3(August), pp.232–238.

Maulvi, F.A. et al., 2017. Application of 3D printing technology in the development

of novel drug delivery systems. , 9(1), pp.44–49.

McCullen, S.D. et al., 2007. Characterization of electrospun nanocomposite scaffolds

and biocompatibility with adipose-derived human mesenchymal stem cells.

International Journal of Nanomedicine, 2(2), pp.253–263.

McKee, M.G. et al., 2004. Correlations of solution rheology with electrospun fiber

formation of linear and branched polyesters. *Macromolecules*, 37(5), pp.1760–

1767.

McManus, M.C. et al., 2006. Electrospun fibrinogen: Feasibility as a tissue

engineering scaffold in a rat cell culture model. *Journal of Biomedical

Materials Research - Part A*, 81A(2), pp.299–309.

Megelski, S. et al., 2002. Micro- and nanostructured surface morphology on

electrospun polymer fibers. *Macromolecules*, 35(22), pp.8456–8466.

Mehrabi Bahar, M. et al., 2015. The role of prophylactic cefazolin in the prevention

of infection after various types of abdominal wall hernia repair with mesh.

Asian Journal of Surgery, 38(3), pp.139–144.

Menei, P. et al., 1994. Fate and biocompatibility of three types of microspheres implanted into the brain. *Journal of Biomedical Materials Research*, 28(9), pp.1079–1085.

Middleton, J.C. & Tipton, A.J., 2000. Synthetic biodegradable polymers as orthopedic devices. *Biomaterials*, 21(23), pp.2335–2346.

Molegraaf, M., Kaufmann, R. & Lange, J., 2017. Comparison of self-gripping mesh and sutured mesh in open inguinal hernia repair: A meta-analysis of long-term results. *Surgery*, pp.1–13.

Moriarty, F., Sebastian, A.J.Z. & Busscher, H.J., 2012. *Biomaterials Associated Infection: Immunological Aspects and Antimicrobial Strategies*, Springer.

Morling, J.R. et al., 2016. Adverse events after first, single, mesh and non-mesh surgical procedures for stress urinary incontinence and pelvic organ prolapse in Scotland, 1997–2016: a population-based cohort study. *The Lancet*, 389(10069), pp.629–640.

Moulton, S.E. & Wallace, G.G., 2014. 3-dimensional (3D) fabricated polymer based drug delivery systems. *Journal of Controlled Release*, 193, pp.27–34.

Mouzam, M.I. et al., 2011. Preparation of a novel floating ring capsule-type dosage form for stomach specific delivery. *Saudi Pharmaceutical Journal*, 19(2), pp.85–93.

Munegato, G. et al., 2017. A new technique for tension-free reconstruction in large

incisional hernia. *Updates in Surgery*, (123456789).

Nair, L.S. & Laurencin, C.T., 2007. Biodegradable polymers as biomaterials. *Progress in Polymer Science (Oxford)*, 32(8–9), pp.762–798.

Nelson, M.T. et al., 2014. Preferential, enhanced breast cancer cell migration on biomimetic electrospun nanofiber "cell highways". *BMC cancer*, 14(1), p.825.

Ng, K.W. et al., 2007. In vivo evaluation of an ultra-thin polycaprolactone film as a wound dressing. *Journal of Biomaterials Science, Polymer Edition*, 18(7), pp.925–938.

von der Ohe, P.C. et al., 2012. Triclosan-the forgotten priority substance? *Environmental Science and Pollution Research*, 19(2), pp.585–591.

Orozco, V.H. et al., 2009. Preparation and characterization of poly(Lactic Acid)- G-maleic anhydride + starch blends. *Macromolecular Symposia*, 277(1), pp.69–80.

Ospina-Orejarena, A. et al., 2016. Grafting collagen on poly (lactic acid) by a simple route to produce electrospun scaffolds, and their cell adhesion evaluation. *Tissue Engineering and Regenerative Medicine*, 13(4), pp.375–387.

Papenburg, B.J. et al., 2009. Development and analysis of multi-layer scaffolds for tissue engineering. *Biomaterials*, 30(31), pp.6228–6239.

Park, H. et al., 2012. Fabrication of levofloxacin-loaded nanofibrous scaffolds using coaxial electrospinning. *Journal of Pharmaceutical Investigation*, 42(2), pp.89–93.

Patel, H., Ostergard, D.R. & Sternschuss, G., 2012. Polypropylene mesh and the host response. *International Urogynecology Journal*, 23(6), pp.669–679.

Patrício, T. et al., 2013. Characterisation of PCL and PCL/PLA scaffolds for tissue engineering. *Procedia CIRP*, 5, pp.110–114.

Piccoli, A. et al., 2002. Determination of triclosan in personal health care products by liquid chromatography (HPLC). *Farmaco*, 57(5), pp.369–372.

Powell, H.M. & Boyce, S.T., 2009. Engineered Human Skin Fabricated Using Electrospun Collagen–PCL Blends: Morphogenesis and Mechanical Properties.*3*, 15(8).

Puppi, D. et al., 2011. Development of 3D wet-spun polymeric scaffolds loaded with antimicrobial agents for bone engineering. *Journal of Bioactive and Compatible Polymers*, 26, pp.478–492.

Qin, S. et al., 2015. Continual cell deformation induced via attachment to oriented fibers enhances fibroblast cell migration. *PLoS ONE*, 10(3), pp.1–16.

Ramot, Y. et al., 2016. Biocompatibility and safety of PLA and its copolymers. *Advanced Drug Delivery Reviews*, 107, pp.153–162.

Reinke, J.M. & Sorg, H., 2012. Wound repair and regeneration. *European Surgical Research*, 49(1), pp.35–43.

Reneker, D.H. & Fong, H., 2006. Polymeric nanofibers: Introduction. *A.C.S. Symposium Series*, 918, pp.1–6.

Robinson, A. a, Belden, J.B. & Lydy, M.J., 2005. Toxicity of fluoroquinolone antibiotics to aquatic organisms. *Environmental Toxicology and Chemistry / SETAC*, 24(2), pp.423–430.

Robson, M.C. et al., 2000. Wound healing trajectories as predictors of effectiveness of therapeutic agents. *Archives of Surgery (Chicago, Ill. : 1960)*, 135(7), pp.773–7.

Ruoslahti, E., 1984. Fibronectin in cell adhesion and invasion. *Cancer and Metastasis Review*, 3(1), pp.43–51.

Sachs, E., Cima, M. & Cornie, J., 1990. Three-dimensional printing: rapid tooling and prototypes directly form a CAD model. *CIRP Annals - Manufacturing Technology*, 39(1), pp.201–204.

Sandler, N. et al., 2011. Inkjet printing of drug substances and use of porous substrates-towards individualized dosing. *J Pharm Sc*, 100(8), pp.3386–3395.

Schmidt, D.R., Waldeck, H. & Kao, W.J., 2009. Protein adsorption to biomaterials. In D. A. Puleo & R. Bizios, eds. *Biological Interactions on Materials Surfaces*. New York: Springer, pp. 1–18.

Schramm, G., 2016. *A Practical Approach to Rheology and Rheometry* 2nd Edition., Karlsruhe, Germany: Thermo Electron (Karlsruhe) GmbH.

Sebe, I. et al., 2013. Polymer structure and antimicrobial activity of polyvinylpyrrolidone-based iodine nanofibres prepared with high-speed rotary spinning technique. *International Journal of Pharmaceutics*, 458(1), pp.99–103.

Sell, S.A. et al., 2009. Electrospinning of collagen/biopolymers for regenerative medicine and cardiovascular tissue engineering. *Advanced Drug Delivery Reviews*, 61(12), pp.1007–1019.

Shah, N. et al., 2014. Fundamentals of Amorphous Systems: Thermodynamic Aspects *M. J. Rathbone, ed., NewYork Heidelberg Dordrecht London: Springer US*.

Shang, S. et al., 2010. The effect of electrospun fibre alignment on the behaviour of rat periodontal ligament cells. *European Cells and Materials*, 19, pp.180–192.

Signori, F., Coltelli, M.B. & Bronco, S., 2009. Thermal degradation of poly(lactic acid) (PLA) and poly(butylene adipate-co-terephthalate) (PBAT) and their blends upon melt processing. *Polymer Degradation and Stability*, 94(1), pp.74–82.

Sill, T.J. & von Recum, H.A., 2008. Electrospinning: Applications in drug delivery and tissue engineering. *Biomaterials*, 29(13), pp.1989–2006.

Sisirak, M., Zvizdic, A. & Hukic, M., 2010. Methicillin-resistant *Staphylococcus aureus* (MRSA) as a cause of nosocomial wound infections. *Bosn. J. Basic Med. Sci.*, 10(1), pp.32–37.

Sivashankari, P.R. & Prabaharan, M., 2016. Prospects of chitosan-based scaffolds for growth factor release in tissue engineering. *International Journal of Biological Macromolecules*, 93, pp.1382–1389.

Sohrabi, A. et al., 2013. Sustained drug release and antibacterial activity of

ampicillin incorporated poly(methyl methacrylate)-nylon6 core/shell nanofibers. *Polymer (United Kingdom)*, 54(11), pp.2699–2705.

Solomkin, J.S. et al., 2010. Diagnosis and management of complicated intra-abdominal infection in adults and children: Guidelines by the Surgical Infection Society and the Infectious Diseases Society of America. *Clinical Infectious Disease*, 50, pp.133–64.

Song, B., Wu, C. & Chang, J., 2012. Dual drug release from electrospun poly(lactic-co-glycolic acid)/mesoporous silica nanoparticles composite mats with distinct release profiles. *Acta Biomaterialia*, 8(5), pp.1901–1907.

Steinberg, J.P., Clark, C.C. & Hackman, B.O., 1996. Nosocomial and community-acquired Staphylococcus aureus bacteremias from 1980 to 1993: impact of intravascular devices and methicillin resistance. *Clin Infect Dis.*, 23(2), pp.255–259.

Sukigara, S. et al., 2003. Regeneration of Bombyx mori silk by electrospinning - Part 1: Processing parameters and geometric properties. *Polymer*, 44(19), pp.5721–5727.

Sun, B. et al., 2014. Advances in three-dimensional nanofibrous macrostructures via electrospinning. *Progress in Polymer Science*, 39(5), pp.862–890.

Tahan, N. et al., 2016. Measurement of superficial and deep abdominal muscle thickness: an ultrasonography study. *Journal of Physiological Anthropology*, 35(1), p.17.

Tan, A.R. et al., 2008. Electrospinning of photocrosslinked and degradable fibrous scaffolds. *Journal of Biomedical Materials Research - Part A*, 87(4), pp.1034–1043.

Thomas, V. et al., 2006. Mechano-morphological studies of aligned nanofibrous scaffolds of polycaprolactone fabricated by electrospinning. *Journal of Biomaterials Science, Polymer Edition*, 17(9), pp.969–984.

Thongngam, M. & McClements, D.J., 2005. Influence of pH, ionic strength, and temperature on self-association and interactions of sodium dodecyl sulfate in the absence and presence of chitosan. *Langmuir*, 21(1), pp.79–86.

Tillman, B.W. et al., 2009. The in vivo stability of electrospun polycaprolactone-collagen scaffolds in vascular reconstruction. *Biomaterials*, 30(4), pp.583–588.

Tiwari, G. et al., 2012. Drug delivery systems: An updated review. *International Journal of Pharmaceutical Investigation*, 2(1), pp.2–11.

Toncheva, A. et al., 2016. Antibacterial PLA/PEG electrospun fibers: Comparative study between grafting and blending PEG. *European Polymer Journal*, 75, pp.223–233.

Toncheva, A. et al., 2011. Electrospun poly(L-lactide) membranes containing a single drug or multiple drug system for antimicrobial wound dressings. *Macromolecular Research*, 19(12), pp.1310–1319.

Topuz, F. & Uyar, T., 2017. Electrospinning of gelatin with tunable fiber morphology from round to flat/ribbon. *Materials Science and Engineering C*,

80, pp.371–378.

Unger, M., Vogel, C. & Siesler, H.W., 2010. Molecular weight dependence of the thermal degradation of poly(epsilon-caprolactone): a thermogravimetric differential thermal Fourier transform infrared spectroscopy study. *Applied spectroscopy*, 64(7), pp.805–9.

Del Valle, L.J. et al., 2011. Electrospinning of polylactide and polycaprolactone mixtures for preparation of materials with tunable drug release properties. *Journal of Polymer Research*, 18(6), pp.1903–1917.

Venugopal, J., Zhang, Y.Z. & Ramakrishna, S., 2005. Fabrication of modified and functionalized polycaprolactone nanofibre scaffolds for vascular tissue engineering. *Nanotechnology*, 16(10), pp.2138–42.

Vorng, J.-L. et al., 2016. Semi-empirical rules to determine drug sensitivity and ionization efficiency in SIMS using a model tissue sample. *Analytical Chemistry*, 88, pp.11028–11036.

Wang, J. et al., 2013. Prospective randomized, double-blind, placebo controlled trial to evaluate infection prevention in adult patients after tension-free inguinal hernia repair. *International Journal of Clinical Pharmacology & Therapeutics*, 51(12), pp.924–931.

Wang, M. et al., 2010. Sustained antibacterial activity from triclosan-loaded nanostructured mesoporous silicon. *Molecular Pharmaceutics*, 7(6), pp.2232–2239.

Wang, Y. et al., 2017. Electrospun PBLG/PLA nanofiber membrane for constructing in vitro 3D model of melanoma. *Materials Science and Engineering C*, 76, pp.313–318.

Wang, Z.X. et al., 2013. Systematic review and meta-analysis of triclosan-coated sutures for the prevention of surgical-site infection. *British Journal of Surgery*, 100(4), pp.465–473.

Webber, M.A. et al., 2017. Quinolone-resistant gyrase mutants demonstrate decreased susceptibility to triclosan. *Journal of Antimicrobial Chemotherapy*, (October), pp.2755–2763.

Weltz, A.S. et al., 2017. Operative outcomes after open abdominal wall reconstruction with retromuscular mesh fixation using fibrin glue versus transfascial sutures. *The American Surgeon*, 83(9), pp.937–942.

Whited, B.M. & Rylander, M.N., 2014. The influence of electrospun scaffold topography on endothelial cell morphology, alignment, and adhesion in response to fluid flow. *Biotechnology and Bioengineering*, 111(1), pp.1–22.

van Winterswijk, P.J. & Nout, E., 2007. Tissue engineering and wound healing: An overview of the past, present, and future. *Wounds*, 19(10).

Woodruff, M.A. & Hutmacher, D.W., 2010. The return of a forgotten polymer - Polycaprolactone in the 21st century. *Progress in Polymer Science (Oxford)*, 35(10), pp.1217–1256.

Wu, W. et al., 2009. A programmed release multi-drug implant fabricated by three-

dimensional printing technology for bone tuberculosis therapy. *Biomedical Materials (Bristol, England)*, 4(6), p.65005.

Yang, L. et al., 2015. Bacteria in hernia sac: an important risk fact for surgical site infection after incarcerated hernia repair. *Hernia*, 19(2), pp.279–283.

Yao, F. & Weiyuan, J.K., 2010. Drug release kinetics and transport mechanisms of non- degradable and degradable polymeric delivery systems. *Expert Opinion Drug Delivery*, 7(4), pp.429–444.

Zahedi, P. et al., 2012. Preparation and performance evaluation of tetracycline hydrochloride loaded wound dressing mats based on electrospun nanofibrous poly(lactic acid)/poly(ϵ-caprolactone) blends. *Journal of Applied Polymer Science*, 124, pp.4174–4183.

Zamani, M., Prabhakaran, M.P. & Ramakrishna, S., 2013. Advances in drug delivery via electrospun and electrosprayed nanomaterials. *International Journal of Nanomedicine*, 8, pp.2997–3017.

Zhang, X.-Q., Intra, J. & Salem, A.K., 2008. Comparative study of poly (lactic-co-glycolic acid)-poly ethyleneimine-plasmid DNA microparticles prepared using double emulsion methods. *Journal of Microencapsulation*, 25(1), pp.1–12.

Zheng, H. et al., 2002. Recurrent inguinal hernia: Disease of the collagen matrix? *World Journal of Surgery*, 26(4), pp.401–408.

Zogbi, L. et al., 2010. Retraction and fibroplasia in a polypropylene prosthesis: Experimental study in rats. *Hernia*, 14(3), pp.291–298.

Appendix A

Descriptive Statistics

	N total	Mean	Standard Deviation	SE of mean	Lower 95% CI of Mean	Upper 95% CI of Mean	Coefficient of Variation	Minimum	Median	Maximum
PCL	50	2.01856	0.45108	0.06379	1.89037	2.14676	0.22346	1.415	1.902	2.9762
PCL-IRG	50	1.64954	0.40205	0.05686	1.53528	1.7638	0.24373	1.04399	1.61595	2.763
PCL-LEVO	50	2.87246	1.66351	0.23526	2.3997	3.34523	0.57912	0.304	2.375	8.291
PCL-COLLAGEN	50	0.78202	0.53321	0.07541	0.63049	0.93356	0.68183	0.00421	0.729	1.877
PCL-COLLAGEN-IRG	50	0.89251	0.2996	0.04237	0.80736	0.97765	0.33568	0.3108	0.90015	1.7255
PCL-COLLAGEN-LEVO	50	1.51712	1.073	0.15175	1.21218	1.82206	0.70726	0.04096	1.53	3.76

One Way ANOVA
  Means Comparisons
    Scheffe Test

	MeanDiff	SEM	F Value	Prob	Alpha	Sig	LCL	UCL
PCL-IRG PCL	-0.36903	0.17622	0.87711	0.49674	0.05	0	-0.95937	0.22132
PCL-LEVO PCL	0.8539	0.17622	4.69628	3.84321E-4	0.05	1	0.26355	1.44424
PCL-LEVO PCL-IRG	1.22292	0.17622	9.63254	1.57402E-8	0.05	1	0.63258	1.81327
PCL-COLLAGEN PCL	-1.23654	0.17622	9.84825	1.01833E-8	0.05	1	-1.82689	-0.6462
PCL-COLLAGEN PCL-IRG	-0.86752	0.17622	4.84725	2.82165E-4	0.05	1	-1.45786	-0.27717
PCL-COLLAGEN PCL-LEVO	-2.09044	0.17622	28.146	2.72922E-23	0.05	1	-2.68079	-1.50009
PCL-COLLAGEN-IRG PCL	-1.12606	0.17622	8.16701	3.09283E-7	0.05	1	-1.7164	-0.53571
PCL-COLLAGEN-IRG PCL-IRG	-0.75703	0.17622	3.69122	0.00296	0.05	1	-1.34738	-0.16669
PCL-COLLAGEN-IRG PCL-LEVO	-1.97996	0.17622	25.24949	3.55999E-21	0.05	1	-2.5703	-1.38961
PCL-COLLAGEN-IRG PCL-COLLAGEN	0.11048	0.17622	0.07862	0.99547	0.05	0	-0.47986	0.70083
PCL-COLLAGEN-LEVO PCL	-0.50144	0.17622	1.61952	0.15466	0.05	0	-1.09179	0.0889
PCL-COLLAGEN-LEVO PCL-IRG	-0.13242	0.17622	0.11294	0.98946	0.05	0	-0.72276	0.45793
PCL-COLLAGEN-LEVO PCL-LEVO	-1.35534	0.17622	11.83149	1.93333E-10	0.05	1	-1.94569	-0.765
PCL-COLLAGEN-LEVO PCL-COLLAGEN	0.7351	0.17622	3.48042	0.00451	0.05	1	0.14475	1.32544
PCL-COLLAGEN-LEVO PCL-COLLAGEN-IRG	0.62461	0.17622	2.51284	0.03011	0.05	1	0.03427	1.21496

Sig equals 1 indicates that the difference of the means is significant at the 0.05 level.
Sig equals 0 indicates that the difference of the means is not significant at the 0.05 level.

Appendix B

Descriptive Statistics

	N total	Mean	Standard Deviation	SE of mean	Lower 95% CI of Mean	Upper 95% CI of Mean	Coefficient of Variation	Minimum	Median	Maximum
PLA	50	2.7328	0.38394	0.0543	2.62369	2.84192	0.14049	1.8628	2.73275	3.6213
PLA-IRG	50	2.47521	0.64137	0.0907	2.29293	2.65748	0.25912	1.2802	2.4182	3.7815
PLA-LEVO	50	2.08062	0.35799	0.05063	1.97888	2.18236	0.17206	1.3224	2.08355	3.081
PLA-COLLAGEN	50	1.66621	0.40745	0.05762	1.55041	1.782	0.24454	1.0599	1.57191	3.0151
PLA-COLLAGEN-IRG	50	1.69732	0.49899	0.07057	1.55551	1.83913	0.29398	1.005	1.6365	3.63
PLA-COLLAGEN-LEVO	50	0.9777	0.71047	0.10048	0.77578	1.17961	0.72668	0.1224	0.9213	3.668

One Way ANOVA
  Means Comparisons
    Scheffe Test

	MeanDiff	SEM	F Value	Prob	Alpha	Sig	LCL	UCL
PLA-IRG PLA	-0.2576	0.1035	1.23898	0.2908	0.05	0	-0.60432	0.08913
PLA-LEVO PLA	-0.65218	0.1035	7.94193	4.89952E-7	0.05	1	-0.99891	-0.30546
PLA-LEVO PLA-IRG	-0.39459	0.1035	2.90719	0.01404	0.05	1	-0.74131	-0.04786
PLA-COLLAGEN PLA	-1.0666	0.1035	21.24171	3.90619E-18	0.05	1	-1.41332	-0.71987
PLA-COLLAGEN PLA-IRG	-0.809	0.1035	12.22047	8.96397E-11	0.05	1	-1.15573	-0.46228
PLA-COLLAGEN PLA-LEVO	-0.41442	0.1035	3.20671	0.00778	0.05	1	-0.76114	-0.06769
PLA-COLLAGEN-IRG PLA	-1.03548	0.1035	20.02034	3.51241E-17	0.05	1	-1.3822	-0.68876
PLA-COLLAGEN-IRG PLA-IRG	-0.77788	0.1035	11.29843	5.57007E-10	0.05	1	-1.12461	-0.43116
PLA-COLLAGEN-IRG PLA-LEVO	-0.3833	0.1035	2.74322	0.01932	0.05	1	-0.73002	-0.03657
PLA-COLLAGEN-IRG PLA-COLLAGEN	0.03112	0.1035	0.01808	0.99987	0.05	0	-0.31561	0.37784
PLA-COLLAGEN-LEVO PLA	-1.75511	0.1035	57.51689	1.34138E-41	0.05	1	-2.10183	-1.40838
PLA-COLLAGEN-LEVO PLA-IRG	-1.49751	0.1035	41.87248	1.73035E-32	0.05	1	-1.84424	-1.15079
PLA-COLLAGEN-LEVO PLA-LEVO	-1.10293	0.1035	22.71329	2.8818E-19	0.05	1	-1.44965	-0.7562
PLA-COLLAGEN-LEVO PLA-COLLAGEN	-0.68851	0.1035	8.85132	7.66839E-8	0.05	1	-1.03523	-0.34179
PLA-COLLAGEN-LEVO PLA-COLLAGEN-IRG	-0.71963	0.1035	9.66949	1.46079E-8	0.05	1	-1.06635	-0.3729

Sig equals 1 indicates that the difference of the means is significant at the 0.05 level.
Sig equals 0 indicates that the difference of the means is not significant at the 0.05 level.

Appendix C

	Tensile Strength (MPa) *n* = 3	Elasticity (MPa)	Maximum Extension (mm)
PCL	12.06 ± 0.54	17.35 ± 0.24	40.34 ± 2.47
PCL-IRG	3.25 ± 0.21	13.01 ± 0.13	30.23 ± 1.39
PCL-LEVO	3.33 ± 0.94	6.88 ± 0.76	22.14 ± 1.97
PCL-COLLAGEN	7.86 ± 0.92	4.02 ± 0.25	29.24 ± 3.18
PCL-COL-IRG	1.91 ± 0.40	1.01 ± 0.83	20.83 ± 0.88
PCL-COL-LEVO	7.81 ± 0.33	12.88 ± 0.11	26.23 ± 0.41
PLA	2.32 ± 0.49	20.21 ± 0.66	14.22 ± 1.73
PLA-IRG	1.21 ± 0.18	37.1 ± 0.35	3.27 ± 1.16
PLA-LEVO	4.82 ± 0.64	49.18 ± 0.19	20.82 ± 2.41
PLA-COLLAGEN	5.6 ± 0.77	91.04 ± 0.87	13.02 ± 1.12
PLA-COL-IRG	7.13 ± 0.53	66.3 ± 0.34	12.27 ± 1.69
PLA-COL-LEVO	5.23 ± 0.44	30.51 ± 0.24	9.26 ± 2.45